The head-on collision of a combustion wave with a shock wave and with a rarefaction wave : a one-dimensional gasdynamical analysis

Please check the document version of this publication:

THE HEAD-ON COLLISION OF A
COMBUSTION WAVE WITH A
SHOCK WAVE, AND WITH
A RAREFACTION WAVE

G. BROEKSTRA

THE HEAD-ON COLLISION OF A COMBUSTION WAVE WITH A SHOCK WAVE, AND WITH A RAREFACTION WAVE

a one-dimensional gasdynamical analysis

GERRIT BROEKSTRA

GEBOREN TE ALKMAAR

Dit proefschrift is goedgekeurd door de promotor Prof.Dr.Ir. G. Vossers
en de coreferent Prof.Dr.Ir. C. Boelhouwer

to my parents
to Frieda and Barbara

CONTENTS

6

LIST OF PRINCIPAL SYMBOLS

Latin symbols

a_1	constant in isentropic equation	
a_i	number of moles of ith reactant	
A	proportionality constant	
b	plate thickness at second break point in u_{fs}-d curve	m
b_i	number of moles of ith product	
c	sound wave velocity	m/s
c_{p_i}	heat capacity at constant pressure of ith species	J/mole K
C_v	specific heat at constant volume	J/kg K
C_p	specific heat at constant pressure	J/kg K
d	thickness of plate	m
D	detonation wave velocity	m/s
e	specific internal energy	J/kg
E	$= e + \frac{1}{2}u^2 + Q$	J/kg
	or, apparent activation energy	J/mole
h_i	enthalpy of ith species	J/mole
H	specific enthalpy	J/kg
ΔH_i°	heat of formation of ith species at 298.15 K	J/mole
ΔH_i	heat of formation of ith species at temperature T	J/mole
ΔH_i^T	enthalpy of ith species at temperature T with respect to T = 298.15 K	J/mole
J	mechanical equivalent of heat = 4.184	J/cal
k_i	equilibrium constant of ith species	
l	length of reaction zone	m
l_{cw}	length of combustion wave zone	m
l_{ind}	length of induction zone	m
m	mass stream	kg/m^2 s
	or, molecular weight	kg/mole
m_i	molecular weight of ith species·	kg/mole

Ma	Mach number	
p	pressure	N/m^2
p_i	partial pressure of ith species	N/m^2
P	Riemann invariant	m/s
q	pseudo-viscosity term	N/m^2
Q	Riemann invariant	m/s
	or, partial specific heat of explosion	J/kg
Q_t	total specific heat of explosion	J/kg
R	universal gas constant	J/mole K
S	specific entropy	J/kg K
t	time	s
T	temperature	K
u	particle velocity	m/s
U	shock wave velocity	m/s
U_{CW}	combustion wave velocity	m/s
v	particle velocity with respect to wave	m/s
V	specific volume	m^3/kg
x	Lagrangian distance coordinate	m
X	Eulerian distance coordinate	m
y	Lagrangian mass coordinate	kg/m^2
y_i	mole fraction of ith species	
Z	Eulerian distance coordinate $\perp$ to X-coordinate	m

Greek symbols

β	reaction coordinate = Q/Q_t	
γ	ratio of specific heats	
ε	total energy (thermal, kinetic and chemical)	J
κ	= $(\gamma+1)/(\gamma-1)$	
ν	Courant number	
ξ	space coordinate attached to shock front	m
ρ	density	kg/m^3
τ	time measured along particle path	s

τ_{ind}	induction time measured along particle path	s
τ^o_{ind}	induction time measured by stationary observer	s
τ_{rel}	heat release "relaxation time"	s

Letter subscripts

e	equilibrium
f	frozen
fs	free-surface
i	incident, or interface
j	refers to jth zone
m	inert material
r	resulting, or behind reflected wave
t	total
tr	total in reflected wave
w	wall

Numerical subscripts (unless otherwise specified)

1	in front of shock wave
2	behind shock wave, or in front of combustion wave
3	behind combustion wave

Letter superscript

n	refers to nth time step

Abbreviations

CJ	Chapman-Jouguet
HE	high explosive
RDX	Cyclotrimethylenetrinitramine (Hexogen)
TNT	Trinitrotoluene
p_{21}	$= p_2/p_1$, etc.
[ ]	concentration usually in [moles/litre]

INTRODUCTION

An explosive may be defined as any substance or device which will produce, upon release of its potential energy, a sudden outburst of gas, thereby exerting high pressures on its surroundings.
Three types of commercial and military explosives may be discerned: mechanical, chemical and atomic.
An example of a mechanical explosion is the famous Krakatao volcanic explosion of 1883. When the volcano ruptured and dumped a great mass of molten lava into the ocean the sudden vaporization of an estimated cubic mile of ocean water caused air and water shock waves which were observed on four continents. This greatest steam explosion of history involved an estimated energy release equivalent to more than 5 million kilotons of TNT.
Chemical explosives may be subdivided in (a) detonating or "high" explosives, and (b) deflagrating or "low" explosives. The latter types are characterized by relatively slow burning rates and low pressures. High explosives, which are characterized by relatively high reaction rates and high pressures, comprise two main types, (a) primary, and (b) secondary explosives. Primary explosives may be ignited by such means as spark, flame or other appropriate heat sources. As an example we mention such sensitive substances as lead azide and mercury fulminate. Many gaseous, vapour and dust-air explosives are primary explosives, since they are readily detonated by means of a heat source of appropriate magnitude. Many residential and industrial accidents and fatalities have been caused by these extremely dangerous explosion hazards. Secondary explosives such as TNT, RDX and Ammonium nitrate usually require the use of shock waves to initiate detonation.

Detonation is a process by which the explosive undergoes chemical reaction within a peculiar type of shock wave called the detonation wave. This wave propagates through the explosive, supported and reinforced by the energy released by chemical reaction, at velocities from about 1.5 km/s to 9 km/s, depending on the heat of explosion, the rate at which this energy is released, the density of the explosive and its physical dimensions. Many military and some commercial high explosives

are applied in practice because of their brisance, or shattering action.
Brisance, which can be identified with detonation pressure, is a term
used to describe the ability of the explosive to shatter or fragment
hard objects in direct contact with the explosive. The object in con-
tact with the explosive in turn influences the detonation process.
The basic mechanisms underlying the interaction of detonation waves with
their immediate surroundings are at present poorly understood. In order
to gain a better insight into the nature and origin of such complicated
interactions a possible approach of the problem is suggested in this
work. The essential part of the approach is the concept of a detonation
wave which is assumed to consist of two elementary waves, i.e. a shock
wave followed by a combustion wave. Interactions of these elementary
waves provide then a means of studying interactions of detonation waves
with their surroundings.

This work is arranged in such a way that PART A deals with the non-
reactive waves, i.e. shock, compression and rarefaction waves (Chapter
AI), and with the reactive waves, i.e. detonation and combustion waves
in gaseous mixtures (Chapter AII). In the same Chapter we present our
accurate calculations of detonation wave properties and our measure-
ments of detonation velocities and pressures of stoichiometric hydrogen-
oxygen and equimolar acetylene-oxygen mixtures.
In PART B - Chapter BI we derive the loci of the states that may be
reached from a given state in front of or behind the elementary waves.
These loci constitute the ingredients for the study of two interaction
rules concerning the head-on collision of a combustion wave with a shock
wave, and with a rarefaction wave, which we derive in PART B - Chapter
BII.
As an application of these rules PART C is devoted to a theoretical and
experimental study of the reflection of a gaseous detonation wave
against a solid wall. For this purpose this author developed a computer
program for the approximate numerical solution of the reflection pro-
blem. We modelled the detonation wave by means of three models, each of
which is less restrictive than the preceding one. We also developed
special pressure bar transducers for the measurement of the reflection
pressure.

As another application PART D deals with some aspects of the determination of reaction zone lengths of solid high explosives.
We developed a computer program for the approximate numerical solution of the transmission of a detonation wave into an inert medium.

PART A - CONCEPTS OF GASDYNAMICS

This part is devoted to the study of some concepts of non-reactive and reactive gasdynamics. In Chapter AI some properties of the elementary waves of non-reactive gasdynamics, i.e. rarefaction, compression and shock waves, are shortly summarized for the purpose of further reference. In Chapter AII we discuss some properties of detonation waves. Here we introduce the combustion wave as an elementary wave of reactive gasdynamics.

Chapter AI - Concepts of Non-Reactive Gasdynamics

Gasdynamics concerns itself with the study of the motion of gases. This motion is said to be steady or stationary, if the parameters characterizing the motion and state of the gas are invariant with time. If these parameters change with time, the motion is called unsteady.

Since the phenomena occurring during the motion of the gas considered in gasdynamics are macroscopic, a gas is regarded to be a continuous medium, i.e. it is assumed that a volume element of the medium, however small, still contains a very large number of molecules. Accordingly, when we speak of a "particle", we do not mean a single molecule, but a physically small volume element, i.e. very small compared with the volume of the medium under consideration, but still containing many molecules.

The state of a moving gas is mathematically described by the laws of conservation of mass, momentum and energy, supplemented by the equation of state of the gas. We shall investigate plane one-dimensional motion of a gas, i.e. that type of motion for which all quantities are identical in the planes X = constant, and depend only on time for a given value of the coordinate X.

We can study the motion of a gas by two methods. In one we can determine the parameters characterizing the motion and state of the gas at a given point in space and at a given instant of time; in the other we follow the fate of individual particles of the gas. The first form of the resulting equations is called the Eulerian form, while the second is termed the Lagrangian form. The Lagrangian scheme is particularly

convenient when we consider internal processes involving individual
particles of the gas, such as chemical reactions, where progress with
time depends on the changes of both density and temperature of each
particle.
Before proceeding with the gasdynamical equations we would like to make
the following remarks. Classical gasdynamics deals with the study of
motion of a gas in which it is possible to neglect the dissipative pro-
cesses due to viscosity and heat exchange between the particles and
with bodies in contact with the gas. Gravitational effects are also
neglected. When there are also no sources or sinks of heat produced in
the gas, this is tantamount to assuming that as a particle moves about,
the specific entropy of the moving particle remains constant, i.e. the
changes in state of the particle are adiabatic. The word isentropic,
while being perhaps more accurate here, is reserved in gasdynamics for
the concept of constant entropy.

For the derivations of the Eulerian and Lagrangian equations of motion
the reader is referred to some excellent textbooks on gasdynamics as,
for example, those of Courant and Friedrichs[1], Stanyukovich[2], and
Zeldovich and Raizer[3]. In Chapter AI-§1 we derive some properties of
rarefaction and compression waves in an ideal gas. For the sake of sim-
plicity of the equations we have assumed for the greater part of this
thesis that the gas is a constant gamma-constant molecular weight ideal
gas. In Chapter AI-§2 we derive some properties of steady shock waves,
which will be referred to in subsequent sections.

AI-§1 The rarefaction and compression wave in an ideal gas

The Eulerian equations of gasdynamics for plane adiabatic motion of an
ideal gas may be transformed in the so-called characteristic form
[1,2,3]. The flow can then be described by two variables, the particle
velocity $u(X,t)$, and, for example, the velocity of sound $c(X,t)$ as
functions of the Eulerian distance coordinate X, and time t. The velo-
city of sound is uniquely related to the other thermodynamic variables
by the isentropic relations $p = p(c)$ and $\rho = \rho(c)$, where p is the pres-
sure and ρ is the density.

The Eulerian equations are transformed so that they contain derivatives along the two families of characteristic curves, or characteristics, only. For an ideal gas with constant specific heat ratio γ the equations become [3]

$$P = u + \frac{2c}{\gamma-1} = \text{const.} \quad \text{along P characteristics:} \quad \frac{dX}{dt} = u + c \qquad \text{AI-1-1}$$

$$Q = u - \frac{2c}{\gamma-1} = \text{const.} \quad \text{along Q characteristics:} \quad \frac{dX}{dt} = u - c \qquad \text{AI-1-2}$$

where P and Q are called the Riemann invariants. The latter variables may be used to describe the motion of the gas in place of the old variables, u and c. They are uniquely related to the variables u and c by Eqs. A-1-1 and A-1-2. Solving these equations we find

$$u = \frac{P+Q}{2} \quad ; \quad c = \frac{\gamma-1}{4} (P-Q) \qquad \text{AI-1-3}$$

Considering the invariants as functions of X and t, the equations of the characteristics may be written as

$$P: \frac{dX}{dt} = F(P, Q) \quad ; \quad Q: \frac{dX}{dt} = G(P, Q) \qquad \text{AI-1-4}$$

Here, F and G are known functions; for an ideal gas they become

$$F \equiv \frac{\gamma+1}{4} P + \frac{3-\gamma}{4} Q \quad ; \quad G \equiv \frac{3-\gamma}{4} P + \frac{\gamma+1}{4} Q \qquad \text{AI-1-5}$$

Eq. AI-1-4 shows that the characteristics have a property that permits them to preserve a constant value of one of the invariants. Since P = const. along a specific P characteristic, a change in slope of the characteristic is determined only by a change in the invariant Q. Similarly, Q = const. along a Q characteristic and a change in slope is determined only by a change in the P invariant.

Let an ideal gas in a tube occupy a half space bounded on the left, for example, by a piston. If at initial time t = 0 the invariant $Q(X, 0)$ = const. in the entire region occupied by the gas, then at subsequent times Q will also remain constant in the entire region, $Q(X, t)$ = const. Any disturbance created at the boundary, for example by an acceleration of the piston, is propagated to the right as P

characteristic waves. All Q characteristics that arrive at the boundary are reflected as P characteristic waves. It follows from Eq. AI-1-4 that these P waves constitute a family of straight lines in the X,t-plane (F = const., because P is constant along the characteristics and Q is constant by assumption).

The velocity of the P waves, $dX/dt = u+c$, is greater than the particle velocity u; consequently, a particle path enters each P wave from the right, i.e. comes from the side with greater values of X. This fact is indicated by calling such waves "forward facing". If, on the other hand, P = const. in a flow region, the Q characteristics are straight lines in the X,t-plane and the waves are called "backward facing".

Let u_1 and c_1 be the particle and sound velocity respectively in a region of constant or uniform flow, where Q(X,t) = const. Then, throughout a forward facing wave region, we have from Eq. AI-1-1

$$Q = u - \frac{2c}{\gamma-1} = u_1 - \frac{2c_1}{\gamma-1} = \text{const.} \qquad \text{AI-1-6}$$

From this we derive

$$u = u_1 + \frac{2}{\gamma-1}(c-c_1) \quad ; \quad c = c_1 + \frac{\gamma-1}{2}(u-u_1) \qquad \text{AI-1-7}$$

Since $c^2 = dp/d\rho > 0$, and $dc/d\rho > 0$, so that the pressure and density change in the same sense as the velocity of sound, they also change in the same sense as the particle velocity in a forward facing wave. We distinguish two types of elementary waves; a wave is called a rarefaction wave, if pressure and density of a gas particle decrease on crossing the wave from "head" to "tail" of the wave, and is called a compression wave, if pressure and density increase on crossing the wave. The propagation velocity of forward facing P waves is given by AI-1-1 and with AI-1-7 becomes

$$\frac{dX}{dt} = u + c = \frac{\gamma+1}{2}u + c_1 - \frac{\gamma-1}{2}u_1 \qquad \text{AI-1-8}$$

The rate of change of this velocity with respect to the particle velocity is then

$$\frac{d(u+c)}{du} = \frac{\gamma+1}{2} > 0 \qquad \text{AI-1-9}$$

For a region of backward facing Q characteristic waves we have

$$P = u + \frac{2c}{\gamma-1} = u_1 + \frac{2c_1}{\gamma-1} = \text{const.} \qquad \text{AI-1-10}$$

From this we derive

$$u = u_1 - \frac{2}{\gamma-1}(c-c_1) \quad ; \quad c = c_1 - \frac{\gamma-1}{2}(u-u_1) \qquad \text{AI-1-11}$$

It is shown that pressure and density change in the opposite sense as the particle velocity in a backward facing wave. The propagation velocity of Q waves is given by Eq. AI-1-2 and with AI-1-11 becomes

$$\frac{dX}{dt} = u - c = \frac{\gamma+1}{2}u - c_1 - \frac{\gamma-1}{2}u_1 \qquad \text{AI-1-12}$$

The rate of change of this velocity with respect to the particle velocity is then

$$\frac{d(u-c)}{du} = \frac{\gamma+1}{2} > 0 \qquad \text{AI-1-13}$$

The above results indicate that, if the particle velocity u increases in crossing both a forward facing and a backward facing wave, the propagation velocity of these waves increases too, and mutatis mutandis.
Eq. AI-1-9 indicates that in a forward facing compression wave, where pressure and density and, hence the particle velocity increase from head to tail of the wave, the velocity of the characteristic waves that constitute the compression wave becomes greater from head to tail. Consequently, a compression wave consists of a family of straight converging lines in the X,t-plane and the profiles of the variables as a function of X steepen in the course of time. A similar conclusion may be drawn from Eq. AI-1-13 for a backward facing compression wave. It may be clear that the characteristics of a compression wave will eventually overtake each other, producing a discontinuity surface or shock wave. Starting with this time, however, the variables in a certain region of the flow would no longer be unique functions of X. Since this is impossible, then it follows that a condition appears which makes the above relations invalid. In fact, these relations are based on the assumption that the

gradients of velocity and temperature are small. Otherwise taking into
account the effect of irreversible thermodynamic processes caused by
viscosity and heat conduction shock wave "discontinuities" should be
regarded as thin layers of finite thickness (of the order of a few
molecular mean free paths), where the flow variables change exceeding-
ly sharply, but continuously.

On the other hand, according to Eq. AI-1-9, in a forward facing rare-
faction wave, where pressure and density and, hence the particle
velocity decrease from head to tail across the wave, the velocity of
the characteristic waves becomes smaller from head to tail. Similarly,
a backward facing rarefaction wave consists of a family of straight
diverging lines and the profiles of the variables as functions of X
flatten out in the course of time. We finally note that, if all diver-
ging characteristics of a rarefaction wave originate from the same
point in the X,t-plane, this wave is called a centered rarefaction
wave.

AI-§2 The shock wave in an ideal gas

In the preceding section we have seen that a compression wave will
eventually steepen into a shock wave. The "jump" conditions across the
shock wave have been derived[1] from the integral form of the laws of
conservation of mass, momentum and energy, for vanishing thickness of
the shock transition zone. In the mathematical idealization the narrow
shock transition zone is replaced by a discontinuous jump in the flow
variables. The following three basic Rankine-Hugoniot relations have
been derived.

mass: $\qquad \rho_2 v_2 = \rho_1 v_1 = m$ $\hspace{3cm}$ AI-2-1

momentum: $\quad p_2 + \rho_2 v_2^2 = p_1 + \rho_1 v_1^2$ $\hspace{2.5cm}$ AI-2-2

energy: $\quad e_2 + \dfrac{p_2}{\rho_2} + \tfrac{1}{2}v_2^2 = e_1 + \dfrac{p_1}{\rho_1} + \tfrac{1}{2}v_1^2$ $\hspace{1.5cm}$ AI-2-3

where subscripts 1 and 2 refer to the states of the gas in front of and
behind the shock wave respectively. If U is the propagation velocity of

the shock wave in a laboratory frame of reference, then $v_1 = u_1 - U$ is
the velocity at which the undisturbed gas flows into the discontinuity,
or the particle velocity with respect to a coordinate system attached
to the shock front. Likewise, $v_2 = u_2 - U$ is the particle velocity behind
the shock wave with respect to the coordinate system attached to the
shock front. The specific internal energy is given by e, while m stands
for the mass stream through the shock wave in the coordinate system
attached to the shock front.

Solving v_1 and v_2 from Eqs. AI-2-1 and AI-2-2 gives

$$v_1^2 = \frac{p_2 - p_1}{\rho_1 \left(1 - \frac{\rho_1}{\rho_2}\right)} = \frac{c_1^2}{\gamma} \frac{p_{21} - 1}{1 - \rho_{12}} \qquad \text{AI-2-4}$$

$$v_2^2 = \frac{p_2 - p_1}{\rho_2 \left(\frac{\rho_2}{\rho_1} - 1\right)} = \frac{c_2^2}{\gamma} \frac{1 - \rho_{12}}{p_{21} - 1} \qquad \text{AI-2-5}$$

where $p_{21} = p_2/p_1$ and $\rho_{12} = \rho_1/\rho_2$. The former equation constitutes a
linear relation between p_{21} and ρ_{12} for given v_1 and fixed initial con-
ditions, and is known as the Rayleigh line.

Substitution of these two equations into AI-2-3 gives the Hugoniot re-
lation or shock adiabatic

$$e_2 - e_1 = \frac{c_1^2}{\gamma} (1 + p_{21})(1 - \rho_{12}) \qquad \text{AI-2-6}$$

With the equation of state of an ideal gas with constant specific heat
ratio in the form

$$e = \frac{p}{(\gamma - 1)\rho} \qquad \text{AI-2-7}$$

the Hugoniot relation may be written in explicit from

$$\rho_{12} = \frac{\kappa + p_{21}}{\kappa p_{21} + 1} \qquad \text{AI-2-8}$$

where $\kappa = (\gamma + 1)/(\gamma - 1)$.

Substitution of Eq. AI-2-8 into AI-2-4 and AI-2-5 gives

$$Ma_1^2 = \frac{(\gamma+1)p_{21}+(\gamma-1)}{2\gamma} \qquad\qquad AI-2-9$$

$$Ma_2^2 = \frac{(\gamma+1)p_{12}+(\gamma-1)}{2\gamma} \qquad\qquad AI-2-10$$

where the Mach numbers $Ma_1 = v_1/c_1$ and $Ma_2 = v_2/c_2$, which are positive quantities.

Since $p_{21} > 1$, we find $Ma_1 > 1$ and $Ma_2 < 1$. Consequently, the gas flows into the shock wave with supersonic velocity and flows out of the wave with subsonic velocity. Or, in other words, a shock wave propagates with supersonic velocity with respect to the gas ahead of and with subsonic velocity with respect to the gas behind the wave.

The above conclusions will be used for further reference in this work.

Chapter AII - Concepts of reactive gasdynamics

This Chapter deals with some properties of steady plane reaction waves in ideal gases that are capable of heat release by exothermic chemical reactions.

The classification of reaction waves was based by Jouguet[4] on the adiabatic curve of Hugoniot for complete heat release (see Chapter AII-§2). Those reaction waves, whose properties are described by the upper branch of the Hugoniot curve, are called detonation waves and those pertaining to the lower branch deflagration waves.

A deflagration wave is, in fact, a flame which propagates in a stationary gas by means of thermal conductivity and diffusion of chemical active particles. The propagation velocity of a deflagration wave is thus determined by the coefficients of thermal conductivity and diffusion and the chemical reaction rates. For air mixtures of hydrocarbons this velocity amounts to 0.3-0.4 m/s. The combustion in a deflagration wave is accompanied by a decrease in pressure and density; the products of combustion move in a direction opposite to that of the front of the flame.

This study will be concerned with detonation waves. A detonation wave consists of a shock wave which initiates chemical reaction behind its

front as a result of heating by adiabatic compression. The propagation
velocity, which is generally constant, amounts to several km/s for
gaseous mixtures. The pressure and density in a detonation wave increase
considerably compared with the initial mixture. The combustion products
in the detonation wave move in the same direction as the front of the
wave.

The physical model of a detonation wave, in particular its structure
and stability, is still unclear in many respects. In Chapter AII-§1 we
will give a short survey of the development of detonation wave models.
In Chapter AII-§2 some items of classical detonation wave theory are
discussed, which is illustrated with some of our calculations for a
constant gamma- constant molecular weight gas. In Chapter AII-§3 we pre-
sent our accurate calculations of detonation wave properties of stoi-
chiometric hydrogen-oxygen and equimolar acetylene-oxygen mixtures at
several initial pressures. In the same Chapter we present our measure-
ments of detonation wave velocities and pressures of these mixtures.
The rarefaction wave (Taylor wave) behind the detonation wave, in which
the detonation products expand, is treated in Chapter AII-§4. In Chapter
AII-§5 we will introduce the concept of the combustion wave, which from
the point of view of gasdynamics is defined as that part of the detona-
tion wave in which all the heat by chemical reaction is released.

AII-§1 Survey of detonation wave models

In the last decade a number of excellent reviews have appeared on the
three fundamental problems of detonation wave theory, i.e. the develop-
ment of the wave, its stability and its structure. Of these we mention
those by Oppenheim, Manson and Wagner[5], Shchelkin and Troshin[6],
Soloukhin[7,8], Shchelkin[9], van Tiggelen and de Soete[10], Strehlow[11,12]
and Edwards[13]. Especially the Russian authors have given detailed ac-
counts of the modern explanation of detonation wave structure and stabi-
lity. It seems rather unnecessary to review the complete literature
again in the present report and interested readers are referred to these
survey papers. We will restrict the attention to some of the highlights
in the development of detonation wave models.

The gasdynamics theory of detonation waves has been developed at the beginning of this century. The simplest classical one-dimensional model of a plane detonation wave in a tube was proposed by Chapman[14] and Jouguet[4]. According to this model the detonation wave consists of a shock wave in which chemical reaction occurs instantaneously. Immediately behind the shock wave the combustion products expand in the Taylor wave. The pressure distribution in the Chapman-Jouguet (CJ) model is shown schematically in Fig. AII-1a. From the laws of conservation of mass, momentum and energy an infinite number of detonation velocities are found for each given gaseous mixture. It was shown by Chapman and Jouguet that only one of these corresponds to the experimentally observed velocity.
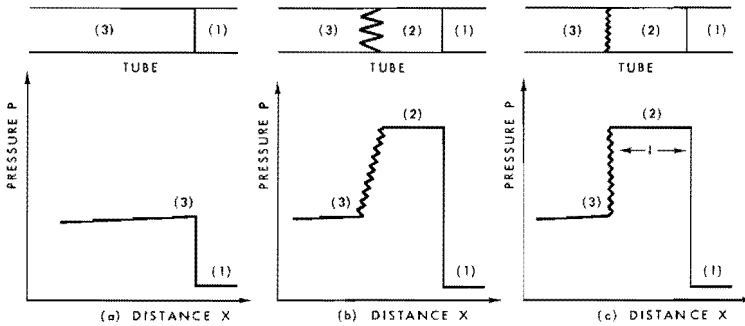
Fig. AII-1   Pressure distributions in CJ model (a) and ZND models
(b and c)

This detonation velocity is selected by determining the point of tangency of the Rayleigh line with the Hugoniot curve for complete heat release. This selection rule is known as the CJ hypothesis. At this point of tangency the entropy is a minimum on the Hugoniot curve and the detonation velocity relative to the velocity of the combustion products is equal to the speed of sound in them (see Chapter AII-§2). Rarefaction and compression waves appearing behind the detonation wave, which move with the speed of sound, do not overtake the front and it propagates without attenuating or becoming stronger.
Although the CJ model of the detonation wave is sufficient to determine

the detonation velocity and the state of the combustion products, many features of detonation waves are connected with the finite rate of chemical reactions. Zeldovich[15,16], Von Neumann[17] and Doering[18], independently from each other, drew attention to the fact that the gas in a detonation wave does not ignite instantaneously. As a consequence, according to this ZND model the detonation wave should consist of a shock wave that compresses and heats the gas followed by a zone of chemical reaction. Thus a detonation wave is a complex consisting of a shock wave and a combustion zone. The pressure distribution in the ZND model is shown schematically in Fig. AII-1b.

The constant part of the profile behind the shock front is determined by the induction period of the inflammation reaction. The drop in pressure depends on the course of the chemical reaction, which is indicated by the wavy line in Fig. AII-1.

The structure of the reaction zone is determined by simultaneously solving the gasdynamical equations of the conservation of mass, momentum and energy and the equations of chemical kinetics. Duff[19] integrated numerically a system of simultaneous kinetic equations with the state point constrained to the Rayleigh line to calculate the reaction zone structure for a $2H_2+O_2+Xe$ detonation at an initial pressure of 30 mm Hg. Experimental measurements of the density profile in the detonation wave had been made by Kistiakowsky and Kydd[20] with an X-ray densitometer. The results of the computations suggested that all of the qualitative features of the detonation profile observed could be explained in terms of a straightforward kinetic mechanism and reasonable rate constants. He found that the largest part of the reaction zone is governed by the induction zone with almost no change in the thermo and gasdynamical variables. Branching chain reactions control this induction zone producing a large amount of free atoms and radicals, while the energy change is small due to the approximate stoichiometry of the chain. The remainder of the profile and almost all of the extremely rapid changes of the variables is governed by the rate of recombination of the large excess of atoms and radicals.

Cook and Keyes[21] and Soloukhin[7] reached similar conclusions for the ZND model. It was found that the duration of the induction period could

be more than 90% of the total chemical reaction time, if the activation energy of the process is sufficiently high (E = 20 to 40 kcal/mole), as is the case for most gaseous detonations.

Therefore the pressure distribution in a detonation wave is often treated under the assumption that after the induction period neither the pressure nor any other variables have changed, and that after its completion the mixture is instantaneously combusted. For this reason the detonation wave may be treated as a so-called double discontinuity[6], i.e. a shock wave followed by a discontinous combustion wave. The elevated pressure part of the detonation wave is called the Von Neumann spike (Fig. AII-1c).

Extensive experimental work has been undertaken to examine the validity of the ZND model. Much of the initial work was done by Kistiakowsky[22] and his coworkers and Manson c.s.[23]. They established that observed detonation wave velocities were within 1% of the equilibrium values based on the CJ hypothesis. It should, however, not be concluded that hence the CJ theory is valid, because the velocity is relatively insensitive to the details of the assumed model. A major difficulty is encountered in any attempt to examine the profile of the front of a plane detonation wave, due to the extreme spatial compression of events. For example, in the detonation of a mixture of hydrogen with oxygen, the period of induction is approximately 1 microsecond at atmospheric pressure[7]. Consequently, techniques with a time resolution of the order of 1 or 2 μs will give an imperfect representation of the detonation wave structure. In spite of this, support for the ZND model was provided by X-ray absorption studies[20,24] and pressure recordings[25,26], which established beyond question the existence of the Von Neumann spike. Moreover, extrapolated values of peak pressures and densities are in reasonable agreement with calculated values behind the shock front. Just and Wagner[27] employed optical techniques to measure the overall thickness of the induction zone. It was later found with refined techniques by Soloukhin[28] in C_2H_2-O_2 mixtures that the observed reaction zone thickness was one order of magnitude larger than expected on the basis of kinetic data.

Jones and Vlases[29,13] measured the pressure arising from the normal reflection of a plane detonation wave at a rigid surface with a modified Baganoff gauge[30]. This gauge has a rise time of 0.05 μs, although the total time of measurement is limited to somewhat less than 2.5 μs. The observed peaks correspond to calculated equilibrium values behind the reflected Von Neumann spike.

Gaydon and Hurle[31], using the spectrum line reversal technique, measured accurately the CJ temperatures of $CO-O_2$ mixtures, which showed to be in agreement with expected values. Soloukhin[28] concluded later that calculated and measured CJ temperatures in subatmospheric $C_2H_2-O_2$ mixtures agreed well. However, within the detonation zone he found temperature peaks in excess of the CJ values.

Up till approximately 1960 the ZND model of the detonation wave has been quite successful in explaining various wave properties. Convincing evidence, however, has been offered in the last decade that the gas flow in the reaction zone is far from one-dimensional and is accompanied by transverse perturbations.

As early as 1926 Campbell and Woodhead[32] discovered spinning detonation, which phenomenon does not fit in the ZND model and which was considered for many years to be an exceptional form of detonation.

It was shown by several Russian investigators (Shchelkin[9] among others) that detonational spin occurs always and in all mixtures near the propagation limits of detonation, by whichever method these limits are obtained: by decreasing the diameter of the tube, by decreasing the initial pressure of the mixture or by changing the concentration of the combustion component. Spin detonation is a non-planar process. Combustion in the form of a nucleus propagates in a forward direction along the tube axis and simultaneously rotates about the tube axis, so that a spiral movement is observed. It was found that spinning detonation consists of a complex triple Mach configuration, behind the fronts of which combustion is initiated. On departing from the limiting mixture composition for the propagation of detonation it was shown that the number of spin nuclei increases and the spin becomes multiple. Eventually, the detonation becomes "normal" and planar.

It turned out that not only spinning detonation, but also "normal" detonation has actually a three-dimensional structure. White[33] took a series of interferograms, from which it appeared that detonation waves were of a turbulent nature, but later distinct transverse waves were found.

The structural stability of the ZND model was then analysed by Shchelkin[34]. He found that, due to the exponential temperature dependence of the induction time, a detonation wave is structurally unstable. It is worthwhile to consider briefly the physical arguments for the instability model proposed by Shchelkin. Consider the "square" wave model of Fig. AII-1c, where it is supposed that after a certain induction period τ_{ind} the gaseous mixture will react instantaneously.

D is the detonation velocity, u_2 is the particle velocity behind the shock front, l is the length of the induction zone ($l = (D-u_2)\tau_{ind}$) and p_1, p_2 and p_3 the undisturbed pressure, the shock pressure and the CJ pressure respectively.

The dependence of the induction time τ_{ind} on temperature T and apparent activation energy E is expressed as

$$\tau_{ind} = A\ e^{E/RT} \qquad\qquad \text{AII-1-1}$$

where R is the gas constant and A a pre-exponential factor, which is assumed to be independent of temperature and pressure.

Consider a sudden small perturbation bcb on the reaction plane JJ as shown in Fig. AII-2 resulting from, for example, a small inhomogeneity
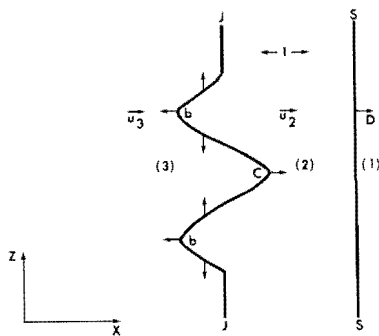
Fig. AII-2 Schematic view of weak perturbation bcb in the induction zone

in the composition of the mixture. Shchelkin assumed that, when the per-
turbation is formed, the pressure at the CJ plane JJ remains at p_3 and
the pressure between the shock front SS and JJ is p_2. The regions bb
will tend to expand along the direction of the plane JJ due to the pres-
sure difference. Rarefaction waves will be generated and propagate into
the regions bb, decreasing the pressure as a result of the expansion,
cooling the reactants and lengthening the induction time τ_{ind} causing
the perturbation to grow in the direction indicated by the arrows. The
burnt products in region c are being compressed as the neighbouring
regions bb expand. The detonation in region c turns out to be "over-
driven" , and the CJ condition is violated at region c. In front of re-
gion c a compression wave starts propagating through the unburnt gas to
the leading SS front. This wave causes still greater adiabatic heating
of the unburnt gas and corresponding shortening of the induction time
τ_{ind}. Eventually the perturbation c approaches the shock front SS.
As a result Shchelkin formulated the following quantitative criterion
for the loss of stability. If a perturbation at the reaction plane
increases the induction time, being the natural time scale for proces-
ses in a detonation wave, by a value approximately equal to, or ex-
ceeding, τ_{ind} the arbitrary initial distortion of the reaction plane
will increase and the wave will loose its stability. If the induction
time increase is small compared to τ_{ind}, the wave will be stable. We
obtain then the instability criterion

$$\frac{d\tau_{ind}}{dT}\Big|_{T_2} (T_2 - T) \geqslant \tau_{ind} \qquad\qquad\qquad \text{AII-1-2}$$

where T and T_2 are the temperatures of the unburnt gas in the perturba-
tion zone after the expansion, and prior to the expansion and behind
the shock front respectively. From AII-1-1 and AII-1-2 we may derive

$$\frac{E}{RT_2} \left(1 - \frac{T}{T_2}\right) \geqslant 1 \qquad\qquad\qquad \text{AII-1-3}$$

At the limit, the adiabatic expansion may have cooled the unburnt gas
to a temperature $T = T_2(p_3/p_2)^b$, where $b = (\gamma-1)/\gamma$.

Therefore, according to Shchelkin, instability sets in when

$$\frac{E}{RT_2} (1 - (\frac{p_3}{p_2})^b) \geqslant 1.$$
                                                                    AII-1-4

Thus, loss of stability should be observed in mixtures with E > 15 to 20
kcal/mole, that is, in practically all known detonating gas mixtures[34].
The question of stability of one-dimensional detonation waves has been
further investigated theoretically by Erpenbeck[35]. The main results
coincide with those of Shchelkin's first approximation analysis.

Perturbations in the reaction zone propagate to the shock front, result-
ing in "overcompressed" and "undercompressed" regions on the plane
detonation front. In the "overcompressed" regions, the induction time
is considerably reduced and ignition occurs at these local hot spots
(ignition centers) prior to the rest of the front. The ignition
centers travel at a velocity somewhat higher than the CJ velocity along
the surface of the shock front in transverse direction. In fact, the
established microscopic features of a detonation front consist of Mach
wave interactions, which move across the front. The front shape of the
detonation wave undergoes periodic changes resulting from the periodic
collisions of these transverse waves and from corresponding pressure
pulsations at the collision loci. Russian investigators call the
structure to be "multiheaded"; in American literature the term "pulsa-
ting" detonation is mainly used.
The shock wave geometry for a multiheaded detonation wave is depicted
schematically in Fig. AII-3 after Soloukhin[28].
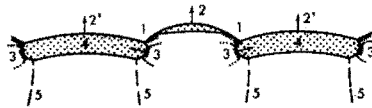
Fig. AII-3 Diagram of multiheaded detonation front; numbers refer to
            text; (5) transverse waves

The gas is continuously burnt in areas (1) immediately behind the over-driven regions of the Mach stem as well as behind the transverse waves (3) after secondary compression. The wave areas like (2) and (2') are the gradually weakened shocks arising from the collisions of two waves (3). The areas (4) between (2') and the reaction plane represent areas of largely unburnt compressed gas.

The triple points (ignition centers) of the Mach waves that run trans-versely across the shock front of the detonation wave have been found to have the property that they will "write" a characteristic cell pattern on a smoked surface. From this it was found by Shchelkin[9] that the average dimensions between two ignition centers are of the order of magnitude of the classical reaction zone thickness. As there are very many of these perturbations on a multiheaded detonation front (the frequency, $D/\Delta z$, where Δz is the linear dimension of a cell written on a smoked surface, amounts to 1 MHz at atmospheric pressure), a mathematical analysis of the overall detonation process seems at present far away. It was attempted, however, by White[33] to make a qualitative analysis. He assumed that the pulsating motion could be considered in the form of isotropic turbulence. Including the pulsation components of velocity, density and pressure in the conservation laws, the final state on the equilibrium Hugoniot will vary in this case and will differ from the one-dimensional state, because part of the thermal energy generated will be transformed into pulsating motion energy. The assumption of isotropic turbulence somewhat clarifies the picture of the effect of pulsating motion on the gas flow; however, this assumption is not true. In fact, behind the shock front it is not a disordered turbulent mixing that exists, but a system of finite waves. Therefore, his analysis is primarily of qualitative interest and may be useful for constructing a more detailed scheme for detonation.

The items discussed in this Chapter clearly illustrate the complex phenomenon of detonative combustion. Despite this complexity the ZND model of a one-dimensional steady detonation wave as a double discontinuity of a shock wave and a combustion wave is still the most useful concept for a quantitative understanding of the behaviour of detonation waves. It should, however, be stressed that an analysis by means of the

ZND model should be confirmed by experiments. A telling example of the application of the ZND model has been obtained in the understanding of the process of one-dimensional initiation of detonation (flame to detonation transition) behind a reflected shock wave in a conventional shock tube[6,8,36]. The gasdynamics of this complicated process has been modelled by Gilbert and Strehlow[37] using the method of characteristics. They assumed that each element of gas reacts with kinetics which are dependent only on the previous temperature- pressure-time history and that the gasdynamics of the process may be modelled in a conventional manner. The results of this analysis agreed very well with experimental observations. We will refer to these models later.

AII-§2 Classical theory of detonation waves

The theory of steady plane one-dimensional detonation waves can be found in some excellent textbooks[15,2]. A short review of the theory has recently been given by this author[38].

From a gasdynamical point of view the ZND model of a steady plane detonation wave consists of a shock wave followed by a combustion wave. The shock wave moves with constant velocity into the undisturbed gas of uniform flow properties (subscript 1, Fig. AII-4). Between the shock wave and the combustion wave there is a region of compressed, yet unreacted gas (induction zone), also of uniform flow properties (subscript 2). For the time being it will be assumed that the flow of combustion products behind the combustion wave (subscript 3) is uniform
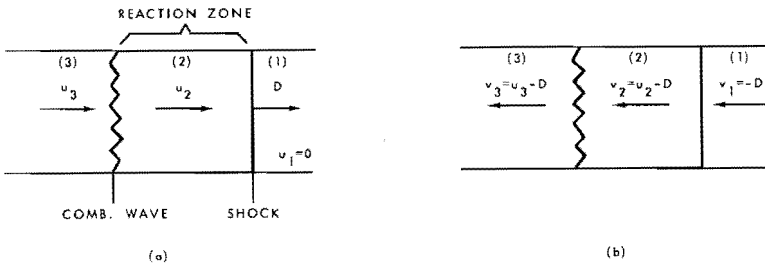
Fig. AII-4   Stationary detonation wave in a tube;
(a) in a laboratory frame of reference;
(b) in a reference frame attached to the shock front

too. In Chapter AII-§4 we will study this flow in some detail.
For the sake of simplicity of the equations it will be assumed that the
gas is a constant gamma gas. The general conclusions will not be effec-
ted by this assumption. A coordinate system is thought to be attached
to the shock front. The following system of equations may then be de-
rived

mass: $\qquad \rho_3 v_3 = \rho_2 v_2 = \rho_1 v_1$ $\hfill$ AII-2-1

momentum: $\quad p_3 + \rho_3 v_3^2 = p_2 + \rho_2 v_2^2 = p_1 + \rho_1 v_1^2$ $\hfill$ AII-2-2

energy: $\qquad e_3 + \dfrac{p_3}{\rho_3} + \tfrac{1}{2} v_3^2 = e_2 + \dfrac{p_2}{\rho_2} + \tfrac{1}{2} v_2^2 + Q_t = e_1 + \dfrac{p_1}{\rho_1} + \tfrac{1}{2} v_1^2 + Q_t$ $\quad$ AII-2-3

where Q_t is the heat of explosion.

We note that the system of equations obtained by taking the equations on
both sides of the second equality sign represent the jump conditions
across a shock wave. We have studied these equations in Chapter AI-§2.
The system obtained by taking the equations on both sides of the first
equality sign represent the transition conditions across the combustion
wave. This system will be discussed separately in Chapter AII-§5.
The system of equations represented by the two outer equations describe
the transition across the complete detonation wave. We will first study
some implications of the latter system.

Combination of the two outer equations of AII-2-1 and AII-2-2 gives an
expression for the detonation velocity D and the particle velocity u_3

$$D^2 = \frac{c_1^2}{\gamma} \ \frac{p_{31}-1}{1-\rho_{13}} \hfill \text{AII-2-4}$$

$$u_3^2 = D^2 \ (1-\rho_{13})^2 = \frac{c_1^2}{\gamma} \ (p_{31}-1) \ (1-\rho_{13}) \hfill \text{AII-2-5}$$

Eq. AII-2-4 is commonly called the equation of a Rayleigh line. In the
ρ_{13}, p_{31}-plane this equation represents a straight line through the
initial and final state points for given initial conditions and D. All
three conservation equations may be combined to give the Hugoniot equa-

tion for complete heat release

$$e_3 - e_1 = Q_t + \frac{1}{2}\frac{c_1^2}{\gamma}(p_{31}+1)(1-\rho_{13}) \qquad \text{AII-2-6}$$

Substituting the equation of state of an ideal gas with constant specific heat ratio, this latter equation may be written in explicit form

$$p_{31} = \frac{\kappa - \rho_{13} + 2\gamma \dfrac{Q_t}{c_1^2}}{\kappa \rho_{13} - 1} \qquad \text{AII-2-7}$$

Differentiating this equation twice shows that in the ρ_{13}, p_{31}-plane the Hugoniot curve for complete heat release has a similar shape as the shock adiabatic, i.e. it is a decreasing function with its convexity facing the negative direction of the axis of coordinates.
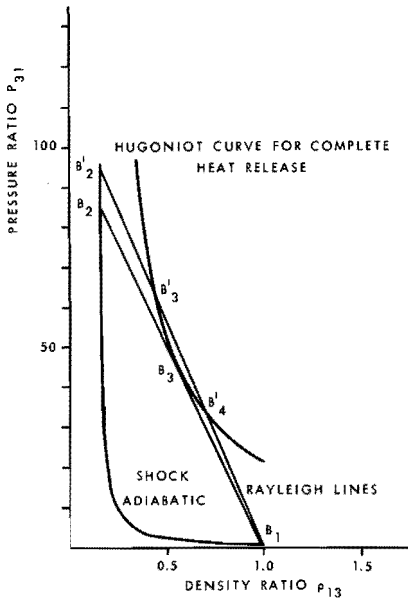
Fig. AII-5 Shock adiabatic, Hugoniot curve and Rayleigh lines computed
for a $C_2H_2 + O_2$ mixture initially at atmospheric pressure

It was found by Jouguet[4] that two branches of the Hugoniot curve with physically possible states may be discerned; one, the upper or detonation branch for which $\rho_{13} < 1$ and the other, the lower or deflagration branch for which $p_{31} < 1$. We will be concerned with the detonation branch. In Fig. AII-5 we have depicted in the ρ_{13},p_{31}-plane the shock adiabatic curve $B_1B_2B_2'$, which passes through the initial state point $(1,1)$, the Hugoniot curve $B_4'B_3B_3'$ for complete heat release and two Rayleigh lines, one of which B_1B_2' intersects the Hugoniot curve in two points B_4' and B_3', while the other B_1B_2 is tangent to this curve. The initial state $(1,1)$ is given by point B_1. The state (2) of the compressed unreacted gas behind the shock wave is given by point B_2 (or B_2') on the shock adiabatic. The final state (3) of the combustion products is given by point B_3 (or B_3') on the Hugoniot curve for complete heat release.

We have calculated these curves for $\gamma = 1.32$ and $Q_t/c_1^2 = 50.23$, which closely resembles a detonation wave in an equimolar acetylene-oxygen mixture with initial conditions $p_1 = 1.0132 \ 10^5$ N/m^2 and $\rho_1 = 1.187$ kg/m^3 (see Appendix III).

It may be clear from the analysis that after the initial jump in pressure and density across the shock wave both pressure and density decrease during the transition to state (3), while the states intermediat between (2) and (3) are all represented by points on a Rayleigh line. The tangent of the slope angle with respect to the abscissa axis of a Rayleigh line, $\tan \alpha$, is written as

$$\tan \alpha = - \frac{p_{31}-1}{1-\rho_{13}} = - \gamma \frac{D^2}{c_1^2} = - \gamma \ Ma_1^2 \qquad \text{AII-2-}$$

where $Ma_1 = D/c_1$ is the Mach number of the detonation wave. It follows that the Rayleigh line which is tangent to the detonation branch corres ponds to the minimum velocity of the detonation wave that may be obtained from all possible velocities allowed by the conservation laws. The tangent of the slope angle with respect to the abscissa axis, $\tan \theta$ of the tangent of the Hugoniot curve is given from AII-2-7 as

$$\tan \theta = \frac{dp_{31}}{d\rho_{13}} = - \frac{1+\kappa p_{31}}{\kappa \rho_{13}-1} \qquad \text{AII-2-}$$

Equating AII-2-9 and AII-2-8 gives the coordinates of point B_3

$$(p_{31})_{B_3} = \frac{1+\gamma Ma_1^2}{\gamma+1} \qquad \text{AII-2-10}$$

$$(\rho_{13})_{B_3} = \frac{1 + \gamma Ma_1^2}{(\gamma+1)Ma_1^2} \qquad \text{AII-2-11}$$

Substitution of the latter two equations into AII-2-7 gives the value of the minimum Mach number that may be obtained

$$Ma_{1min}^2 = (1 + (\gamma^2-1)\frac{Q_t}{c_1^2}) + \{(1 + (\gamma^2-1)\frac{Q_t}{c_1^2})^2 - 1\}^{\frac{1}{2}} \qquad \text{AII-2-12}$$

It will be seen from this equation that the minimum Mach number of detonation is always greater than 1. This is to be expected because of the supersonic velocity of the preceding shock wave. If the total amount of heat released becomes infinitely small the Mach number approaches unity and the detonation wave degenerates into a sound wave.

The equation of an isentropic curve for an ideal gas may be written as

$$p_{31} = \frac{a_1}{\rho_{13}^\gamma} \qquad \text{AII-2-13}$$

where a_1 is a constant.
Differentiating this equation twice shows that this curve in the ρ_{13}, p_{31}-plane has the same general shape as the shock adiabatic and the Hugoniot curve. The tangent of the slope angle with respect to the abscissa axis of the tangent to an isentropic curve is then

$$\tan \phi = \frac{dp_{31}}{d\rho_{13}} = -\gamma \frac{p_{31}}{\rho_{13}} \qquad \text{AII-2-14}$$

At point B_3, upon substitution of the coordinates of point B_3, we obtain

$$(\tan \phi)_{B_3} = -\gamma \frac{(p_{31})_{B_3}}{(\rho_{13})_{B_3}} = -\gamma \, Ma_1^2 \qquad \text{AII-2-15}$$

Comparison with the tangent of the Rayleigh line through point B_3 gives

$$(\tan \alpha)_{B_3} = (\tan \phi)_{B_3} = -\gamma \, Ma_1^2 \qquad\qquad AII-2-16$$

This result means that the Rayleigh line which is tangent to the Hugoniot curve for complete heat release at point B_3 is also tangent to the isentropic curve which passes through this point. It is easy to show that on the detonation branch of the Hugoniot the entropy at point B_3 takes on a minimum value. If, however, we follow the variation in entropy along the line $B_2 B_3$, then the point B_3 corresponds to the maximum value of the entropy on this Rayleigh line. We will give an example of this calculation in Chapter AII-§5.

We may derive one more interesting equation from the equality AII-2-16. Taking into account AII-2-5 we find

$$c_3 = D - u_3 \qquad\qquad AII-2-17$$

which means, that the velocity of the products of combustion with respect to the wave front is equal to the local velocity of sound. A more detailed discussion of the equality is given in Appendix I.
It may also be shown that for an overcompressed or strong detonation (points above B_3 on the detonation branch) we have

$$c_3 > D - u_3 \qquad\qquad AII-2-18$$

and for a weak detonation (points below B_3 on the detonation branch)

$$c_3 < D - u_3 \qquad\qquad AII-2-19$$

If we define the local Mach number $Ma_3 = (D-u_3)/c_3$, we may summarize the latter three equations for the points representing the states of the combustion products on the Hugoniot curve for complete heat release

at B_3 : $Ma_3 = 1$, which corresponds to sonic flow;

above B_3 : $Ma_3 < 1$, which corresponds to subsonic flow;

below B_3 : $Ma_3 > 1$, which corresponds to supersonic flow.

We will not discuss the details of the possibility of the physical realization of all states on the detonation branch here. This subject will be discussed in some detail in Chapter AII-§5. We merely state that the points on the Hugoniot curve below point B_3 are not attainable. The state points above point B_3 may be realized.

It may be clear from the above analysis that the conservation equations supplemented with an equation of state do not allow one to solve the system uniquely. It was postulated by Chapman[14] and Jouguet[4] that most detonations encountered in practice (so-called self-maintaining or unsupported detonations) have a velocity corresponding with sonic flow with respect to the wave front at the final state. Point B_3 is therefore called the CJ point. In fact, if the combustion products do not acquire a velocity greater than the one which corresponds to sonic flow - for example, when the detonation gases are driven by a piston with a velocity greater than the particle velocity at the CJ point -, all detonation velocities are at CJ conditions.

Gasdynamics offers us a simple argument for the observed constancy of unsupported CJ detonations. Suppose the detonation is represented by state point B_3', which has a higher propagation velocity than the CJ velocity of point B_3. Expansion and compression waves caused by small irregularities in the flow of the combustion products travel with the local speed of sound with respect to the gas. They are thus able to catch up with the detonation front causing its velocity to change and an unstationary detonation would result. In particular the rarefaction wave which follows the detonation wave in a closed tube (see Chapter AII-§4) will overtake the front, causing it to slow down. The detonation will then eventually approach the CJ point B_3. Here a stable detonation will result. Waves occurring behind the detonation wave are unable to overtake the wave front and influence its propagation.

AII-§3 Computed and experimental detonation wave properties for $2H_2+O_2$ and $C_2H_2+O_2$ mixtures

Sofar the discussion has been restricted to a constant gamma - constant molecular weight gas. Taking into account the proper changes in thermo-

chemical properties of all species involved in the conversion of reactants to products in the detonation wave, the calculation of the CJ and Von Neumann spike parameters becomes quite complicated and requires a large computer program. Since accurate data on detonation wave parameters are scarce in literature we performed these computations ourselves with the best available thermochemical data known at present for stoichiometric hydrogen-oxygen and equimolar acetylene-oxygen mixtures at several initial pressures. The details of the calculations are given in Appendix I.
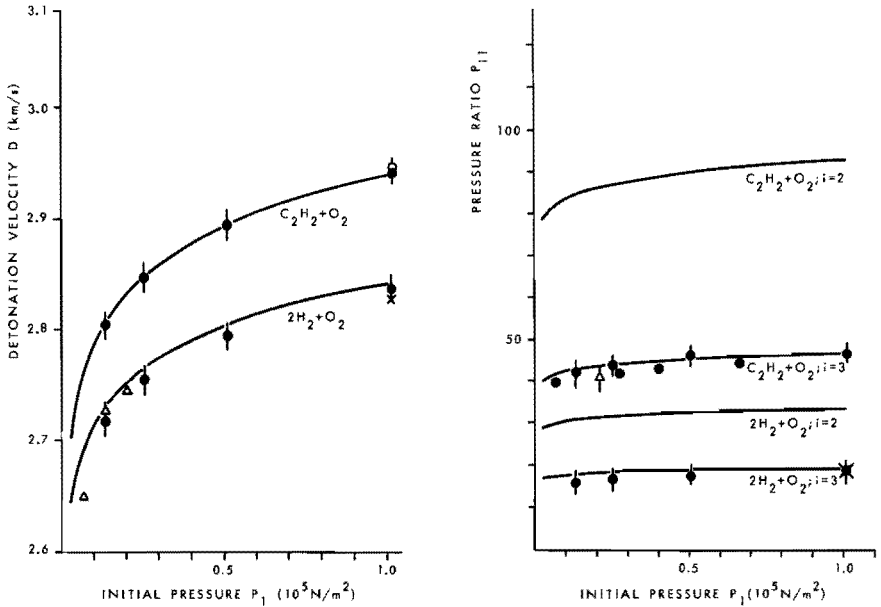
Fig. AII-6 Calculated (——) and measured ($\blacklozenge$) detonation velocities for $C_2H_2+O_2$ and $2H_2+O_2$ mixtures as a function of initial pressure p_1 (see Appendix I and II); experimental values obtained by Ref. 22 (o), Ref. 25 (x) and Ref. 27 ($\triangle$)

Fig. AII-7 Calculated (——) and measured ($\blacklozenge$) CJ (p_{31}) and Von Neumann spike (p_{21}) pressures as a function of initial pressure p_1 for $C_2H_2+O_2$ and $2H_2+O_2$ mixtures (see Appendix I and II); experimental values obtained by Ref. 25 (x), Ref. 43 ($\bullet$) and Ref. 44 ($\triangle$)
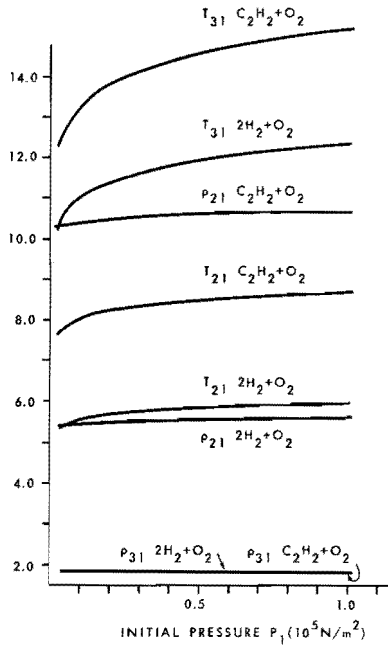
Fig. AII-8 Calculated CJ and Von Neumann spike temperatures and den-
sities as a function of initial pressure p_1 for $C_2H_2+O_2$ and
$2H_2+O_2$ mixtures (see Appendix I)

Results for the aforementioned mixtures are presented in the Tables I-2,
I-4 and I-3, I-5 respectively. The detonation wave velocities calculated
in Appendix I for both mixtures are shown in Fig. AII-6 by solid lines
as a function of initial pressure. We designed a pin-raster-oscilloscope
technique for the measurements of these velocities. The details of this
precise technique are presented in Appendix II. Results of our measure-
ments are given in Fig. AII-6 by the closed circles representing the mean
values and standard deviations. The agreement with theoretical values
is quite favourably especially for the acetylene-oxygen data, which
closely follow the theoretical curve.
Fig. AII-7 gives our calculated CJ and Von Neumann spike pressure ratios
as a function of initial pressure for both mixtures. We constructed a
so-called pressure bar transducer for the measurements of CJ pressures.
The details of this transducer as well as the details of experimenta-

tion are also presented in Appendix II. Results of our measurements
are given in Fig. AII-7 (mean value and standard deviation). They com-
pare quite favourably with the theoretical results. In the same Figure
are also inserted the recently published experimental results of Huni
et al.[43]. They calibrated their pressure transducer in equimolar ace-
tylene-oxygen mixtures. Their calculations, however, are somewhat sim-
plified, so that their results come out to be slightly lower than our
more accurate computations predict. Nevertheless, the trend of their
data follows closely our theoretical curve.

Due to the inadequacy of the gauge response (see Appendix II) to the
Von Neumann spike the measured peak pressures on the records bear no
resemblance to the calculated values. For this reason they have not been
included in the Figures. Finally, Fig. AII-8 summarizes a few results
of our theoretical calculations of temperatures and densities.

In Appendix III we derived some equations that will be used to deter-
mine the CJ parameters for a constant gamma - constant molecular weight
gas.

AII- §4 The Taylor wave

In the laboratory plane one-dimensional detonation waves are usually
obtained from the ignition of a detonable gaseous mixture at the closed
end of a constant area tube (detonation tube). As the combustion pro-
ducts are at rest at this closed end and the combustion products behind
the detonation wave move in a forward direction, there should be a re-
gion of unstationary flow behind the detonation wave. It was shown by
Taylor[39] that the detonation wave borders on a forward facing rarefac-
tion wave (Taylor wave).
The flow in a forward facing rarefaction wave is described by the fol-
lowing equations (see Chapter AI-§1)

$$X = (u+c)t \qquad\qquad\qquad \text{AII-4-1}$$

$$u = u_3 - \frac{2}{\gamma - 1} (c_3 - c) \qquad\qquad \text{AII-4-2}$$

where $X = 0$ at the closed end of the tube.

The detonation velocity, according to the CJ condition, $D = u_3 + c_3$.

Hence the position of the CJ plane is given by

$$X_3 = Dt = (u_3 + c_3)t \qquad\qquad \text{AII-4-3}$$

Substitution of AII-4-1 and AII-4-3 into AII-4-2 gives

$$u = u_3 - \frac{2}{\gamma + 1} (\frac{X_3 - X}{t}) \qquad\qquad \text{AII-4-4}$$

If we neglect the pressure ahead of the detonation front compared with the pressure behind the wave, i.e. $p_3 \gg p_1$, then we obtain from the conservation equations (see Appendix III) $u_3 = c_3/\gamma$. Consequently,

$$\frac{u}{c_3} = \frac{1}{\gamma} (-1 + 2\frac{X}{X_3}) \qquad\qquad \text{AII-4-5}$$

Thus, the velocity of the combustion products decreases linearly with the distance from the CJ plane. When $X = X_3/2$ we have $u = 0$, that is, between this point and the closed end of the tube the combustion products are at rest with respect to the walls of the tube.

The distribution of the pressure is determined analogously

$$\frac{p}{p_3} = (1 - \frac{\gamma - 1}{\gamma} (1 - \frac{X}{X_3}))^{\frac{2\gamma}{\gamma - 1}} \qquad\qquad \text{AII-4-6}$$

We computed the distributions of pressure, density, sound velocity and particle velocity behind a detonation wave in a gas with $\gamma = 1.32$, which closely corresponds to the flow of products of an equimolar acetylene-oxygen mixture (see Fig. AII-9).

The density and pressure distributions of Taylor waves have been experimentally checked by Kistiakowsky and Kydd[20] and Gordon[40] respectively. They found reasonable agreement with theory.
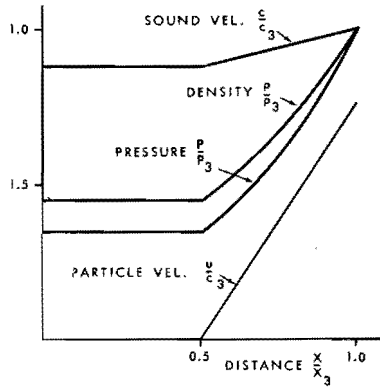
Fig. AII-9 Computed dimensionless sound velocity, density, pressure,
and particle velocity distributions (Taylor wave) along a
detonation tube; $\gamma = 1.32$

It may be noted from AII-4-4 that the particle velocity distribution
- and also the other distributions - is only dependent on the combina-
tion X/t. These motions are called self similar.

AII-§5 The combustion wave

From the point of view of gasdynamics the combustion wave is defined as
that part of the detonation wave where the heat release actually oc-
curs. The reason for considering this part of the detonation wave sepa-
rately as an elementary wave will become clear in what follows. We will
first discuss the relations between the initial and final states of
steady combustion waves. Secondly, we will consider the consequences of
heat release on the motion of the gas in some greater detail.
The initial state for a combustion wave is the state behind a shock
wave (state 2, point B_2 (or point B_2') in Fig. AII-5). It should be kept
in mind that the velocity of the gas behind a shock wave with respect
to this wave is always subsonic, i.e. $Ma_2 = v_2/c_2 < 1$ (see also Chapter
AI-§2). In other words, the velocity of a combustion wave with respect
to its initial state is always subsonic.
The laws of conservation of mass, momentum and energy are given by the

system of equations on both sides of the first equality sign of Eqs.
AII-2-1 through AII-2-3. From these equations we derive the equation
of a

Rayleigh line:
$$v_2^2 = \frac{c_2^2}{\gamma} \frac{1-p_{32}}{\rho_{23}-1}$$
AII-5-1

and
$$v_3^2 = \frac{c_2^2}{\gamma} \rho_{23}^2 \frac{1-p_{32}}{\rho_{23}-1}$$
AII-5-2

and the equation of Hugoniot for complete heat release in explicit form
for the case of an ideal gas with constant specific heat ratio

$$p_{32} = \frac{\kappa - \rho_{23} + 2\gamma\frac{Q_t}{c_2^2}}{\kappa\rho_{23}-1}$$
AII-5-3

Fig. AII-10 shows an example of the Hugoniot curve and two Rayleigh
lines, which we computed for the specific case of $\gamma = 1.32$ and
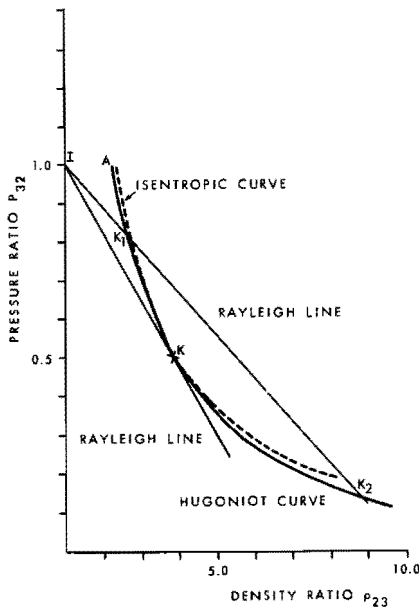
Fig. AII-10   Computed Hugoniot curve, Rayleigh lines and isentropic
curve for a $C_2H_2+O_2$ combustion wave; $\gamma = 1.32$;
$Q_t/c_2^2 = 3.875$

$Q_t/c_2^2 = 3.875$, where the initial conditions are those behind the shock wave represented by state point B_2 (Fig. AII-5).

The tangent of the slope angle with respect to the abscissa axis of a Rayleigh line, which connects the initial state point $(1,1)$ and any point on the Hugoniot curve in the ρ_{23}, p_{32}-plane, is given by

$$\tan \alpha = - \frac{1-p_{32}}{\rho_{23}-1} = - \gamma \frac{v_2^2}{c_2^2} = -\gamma \, Ma_2^2 \qquad\qquad AII-5-4$$

It is seen that $\tan \alpha$ is always negative, which means that in a combustion wave both pressure and density in the final state are lower than in the initial state. The validity of this conclusion is based on the subsonic character of the wave and will become clear in this section. The minimum velocity of the combustion wave with respect to its initial state is formally equal to zero. The state of the products of reaction in this case is given by point A (Fig. AII-10). The coordinates of this point are

$$p_{32} = 1 \quad ; \quad \rho_{23} = 1 + (\gamma-1) \frac{Q_t}{c_2^2} \qquad\qquad AII-5-5$$

More interesting is the maximum velocity of the wave with respect to its initial state. This velocity is determined by the slope of the Rayleigh line IK, which is tangent to the Hugoniot curve at point K. The tangent of the slope angle with respect to the abscissa axis of a tangent to the Hugoniot curve is given by

$$\tan \theta = - \frac{1 + \kappa p_{32}}{\kappa \rho_{23} - 1} \qquad\qquad AII-5-6$$

Equating Eqs. AII-5-4 and AII-5-6 gives the coordinates of point K

$$(p_{32})_K = \frac{1 + \gamma \, Ma_2^2}{1 + \gamma} \qquad\qquad AII-5-7$$

$$(\rho_{23})_K = \frac{1 + \gamma \, Ma_2^2}{(1+\gamma) \, Ma_2^2} \qquad\qquad AII-5-8$$

Substitution of these coordinates into AII-5-3 gives the maximum Mach
number Ma_{2max} that may be obtained

$$Ma^2_{2max} = (1 + (\gamma^2-1) \frac{Q_t}{c_2^2}) - \{(1 + (\gamma^2-1) \frac{Q_t}{c_2^2})^2 - 1\}^{\frac{1}{2}} \qquad AII-5-9$$

It is easily seen from this Equation that the maximum Mach number is al-
ways smaller than one, which should be the case because of the subsonic
character of the wave. It may also be concluded that Ma_2 of all points
on the combustion wave Hugoniot curve is smaller than unity, because,
according to AII-5-4, $Ma_2 < Ma_{2max}$. Fig. AII-11 shows the computed va-
riation of Ma_2 along the Hugoniot curve for our specific case.

We will continue the study of point K. For this purpose we note that the
equation of the isentropic curve is given by

$$p_{32} = \frac{a_1}{p_{23}^\gamma} \qquad AII-5-10$$

The tangent of the slope angle with respect to the abscissa axis of a
tangent to the isentropic curve is written as

$$\tan \phi = - \gamma \frac{p_{32}}{p_{23}} \qquad AII-5-11$$

Substitution of the coordinates of point K into the latter equation gives

$$(\tan \phi)_K = - \gamma Ma_2^2 \qquad AII-5-12$$

Summarizing the above equations we find

$$(\tan \alpha)_K = (\tan \theta)_K = (\tan \phi)_K = - \gamma Ma_2^2 \qquad AII-5-13$$

This result indicates that the Rayleigh line, which is tangent to the
Hugoniot curve for complete heat release at point K, is also tangent to
the isentropic curve which passes through this point. The computed isen-
tropic curve has been drawn in Fig. AII-10.
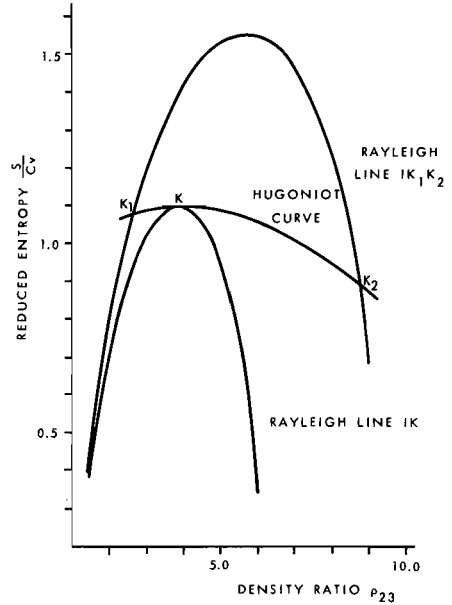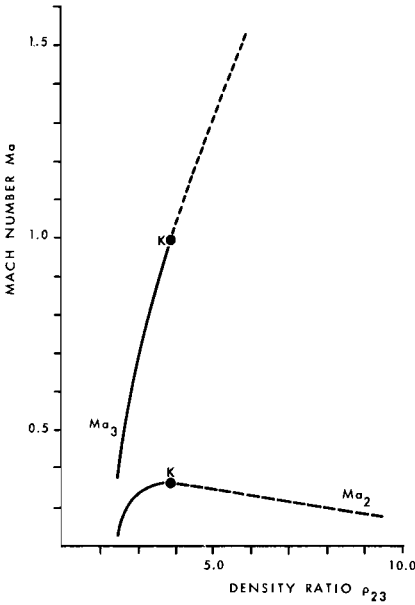
Fig. AII-11 Computed variation of Ma_2 and Ma_3 along the Hugoniot curve
AK_1KK_2 of Fig. AII-10; (——) attainable states; (---)
unattainable states

Fig. AII-12 Computed variation of reduced entropy S/C_v along the
Hugoniot curve AK_1KK_2 and Rayleigh lines IK and IK_1K_2 of
Fig. AII-10

The velocity of sound of the products of combustion c_3 at point K is re-
lated to the slope angle of the tangent of the isentropic curve passing
through this point by the relation

$$\frac{c_3}{(p_2/\rho_2)^{\frac{1}{2}}} = (\gamma p_{32}\rho_{23})^{\frac{1}{2}} = \rho_{23}(-\tan\phi)^{\frac{1}{2}} \qquad\qquad AII-5-14$$

This may be written with the help of Eqs. AII-5-2 and AII-5-4 as

$$\frac{c_3}{(p_2/\rho_2)^{\frac{1}{2}}} = \rho_{23}\frac{1-p_{32}}{\rho_{23}-1} = \frac{v_3}{(p_2/\rho_2)^{\frac{1}{2}}} \qquad\qquad AII-5-15$$
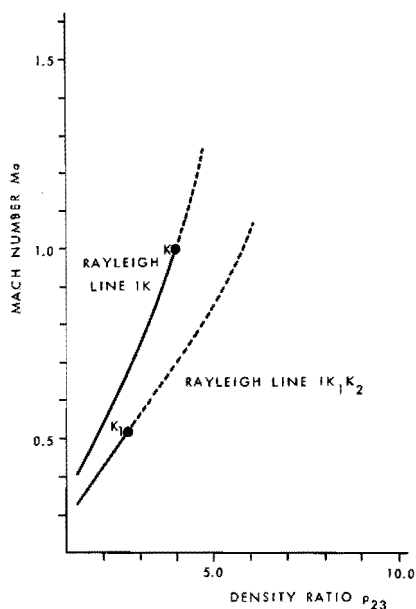
Fig. AII-13 Computed variation of Mach number Ma along the Rayleigh
lines IK and IK_1K_2 of Fig. AII-10
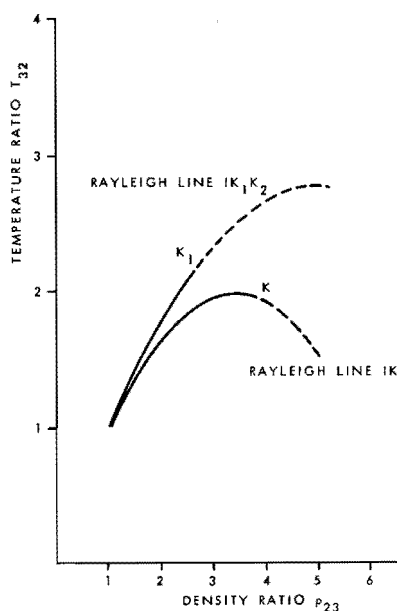
Fig. AII-14 Computed variation of temperature ratio T_{32} along the
Rayleigh lines IK and IK_1K_2 of Fig. AII-10

From this we obtain the result $v_3 = c_3$, which means that at point K the
flow of the products of combustion is sonic in the coordinate system
which is attached to the front of the combustion wave.

We will now show that the entropy at point K on the Hugoniot curve of
complete heat release takes on a maximum value. For this purpose we re-
write the equation for the conservation of momentum as

$$1 + \gamma \, Ma_2^2 = p_{32} + \gamma \rho_{23} \, Ma_2^2 \qquad\qquad AII-5-16$$

By differentiating this expression with respect to the variables and
taking the initial state as constant, we have

$$dp_{32} + \gamma \, Ma_2^2 d\rho_{23} = \gamma \, (1 - \rho_{23}) \, d \, (Ma_2^2) \qquad\qquad AII-5-17$$

Similarly, we rewrite and differentiate the law of conservation of energy

$$\frac{1}{c_2^2} \, dH_3 + \rho_{23}Ma_2^2 d\rho_{23} = \tfrac{1}{2}(1 - \rho_{23}^2) \, d \, (Ma_2^2) \qquad\qquad \text{AII-5-18}$$

The first law of thermodynamics may be written as

$$dH_3 = T_3 dS_3 + \frac{1}{\rho_3} \, dp_3 \qquad\qquad \text{AII-5-19}$$

Eliminating dH_3 from Eqs. AII-5-18 and AII-5-19 gives

$$dp_{32} + \gamma Ma_2^2 d\rho_{23} = \frac{1-\rho_{23}^2}{2\rho_{23}} \, \gamma d \, (Ma_2^2) - \frac{\gamma T_3}{c_2^2 \rho_{23}} \, dS_3 \qquad\qquad \text{AII-5-20}$$

Comparison of AII-5-17 and the latter expression leads to

$$\frac{dS_3}{d(Ma_2^2)} = \frac{c_2^2}{2T_3} \, (1 - \rho_{23})^2 > 0 \qquad\qquad \text{AII-5-21}$$

We have shown that with increasing Mach number Ma_2 the entropy along the Hugoniot curve increases too. We have seen already that at point K the Mach number Ma_2 reaches its maximum value, and so does the entropy. Consequently, all points of the Hugoniot curve, except for point K, are situated below the isentropic curve which passes through K (Fig. AII-10). The isentropic curves, which pass below the point K, intersect the Hugoniot curve twice, once in a point above K and once in a point below K.

Except for a constant the entropy may be written as

$$\frac{S_3}{C_v} = \ln \, (p_{32}\rho_{23}^\gamma) \qquad\qquad \text{AII-5-22}$$

The computed entropy variation along the Hugoniot curve is shown in Fig. AII-12.
From the above considerations it may be clear that the tangent of the

slope angle of a Rayleigh line, tan α, is always larger than the tangent
of the slope angle of the tangent to an isentropic curve, tan φ, for
any point on the Hugoniot curve above point K.

Rewriting AII-5-4 in terms of the Mach number $Ma_3 = v_3/c_3$ of the pro-
ducts of combustion,

$$\tan \alpha = - \gamma \, Ma_3^2 \, \frac{p_{32}}{\rho_{23}} \qquad\qquad \text{AII-5-23}$$

and with AII-5-11 we derive for the points on the Hugoniot curve above K

$$\tan \phi = - \gamma \, \frac{p_{32}}{\rho_{23}} < - \gamma \, Ma_3^2 \, \frac{p_{32}}{\rho_{23}}$$

or, above point K on the Hugoniot curve for complete heat release
$Ma_3 < 1$. Consequently, the flow of the products of combustion with final
states represented by points above point K on the Hugoniot curve is sub-
sonic. Similarly, we may prove that the flow of the combustion products
for the points situated below point K is supersonic, or $Ma_3 > 1$.

Sofar we have not looked into the problem of the realization of the
states that are represented by the Hugoniot curve. We will demonstrate
that the only states that are physically possible are represented by
the points on the Hugoniot curve above point K (branch AK of the curve).
In fact, the states represented by the points below K, e.g. K_2, are
thermodynamically impossible even though they do not contradict the laws
of conservation.

To illustrate this we have computed the entropy along the Rayleigh line
IK_1K_2 (Fig. AII-12). We will see that the entropy at point K_2 is smaller
than at point K_1. During the transition of the gas through the combustion
wave, the state points are given by points on the Rayleigh line from
I to K_1, where at K_1 combustion is completed. After complete heat release
a transition from point K_1 to K_2 would be accompanied by a decrease in
entropy. Such a process would contradict the second law of thermodyna-
mics.

We will now pay some attention to the variation of the flow variables
along a Rayleigh line. In the combustion wave, where the heat releas-

ing reactions do actually take place, the thermo and hydrodynamic va-
riables change continuously from their initial to their final values. We
will represent the course of the chemical reactions by a reaction coor-
dinate β. Let β represent the fraction of heat released at any position
within the combustion wave, so that $(1-\beta)$ represents the unreleased
fraction. Then $\beta = 0$ at the combustion wave front and $\beta = 1$ at the point
of completed combustion. A space coordinate ξ is defined with the value
$\xi = 0$ at the wave front, and the value $\xi = \xi_3 > 0$ at the point where
$\beta = 1$.

For the intermediate states of partial heat release along a Rayleigh line
$(0 \leqslant \xi \leqslant \xi_3)$ we may derive the following laws of conservation.

mass: $\qquad \rho v = \rho_2 v_2$ $\hfill$ AII-5-24

momentum: $\quad p + \rho v^2 = p_2 + \rho_2 v_2^2$ $\hfill$ AII-5-25

energy: $\quad H + \tfrac{1}{2} v^2 = H_2 + \tfrac{1}{2} v_2^2 + \beta Q_t$ $\hfill$ AII-5-26

where the unsubscripted variables refer to intermediate states on a Ray-
leigh line. All variables are functions of ξ only, i.e. $f = f(\xi)$ and
$df = (df/d\xi)d\xi$.

After rewriting these equations somewhat, and taking the total differ-
entials we obtain

$$\frac{dp}{p} + \gamma \, Ma^2 \, \frac{dv}{v} = 0 \qquad\qquad \text{AII-5-27}$$

$$\frac{d\rho}{\rho} + \frac{dv}{v} = 0 \qquad\qquad \text{AII-5-28}$$

$$(\gamma-1) \, Ma^2 \, \frac{dv}{v} + \frac{dT}{T} = \frac{Q_t}{c_p T} \, d\beta \qquad\qquad \text{AII-5-29}$$

$$-\frac{dp}{p} + \frac{dT}{T} + \frac{d\rho}{\rho} = 0 \qquad\qquad \text{AII-5-30}$$

The latter equation is the total differential of the equation of state.
Following Hicks' notation[41] we introduce the quantity N, where

$$N = Ma^2 = \frac{mv^2}{\gamma RT} \qquad\qquad \text{AII-5-31}$$

Differentiation of this expression leads to the useful equation

$$\frac{dv}{v} = \frac{1}{2} \left(\frac{dN}{N} + \frac{dT}{T}\right) \qquad \text{AII-5-32}$$

Elimination of $d\rho/\rho$ and substitution of AII-5-32 into AII-5-27 through AII-5-30 gives the system of equations

$$\frac{\gamma-1}{2} N \frac{dN}{N} + \left(\frac{1}{2}(\gamma-1) N + 1\right) \frac{dT}{T} = \frac{Q_t d\beta}{C_p T} \qquad \text{AII-5-33}$$

$$\frac{1}{2} \frac{dN}{N} - \frac{1}{2} \frac{dT}{T} + \frac{dp}{p} = 0 \qquad \text{AII-5-34}$$

$$\frac{1}{2} \gamma N \frac{dN}{N} + \frac{1}{2} \gamma N \frac{dT}{T} + \frac{dp}{p} = 0 \qquad \text{AII-5-35}$$

These equations can be solved to give the following system of equations

$$\frac{dN}{N} = \frac{1+\gamma N}{1-N} \frac{Q_t d\beta}{C_p T} \qquad \text{AII-5-36}$$

$$\frac{dp}{p} = \frac{-\gamma N}{1-N} \frac{Q_t d\beta}{C_p T} \qquad \text{AII-5-37}$$

$$\frac{dT}{T} = \frac{1-\gamma N}{1-N} \frac{Q_t d\beta}{C_p T} \qquad \text{AII-5-38}$$

$$\frac{d\rho}{\rho} = \frac{-1}{1-N} \frac{Q_t d\beta}{C_p T} \qquad \text{AII-5-39}$$

$$\frac{dv}{v} = \frac{1}{1-N} \frac{Q_t d\beta}{C_p T} \qquad \text{AII-5-40}$$

While the second law of thermodynamics states

$$dS \geqslant \frac{Q_t d\beta}{T} \qquad \text{AII-5-41}$$

The following general conclusions may be drawn. With increasing ξ and hence positive $d\beta > 0$, while $Ma < 1$, the Mach number Ma of the gas increases, the pressure decreases, the density decreases, the velocity with respect to the wave front increases and the entropy increases. The

temperature will increase until $Ma = (1/\gamma)^{\frac{1}{2}}$ and thereafter decreases.
This is caused by the effect that the temperature increase at the front
part of the wave due to heat release is compensated for by the expansion
(cooling) of the gas.

Without taking into account a proper law of heat release, we were thus
able to draw some general conclusions as to the variation of the thermo
and gasdynamic variables along a Rayleigh line. The variations of pres-
sure, entropy, Mach number and temperature as functions of the density
which we computed for the specific case of $\gamma = 1.32$ and $Q_t/c_2^2 = 3.875$
are shown in Figs. AII-10 to AII-14.

It may be noted that the above analysis, from a mathematical point of
view, runs somewhat along the lines of an analysis of a deflagration
wave[6]. It should be stressed again that the mechanism of heat release
and propagation of a deflagration wave is governed by heat conductivi-
ty and diffusion of particles. In a combustion wave, as defined here,
the mechanism of heat release is controlled by the gas which reacts
with kinetics, which are dependent only on the previous thermodynamic
history of the gas particles, without transport effects.

AII-§6 Discussion

In the foregoing we have analysed the properties of one-dimensional de-
tonation waves. Although it is generally recognized that the structure
of the reaction zone is governed by an essentially non-laminar flow
process, our accurate thermochemical calculations of the CJ propagation
velocities and pressures for $2H_2+O_2$ and $C_2H_2+O_2$ mixtures compare quite
favourably with values obtained from our precision measurements in the
range of initial pressures considered.

From a gasdynamics point of view the ZND model of a detonation wave may
be considered to consist of two elementary waves, i.e. a shock wave,
which compresses and heats the gas, and a combustion wave, in which the
heat release due to the conversion of reactants to products actually
occurs. We developed the theory of the combustion wave to some extent
for a constant gamma - constant molecular weight gas.

PART B - WAVE INTERACTIONS

This part is devoted to the study of interactions of elementary waves,
i.e. shock, rarefaction and combustion waves. In Chapter BI the method
of analysis is discussed. The p,u-plane turns out to be a convenient
means for solving interaction problems. In Chapter BII the head-on
collision of a combustion wave with a shock wave, and with a rarefac-
tion wave is studied.

Chapter BI - Method of analysis of elementary waves in the p,u-plane

In many cases of major interest a gas moves initially in elementary
waves, i.e. the non-isentropic shock and combustion waves and the isen-
tropic rarefaction and compression waves.
In addition, a contact discontinuity may be present. Ideally, it is
represented as a discontinuity in temperature, density and entropy.
That is, it is a surface separating two thermodynamically different
states, which are moving at the same flow velocity and pressure. In a
real gas, heat conductivity and diffusivity provide a continuous tran-
sition for the changing flow properties.
If the beginning of the flow consists of elementary waves separated by
uniform flow regions, a fairly complete analysis of the subsequent
phases of motion characterized by the interaction of initially elemen-
tary waves can be achieved. Such waves can be reflected, meet or over-
take one another, so that by interaction a more general state of motion
results.

The interaction of elementary waves in one-dimensional non-reactive
flow, i.e. with the exclusion of our concept of a combustion wave, has
been the subject of many theoretical and experimental investigations.
Courant and Friedrichs[1] published a general analysis of one-dimensional
interactions of shock waves, rarefaction waves and contact surfaces.
They were able to predict the results of interactions of simple waves
for the case of ideal gases by means of an algebraic discussion of the
transition relations for shock and rarefaction waves with the help of
a graphical representation in the p,u-plane.

The Institute of Aerophysics of the University of Toronto has published
a number of UTIA-reports, where these interactions in non-reactive flow
have been exhaustively investigated. Most of the reports are summarized
in Ref. 45. These studies have been concerned with elementary interac-
tions, between two waves colliding, or one wave overtaking another, or
one wave meeting a contact surface.

As the ultimate outcome of such interactions we can, in general, expect
two waves propagating in opposite directions away from the place of
interaction and separated by regions of uniform flow. There are two
such regions, divided by a contact discontinuity separating the two
gases that were initially located on the opposite sides of the place
of interaction.

It may be clear from the following reasoning that after an interaction
only one wave can move in one direction[3]. If two waves were moving in
the same direction, they will always overtake one another after a cer-
tain time; a shock wave will overtake a rarefaction wave; a rarefaction
wave will overtake a shock wave and two shock waves will always over-
take. However, as both waves originate from the same place of interac-
tion, they act as if they had already overtaken one another at the
initial time, and both propagate as a single wave. Therefore it is im-
possible for a second wave to follow the first.

In interactions not involving rarefaction waves, a reflected and trans-
mitted wave always emerge immediately after the collision. Interactions
with rarefaction waves involved, however, lead at first to a period of
penetration. The waves emerging from the zone of penetration are elemen-
tary waves separated by uniform flow regions. In general, from these
interactions, a contact region results, where gradual changes in temp-
erature, density and entropy occur. Pressure and particle velocity are
equal throughout the contact region.

The descriptions in the p,u-plane refer only to uniform terminal states.
Contact discontinuities or regions do not appear in the analysis. Their
existence has to be concluded from entropy considerations.

With the introduction of the combustion wave as an elementary wave,
the number of possible interactions between elementary waves increases

considerably. The combustion wave is, in general, a wave of a certain extent, which means that interactions with a combustion wave always involve a region of penetration.

We will show that from an interaction of two waves, one of which is a combustion wave, three waves will emerge: a combustion wave and a reflected and a transmitted (non-reactive) wave.

BI-§1 Shock wave loci in the p,u-plane

We recall the following expressions. A forward facing wave is a wave moving in the direction of larger values of the coordinate X (or to the right) and a backward facing wave is one moving in the direction of smaller values of X (or to the left).

Before proceeding we recall the term mass stream "m" of a shock wave, which is defined as the amount of mass flowing per unit time through the unit area of the wave, i.e. $m = \rho v$, the product of particle velocity with respect to the wave and density. From Eq. AI-2-1 it is seen that $m = \rho_1 v_1 = \rho_2 v_2$, which means that the mass stream through a steady shock wave is constant.

If a state (1) of a gas and another state (2) are connected through a shock wave, where state (1) or (2) may be either in front of or behind the wave, we may derive from the conservation equations AI-2-1 and AI-2-2

$$\frac{p_2 - p_1}{u_2 - u_1} = -m \qquad\qquad \text{BI-1-1}$$

and

$$\frac{p_2 - p_1}{1/\rho_1 - 1/\rho_2} = m^2 \qquad\qquad \text{BI-1-2}$$

where $u_1 = v_1 + U$ and $u_2 = v_2 + U$ are the particle velocities in a laboratory frame of reference. U is the velocity of the shock wave in the same frame of reference. The significance of BI-1-1 is that the left hand side of the Equation represents the tangent of the slope angle of the straight line in the p,u-plane which connects the state points (1) and (2). Consequently, the steepness of this line represents the absolute value of the mass stream through the shock wave.

Combination of BI-1-1, BI-1-2 and the shock adiabatic equation gives

$$u_2 = u_1 \pm \phi_1 (p_2) \qquad\qquad\qquad BI-1-3$$

where

$$\phi_1(p) = (p-p_1) \left(\frac{2}{\rho_1[(\gamma-1)p_1+(\gamma+1)p]}\right)^{\frac{1}{2}} \qquad\qquad BI-1-4$$

The positive sign applies to forward facing shock waves (this is in-dicated by the symbol "$\vec{S}$"), while the negative sign applies to back-ward facing shock waves ("$\overleftarrow{S}$"). The loci of all states (2) that may be connected with a given state (1) by forward or backward facing shock waves are depicted schematically in Fig. BI-1.

BI-§2 Rarefaction wave loci in the p,u-plane

If a state (1) of a gas and another state (2) are connected through a rarefaction wave, where state (1) or state (2) may be either in front of or behind the wave, we may derive from the constancy of the Riemann invariants across a forward ("$\vec{R}$") or backward ("$\overleftarrow{R}$") facing rarefaction wave

$$u_2 \pm \frac{2c_2}{\gamma-1} = u_1 \pm \frac{2c_1}{\gamma-1} \qquad\qquad\qquad BI-2-1$$

where the top (positive) sign applies to $\overleftarrow{R}$ and the bottom (negative) sign to $\vec{R}$.

From the equation of state for an ideal gas we have

$$\frac{c}{c_1} = \left(\frac{p}{p_1}\right)^{\frac{\gamma-1}{2\gamma}} = \left(\frac{\rho}{\rho_1}\right)^{\frac{\gamma-1}{2}} \qquad\qquad\qquad BI-2-2$$

Substitution of these relations gives the equations for forward (top sign) and backward (bottom sign) facing rarefaction waves in the p,u-plane

$$u_2 = u_1 \pm \psi_1 (p_2) \qquad\qquad\qquad BI-2-3$$

where

$$\psi_1 (p) = \frac{2c_1}{\gamma-1} \left[\left(\frac{p}{p_1}\right)^{\frac{\gamma-1}{2\gamma}} -1\right] \qquad\qquad BI-2-4$$
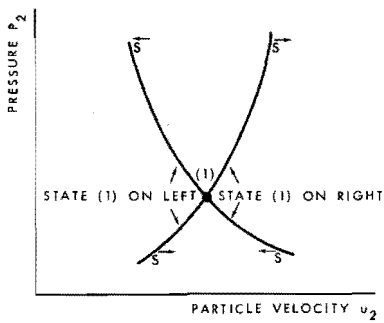
Fig. BI-1   Loci of all states (2) that may be connected with a given
state (1) by a forward or backward facing shock wave
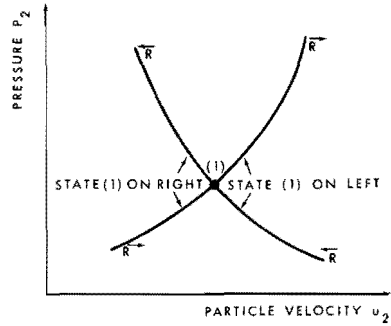
Fig. BI-2   Loci of all states (2) that may be connected with a given
state (1) by a forward or backward facing rarefaction wave
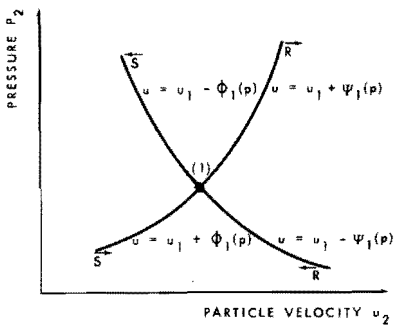
Fig. BI-3   Loci of all states (2) that may be reached from a given
state (1) on the *left* by forward or backward facing waves
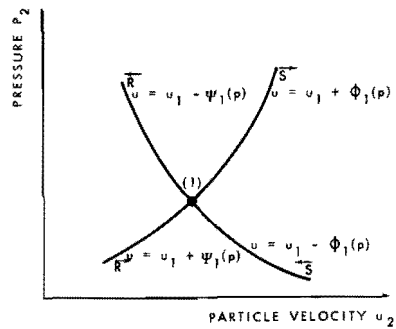
Fig. BI-4   Loci of all states (2) that may be reached from a given
state (1) on the *right* by forward or backward facing waves

The loci of all states (2) that may be connected with a given state (1) by forward or backward facing rarefaction waves are depicted schematically in Fig. BI-2.

Figs. BI-1 and BI-2 may be combined in such a way that one represents all states (2) that may be reached from a given state (1) on the *left* (Fig. BI-3), while the other represents all states (2) that may be reached from a given state (1) on the *right* (Fig. BI-4) by forward or backward facing rarefaction or shock waves.

This combination is justified since at the point of intersection (1) the curves join in a smooth manner. At this point (1) we may derive

$$\phi_1'(p_1) = \psi_1'(p_1) = (\gamma p_1 \rho_1)^{-\frac{1}{2}}$$

and

$$\phi_1''(p_1) = \psi_1''(p_1) = -\frac{\gamma+1}{2} \rho_1^{-\frac{1}{2}} (\gamma p_1)^{-\frac{3}{2}}$$

while $\phi_1'''(p_1) \neq \psi_1'''(p_1)$, although this has little effect at the point of intersection.

BI-§3 The shock tube problem

Suppose that in the plane $X = 0$ of a tube all variables are discontinuous at the initial time $t = 0$, while they are uniform on each side of the discontinuity. For the time being we will assume that the gases are uncapable of heat release.

Such a discontinuity may occur at the instant when a diaphragm which separates two gases at rest, but at different pressures, is removed. It may also occur at the instant when two shock waves collide head-on or overtake one another. As the states and velocities on both sides of the discontinuity will, in general, not satisfy the conservation laws, it cannot propagate as a whole and will break down. We discussed already that we may expect two resulting waves moving away from the original discontinuity in opposite directions, separated by uniform flow regions. As an example we will study the flow in a shock tube.

The shock tube is divided by a thin partition (diaphragm) into two parts. On one side of the diaphragm the tube contains the test gas

(state (1)) at a low pressure and at rest, while on the other side
there is the driver gas (state (4)) at a high pressure and at rest.
In the ideal case we may assume that the diaphragm is removed instan-
taneously, so that the opening time of the diaphragm is infinitely
small. We will also assume that there is no friction with the wall of
the tube and that the gas flow is one-dimensional.
After the diaphragm is removed, the driver gas expands into the direc-
tion of the low pressure section of the tube through a rarefaction
wave, causing a shock wave in the test gas. The two waves are separated
by uniform flow regions on either side of a contact discontinuity se-
parating the two gases that were originally located on the opposite
sides of the diaphragm (states (2) and (3)). The flow resulting from
the removal of the diaphragm is analysed in Fig. BI-5.
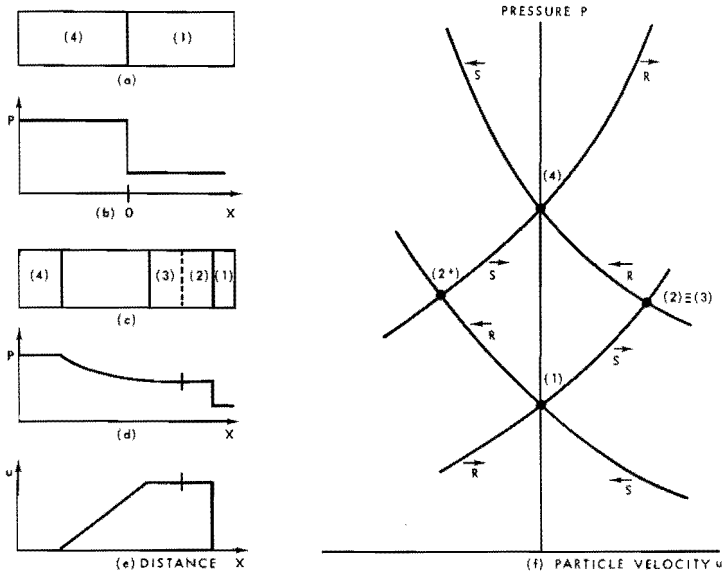
Fig. BI-5 The shock tube problem.
(a) Shock tube, and (b) pressure distribution before dia-
phragm ruptures; (c) shock tube, (d) pressure distribution,
and (e) particle velocity distribution after breaking of
diaphragm; (f) analysis in the p,u-plane

The high pressure section is located on the left, while the low pressure section is situated on the right of the diaphragm. In the p,u-plane we draw through the state points (4) and (1) the loci of Figs. BI-3 and BI-4 respectively. These loci intersect at the points (2) and (2*). State (2*) is impossible, because the two waves are approaching. This would imply a discontinuity at infinity at $t = 0$, and this is contrary to the initial condition that at $t = 0$ the pressure discontinuity is at the origin $X = 0$. The only physically possible solution is that given by state point (2), that is, when the diaphragm ruptures, a shock wave moves into the low pressure section to the right and a rarefaction wave into the high pressure section to the left. A new state (2) is formed, such that $p_4 > p_2 > p_1$ and $u_2 > u_4 = u_1 = 0$. It will be noted that nothing is learned about the formation of a contact discontinuity from this analysis in the p,u-plane, because both pressure and particle velocity across the contact discontinuity are equal. Its existence is deduced from entropy considerations of the shock and rarefaction wave.

BI-§4 Combustion wave loci in the p,u-plane

We will derive the equations for forward and backward facing steady combustion waves that represent the loci of all states that may be connected with a given state in the p,u-plane.

Here, we define the given state (2) as the initial state, i.e. the state of the gas in front of a forward or backward facing combustion wave. State (3) is the final state, i.e. it is located behind the wave. Fig. BI-6 gives schematic representations of the pressure and particle velocity distributions as functions of the position coordinate X for a forward and backward facing combustion wave. As the distribution of the thermo and gasdynamical quantities within the combustion wave is irrelevant for the determination of the terminal states from the initial states, the pressure and particle velocity distributions within the wave have been indicated by a wavy line. The direction of propagation of the wave is shown by an arrow. "l_{cw}" is the (constant) length of the steady combustion wave.
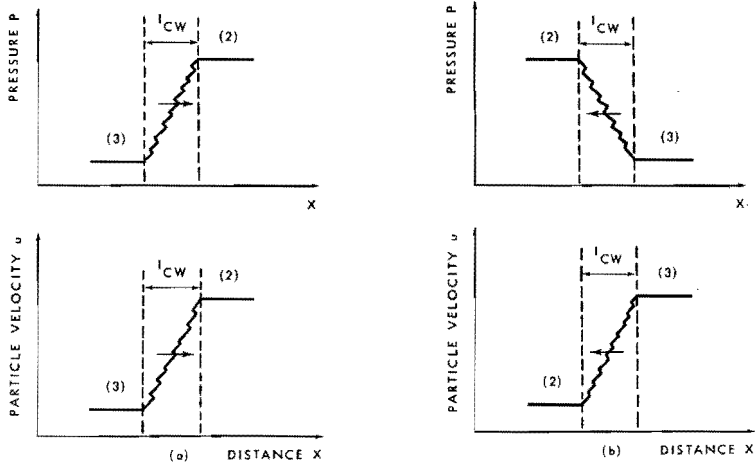
Fig. BI-6   Schematic representation of the pressure and particle velo-
            city distribution for a forward (a) and backward (b) facing
            steady combustion wave

We introduce the symbols $\overrightarrow{CW}$ and $\overleftarrow{CW}$ for a forward and backward facing
combustion wave respectively. Similarly as for the shock wave, we may
speak of the mass stream "m" = ρv of a steady combustion wave, which is
a constant.

From the laws of conservation of mass and momentum (Eqs. on both sides
of the first equality sign of AII-2-1 and AII-2-2) we may derive the
following expressions.

$$\frac{p_3 - p_2}{u_3 - u_2} = -m \qquad\qquad\qquad \text{BI-4-1}$$

and

$$\frac{p_3 - p_2}{1/\rho_2 - 1/\rho_3} = m^2 \qquad\qquad\qquad \text{BI-4-2}$$

where $u_2 = v_2 + U_{CW}$ and $u_3 = v_3 + U_{CW}$ are the particle velocities in a la-
boratory frame of reference. U_{CW} is the velocity of the combustion wave
in the same frame of reference. The significance of BI-4-1 is that the
left hand side of the expression represents the tangent of the slope

angle of the straight line in the p,u-plane which connects the state
points (2) and (3). The steepness of this line represents the absolute
value of the mass stream through the combustion wave.

The Hugoniot equation for complete heat release AII-5-3 may be rewrit-
ten to give ρ_{32} as a function of p_{32}

$$\rho_{32} = \frac{\kappa p_{32} + 1}{p_{32} + 1 + 2\gamma Q_t / c_2^2} \qquad\qquad BI\text{-}4\text{-}3$$

Substitution of BI-4-1 and BI-4-3 into BI-4-2 gives the equations that
represent the loci in the p,u-plane of all states (3) that may be
reached from a given state (2) on the right of a forward facing com-
bustion wave (top sign) and from a given state (2) on the left of a
backward facing combustion wave (bottom sign) respectively.

$$u_3 = u_2 \mp \Omega_2(p_3) \qquad\qquad BI\text{-}4\text{-}4$$

where

$$\Omega_2(p) = \left\{ \frac{2}{\rho_2}(p - p_2) \frac{p - p_2 - \gamma p_2(\gamma-1)Q_t/c_2^2}{(\gamma+1)p + (\gamma-1)p_2} \right\}^{\frac{1}{2}} \qquad BI\text{-}4\text{-}5$$

Unlike the shock and rarefaction loci, these equations do not allow
the interchange of states (2) and (3), i.e. when state (2) would be
defined as the given state behind the combustion wave and state (3)
the state in front of the wave the above equations are not applicable.

We will now discuss some properties of the locus of all states (3) that
may be reached from a given state (2) on the right of a forward facing
combustion wave. A similar discussion may be held for a backward fa-
cing wave.

From the analysis of the properties of combustion waves (Chapter AII-
§5) we may predict qualitatively the general shape of this locus.
For a given state (2) on the right of a forward facing combustion
wave the locus should be a decreasing function ($p_3 < p_2$ and $u_3 < u_2$).
Starting at $Ma_2 = 0$ ($dp/d\Omega_2 = 0$), with increasing Ma_2 the straight line
drawn in the p,u-plane through the initial state point (2) should
intersect the locus in two points, an upper point (3') and a lower

point (3''), such that $p_{3'} > p_{3''}$ and $u_{3'} > u_{3''}$, or, in other words, $Ma_{3'} < 1$ and $Ma_{3''} > 1$. From the discussion in Chapter AII-§5 we know that the upper state point (3') is the only physically possible one. At Ma_{2max} only one state is possible, where $Ma_3 = 1$. Consequently, the line drawn through the initial state point (2) should also be tangent to the locus when $Ma_3 = 1$. Thus, the locus has a point of inflection. As an example, we calculated the combustion wave locus for a specific case ($Q_t/c_2^2 = 3.875$ and $\gamma = 1.32$). The initial state (2) is given by the conditions behind the leading shock wave (Von Neumann spike) of a detonation wave in a $C_2H_2+O_2$ mixture of initial pressure $p_1 = 1.0132$ 10^5 N/m^2 (see also Chapter AII-§2).

Fig. BI-7 shows the calculated combustion wave locus of states (3) that may be obtained from the given state (2). We have also calculated the shock wave locus with the given state (2) on the left of a forward
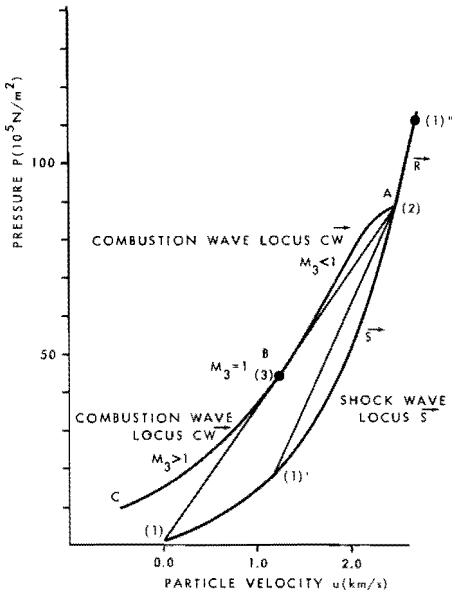
Fig. BI-7   Computed combustion wave locus (ABC) of states (3) that may be reached from a given state (2) in front of a forward facing combustion wave; also the computed forward facing shock and rarefaction wave loci with given state (2) on the left of these waves are given

facing shock wave $\vec{S}$. States (1) and (1') are examples of states on the right (or in front) of the shock waves, that are assumed to run ahead of the combustion wave. Two straight lines have been drawn; one connects states (1) and (2) and is also tangent to the combustion wave locus, and one connects the states (1') and (2). We have seen already that the tangent of the slope angle with respect to the abscissa axis of these lines equals the absolute value m of the mass stream through the shock wave. From Fig. BI-7 we see that the mass stream through the shock wave represented by line 1'-2 (mass stream $|m_{1'-2}|$) is greater than the mass stream $|m_{1-2}|$ through the shock wave represented by line 1-2.

It may be noted that the slope of the line which connects states (2) and (3), which coincides with the line 1-2, also represents the mass stream $|m_{2-3}|$ through the combustion wave.

If a shock wave with velocity U_1 runs ahead of a combustion wave with velocity U_{CW}, so that state (2) is the state of the gas behind the shock wave and ahead of the combustion wave, this means that, if $|m_{2-3}| = \rho_2(U_{CW}-u_2)$ equals $|m_{1-2}| = \rho_2(U_1-u_2)$, both waves run at the same velocity $U_1 = U_{CW}$.

Here, we have found the detonation wave, where, indeed, state (1) represents the initial conditions in front of the $C_2H_2+O_2$ detonation of our example in Chapter AII-§2.

On the other hand, if $|m_{2-3}| = \rho_2(U_{CW}-u_2)$ is smaller than $|m_{1'-2}| = \rho_2(U_1'-u_2)$ and, hence, $U_{CW} < U_1'$, the shock wave "runs away" from the combustion wave. Then an accumulation of mass occurs between the shock wave and the combustion wave in the course of time.

We have also drawn in Fig. BI-7 part of the computed rarefaction wave locus with the given state (2) on the left of a forward facing rarefaction wave. States (1") are possible states on the right (or in front) of the rarefaction wave. If a rarefaction wave runs ahead of a combustion wave, the latter will never be able to overtake the rarefaction wave. In fact, the tail of the rarefaction wave propagates with the velocity of sound with respect to the gas in state (2), while the combustion wave front always has a subsonic velocity with respect to the gas ahead of the wave.

Like in Chapter AII-§2 and §5 we are again faced with the problem of

determination of the final states of the combustion products. We know
already that all states on the branch (2)-(3) ($Ma_3 \leqslant 1$) of the combus-
tion wave locus are physically realizable. As before we may argue that
a steady combustion wave is most likely represented by state point (3),
where $Ma_3 = 1$. Oppenheim[46], studying the development of detonation in
gases, also assumed that this state would be reached. Although this
assumption is reasonable, one should be careful in quantitative calcu-
lations of the distributions of variables within the combustion wave,
where a specific law of heat release is assumed. In applying a parti-
cular law of heat release, which will be discussed later, we found that
Ma_3 depended on this law and could be smaller than unity. It turned
out that this specific law of heat release, which was also used by
Gilbert and Strehlow[37] in their calculations of detonation development,
produced an additional condition for the value of the mass stream
through the combustion wave.

If we assume that the combustion wave has a propagation velocity with
respect to the combustion products equal to the local velocity of sound
in them ($Ma_3 = 1$), this may be expressed with the aid of AII-5-2 as

$$\frac{p_3 - p_2}{1/\rho_2 - 1/\rho_3} = \left(\frac{p_2 - p_3}{u_2 - u_3}\right)^2 = \gamma p_3 \rho_3 \qquad\qquad BI\text{-}4\text{-}6$$

BI-§5 The shock tube problem with combustible gases

We will give a qualitative discussion of the shock tube problem of Chap-
ter BI-§3 with the addition that either the high or low pressure gas
is combustible, which is ignited immediately after removal of the dia-
phragm. We will assume that the amount of heat released as well as the
rate of heat release are given.

Case 1 (Fig. BI-8). The low pressure gas (state (1)) is a combustible
gas, while the high pressure gas (state (4)) is non-combustible. The
initial pressure distribution is given in Fig. BI-8b. Both gases have
a velocity equal to zero. A certain time after removal of the diaphragm
a wave system will have been established (Fig. BI-8c). The high pres-
sure gas has been expanded through a rarefaction wave, which has caused
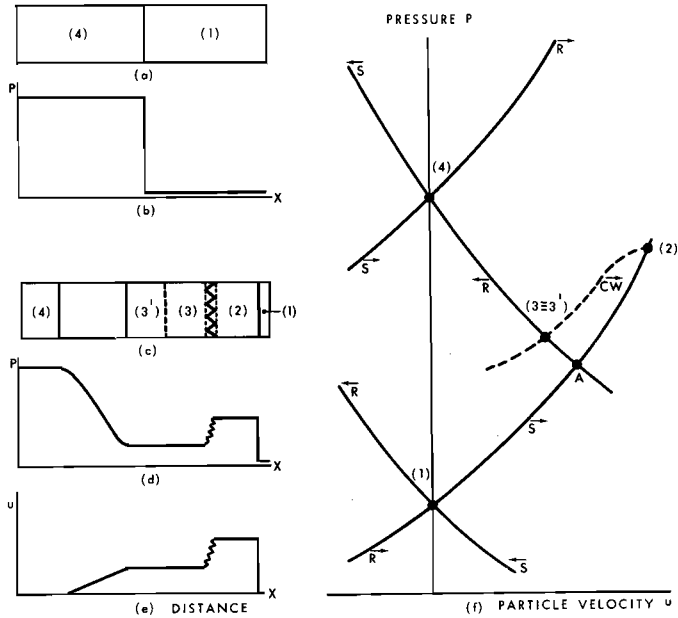
Fig. BI-8 Shock tube problem with combustible gas in low pressure
          section.
          (a) Shock tube, and (b) pressure distribution before dia-
          phragm ruptures; (c) shock tube, (d) pressure, and (e) par-
          ticle velocity distribution after breaking of the diaphragm;
          (f) analysis in the p,u-plane of the resulting waves

a shock wave in the low pressure gas, just as in the case of Fig. BI-5.
Now, the low pressure gas is capable of heat release. Hence, in addi-
tion to the shock and rarefaction wave a combustion wave will originate.
According to the discussion in the previous Chapter the combustion wave
may propagate with the same speed as the shock wave, in which case a
detonation wave has been established. In general, however, depending on
the rate of heat release of the shocked particles the propagation velo-
city of the combustion wave may be lower than the shock wave velocity.
The analysis of the resulting wave system has been given in the p,u-plane
of Fig. BI-8. Without combustion, state point A would have been reached
between the shock and rarefaction wave.
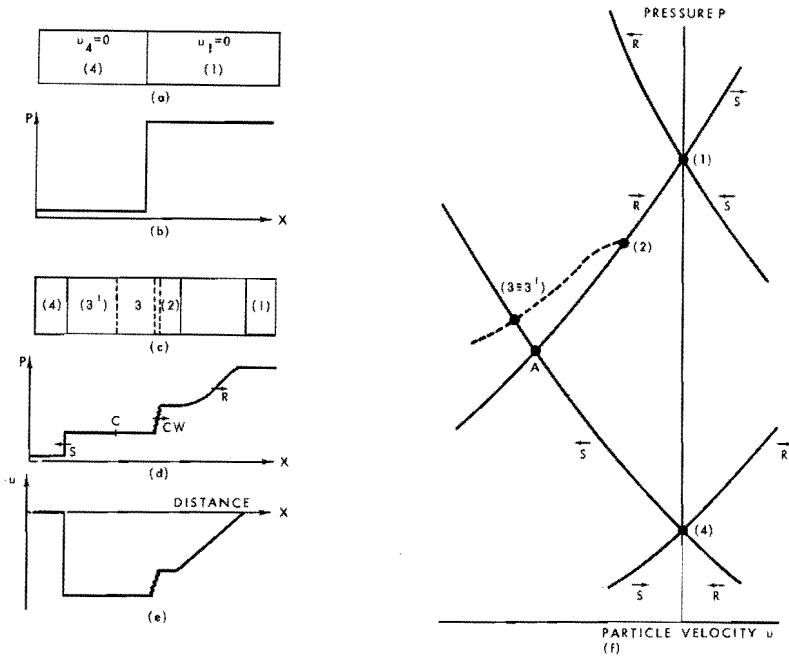
Fig. BI-9 Shock tube problem with combustible gas in high pressure
section.
(a) Shock tube, and (b) pressure distribution before dia-
phragm ruptures; (c) shock tube, (d) pressure, and (e) par-
ticle velocity distribution after breaking of the diaphragm;
(f) analysis in the p,u-plane of the resulting waves

From the $\vec{S}$ locus originating from state point (1) a number of combus-
tion wave loci may be drawn. They will intersect the $\overleftarrow{R}$ locus origina-
ting from state point (4) in a number of points as long as state (2)
is situated on the $\vec{S}$ locus above point A.

The rate of heat release which is determined by the rate of "particle
consumption" in the combustion wave, which is equal to the mass stream
through the wave, determines the slope of the straight line (2)-(3)
and, hence, one specific combustion wave locus. In solving the system
of equations that describe the wave system, which will be done in sub-
sequent sections, we will demonstrate that it has a unique solution.
It will be seen from this analysis that (p_2-p_1) and u_2 are greater

than (p_A-p_1) and u_A respectively. On the other hand, the pressure drop (p_4-p_3) is smaller than the drop (p_4-p_A), which would have resulted without combustion of the low pressure gas. We thus conclude that a stronger shock wave and a weaker rarefaction wave result in the case of combustion of the low pressure gas compared to the case of no combustion.

The pressure and particle velocity distributions at a certain time after removal of the diaphragm are given schematically in Figs. BI-8d and 8e. Like in the case of the shock tube problem of Chapter BI-§3 a contact discontinuity originates which separates the gases that were originally separated by the diaphragm.

Case 2 (Fig. BI-9). The high pressure gas (state (1)) is a combustible gas, while the low pressure gas (state (4)) is non-combustible. The initial pressure distribution is given in Fig. BI-9b. After removal of the diaphragm a wave system originates consisting of a shock wave propagating into the low pressure gas, while the high pressure gas expands through a rarefaction wave. Here, the rarefaction wave is followed by a combustion wave. The analysis in the p,u-plane shows the solution of this shock tube problem. Point A would have been reached without combustion. With combustion a stronger shock and weaker rarefaction wave result.

These case studies are meant to serve as illustration of the effect of the introduction of combustion waves. These shock tube problems, which are somewhat idealized, will not be dealt with any further. Certain features of these problems will, however, be found again in the following Chapter.

Chapter BII - The head-on collision of a combustion wave with a shock
                wave (case 1), and with a rarefaction wave (case 2)

In this Chapter we will demonstrate the validity of two rules that de-
scribe the interaction of two elementary waves, one of which is a com-
bustion wave. In particular, we will restrict the attention to the
study of the head-on collision of a forward facing combustion wave with
a backward facing shock wave, and with a backward facing rarefaction
wave. These two cases will be shown to have important applications in
the field of detonation research.

BII-§1 Qualitative discussion of the collision results

In this section we will give two rules that will be discussed quali-
tatively.

Rule 1. The head-on collision of a backward facing shock wave with a
        forward facing combustion wave will result in a transmitted
        backward facing shock wave and a reflected forward facing
        rarefaction wave.

Rule 2. The head-on collision of a backward facing rarefaction wave
        with a forward facing combustion wave will result in a trans-
        mitted backward facing rarefaction wave and a reflected for-
        ward facing shock wave.

In both cases a forward facing combustion wave follows the reflected
forward facing wave. In addition the interaction results in a contact
discontinuity or region, which is situated behind the combustion wave.
Case 1, which is described by rule 1, is depicted schematically in Fig.
BII-1. Fig. BII-1a gives the pressure and particle velocity distribu-
tions as functions of the distance coordinate X before the interaction.
In front of both waves we find state (0), while behind the shock wave
and combustion wave we find states (1) and (4) respectively. Fig. BII-1b
gives the pressure and particle velocity distributions as functions of
X after the interaction has been completed and uniform states between
the waves have been established. State (2) is the state between the two
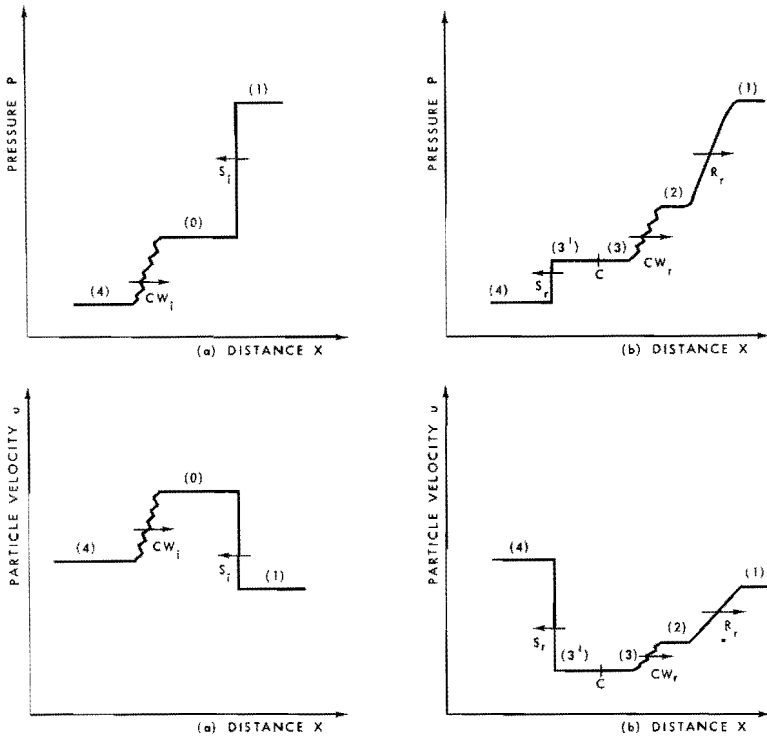
Fig. BII-1   Case 1: head-on collision of a backward facing shock wave
            and a forward facing combustion wave (not to scale);
            (a) X,p- and X,u-plane before the interaction;
            (b) X,p- and X,u-plane after the interaction;
            "C" denotes the position of the contact region

forward facing waves. State (3) is the state behind the combustion wave
and in front of the contact region, while state (3') is the state behind
the backward facing transmitted shock wave.

Case 2, which is described by rule 2, is shown schematically in Fig.
BII-2. The situation before the interaction is depicted in Fig. BII-2a
in the X,p-plane and the X,u-plane, while the situation after the in-
teraction is shown schematically in Fig. BII-2b.

From physical reasoning one may gain some insight in the correctness of
these rules. First we denote the formal similarity of case 1 and 2 with
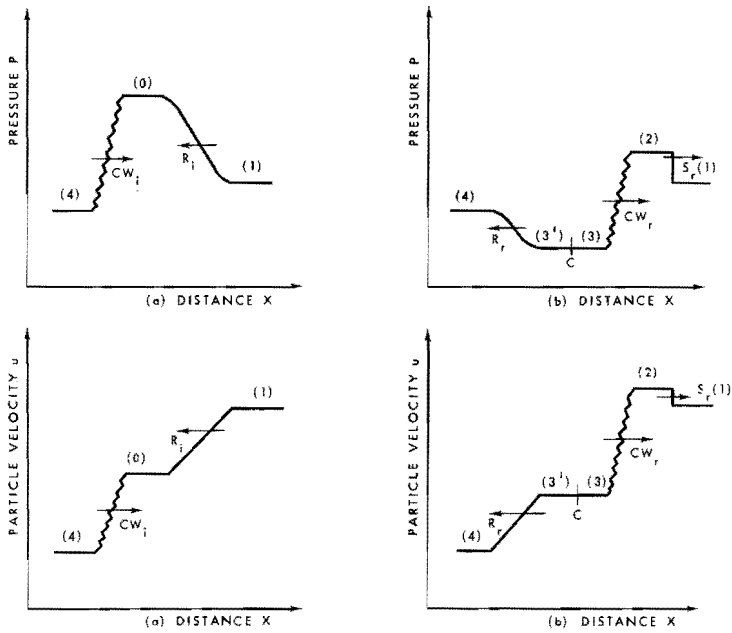
Fig. BII-2 Case 2: head-on collision of a backward facing rarefaction
wave and a forward facing combustion wave (not to scale);
(a) X,p- and X,u-plane before the interaction;
(b) X,p- and X,u-plane after the interaction;
"C" denotes the position of the contact region

the shock tube problems with combustible gases of Fig. BI-9 and Fig.
BI-8 respectively. In both cases the terminal states are similar to
those of the shock tube problems. In fact, the same arguments for the
origin of the waves employed in these problems can be applied here. At
the instant of interaction of the shock wave or rarefaction wave - to
be completely correct we should say: during the short time that the
waves penetrate into each other, due to the finite extent of both com-
bustion and rarefaction waves - with the combustion wave, the cases 1
and 2 show distributions of pressure and particle velocity similar to
those before the removal of the diaphragm in a shock tube.
In other words, in a forward facing combustion wave the particles gra-
dually release heat, accompanied by a pressure drop and acceleration

of the particles in backward direction or away from the wave. A back-
ward facing shock wave running into the direction of the combustion
wave accelerates the particles backwards too. It is quite clear that a
shock wave of some strength will be transmitted through the combustion
wave, due to the pressure difference between states (1) and (4). This
transmitted wave causes a further acceleration of the combusted parti-
cles in backward direction. This implies that the mass stream behind
the combustion wave is increased by the presence of the backward running
shock wave. In order to compensate this increased mass stream the un-
burnt particles ahead of the combustion wave should be accelerated in
backward direction too, in order to "supply" the combustion wave with
"fresh" particles and to satisfy the constancy of the mass stream
through the combustion wave. This is accomplished by the reflected for-
ward facing rarefaction wave.

Analogous reasoning may be held for case 2, where the transmitted rare-
faction wave causes a deceleration of the combusted particles. A re-
flected forward facing shock wave adjusts the mass stream through the
combustion wave by accelerating the particles in forward direction.
To be completely correct, we should replace the term "shock wave" in
the above paragraph by the term "compression wave" where we discussed
case 2. However, as a compression wave will eventually steepen into
a shock wave, we will refer to this final state, where the shock wave
has been formed.

The two rules obtain, moreover, support from the side of acoustical
gasdynamics theory. In the acoustics approximation the pressure differ-
ence across shock, rarefaction and combustion waves becomes infinites-
imally small. The latter wave is then identical to a flame, which pro-
pagates by heat conduction and diffusion. However, from Chapter AII-§5
it may be clear that the mechanism of combustion wave propagation is
unimportant for the determination of the terminal states from a gas-
dynamics point of view. Thanks to the linearity of the relevant equa-
tions Boa-Teh Chu[47] was able to prove the rules 1 and 2 analytically.
His analysis for a compression (expansion) wave in a head-on collision
with a flame front showed that it is transmitted as a weaker compression

(expansion) wave and reflected as a weak expansion (compression) wave. From our calculations we will find that the transmitted finite shock (rarefaction) waves are also of smaller strength than the incident waves. Due to the nonlinear character of the equations that represent finite shock, rarefaction and combustion waves the system of equations that describe the interaction results, cannot be solved analytically. In order to demonstrate the correctness of the rules qualitatively we will call on the schematic description of the interaction in the p,u-plane. Quantitative solutions of the equations will be treated in the following chapters.

BII-§2 Analysis of case 1

We will first analyse case 1 in the p,u-plane. Referring to Fig. BII-la, before the interaction the states (1) and (4) behind the shock wave and behind the combustion wave respectively are connected with a common state (0) in front of both waves. Fig. BII-3 gives an example of the possible locations of these states in the p,u-plane. It may be clear that, for the interaction described by rule 1, always $p_1 > p_0 > p_4$ and u_4, $u_1 < u_0$, which more or less dictates the positions of the state points in the p,u-plane relative to each other. Although it is not essential for the following discussion, we will assume that the Mach
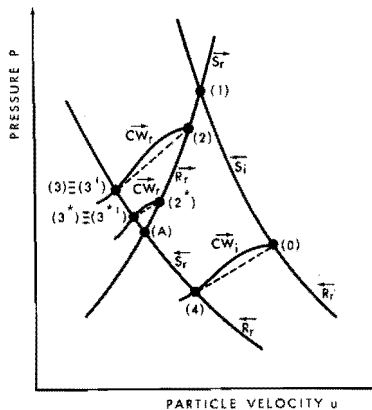
Fig. BII-3 Schematic representation of the case 1 interaction process in the p,u-plane

number $Ma_4 = 1$, which means that we have CJ conditions behind the com-
bustion wave. The slope of the straight line through the original state
points (O) and (4) represents the absolute value of the mass stream
through the combustion wave, which is a maximum when $Ma_4 = 1$. After
the interaction has been completed, state (1) will be on the right of
a forward facing wave, while state (4) will be on the left of a back-
ward facing wave. The corresponding loci in the p,u-plane have been
drawn through these state points. If combustion would be absent after
the interaction, point A would be the terminal state between a back-
ward facing shock wave and a forward facing rarefaction wave. In the
presence of combustion there must also be a forward facing combustion
wave after the interaction. In this case some state point between (1)
and (A), e.g. (2) or (2*), on the $\vec{R}_r$ locus through (1) should be con-
nected via a combustion wave locus $\vec{CW}_r$ with some state point, e.g.
(3) or (3*), on the $\overleftarrow{S}_r$ locus through (4) in order to give a unique
solution for the resulting wave system after the interaction.
We have drawn two of all possible combustion wave loci from (2) and
(2*) respectively. These loci intersect the $\overleftarrow{S}_r$ locus through (4) in
the state points (3) and (3*) respectively. The tangents of the slope
angles of the straight lines (2)-(3) and (2*)-(3*) correspond to the
absolute values of the mass streams through these respective combus-
tion waves. From our quantitative calculations (see Chapter BII-§3)
it turns out that points (2*) below some point (2) on the $\vec{R}_r$ locus
correspond to smaller values of the respective mass streams. Conse-
quently, the straight lines that connect terminal states across the
combustion wave have smaller slopes as points (2) are situated lower
on the $\vec{R}_r$ locus.
If we postulate that the combustion wave which originates from the
interaction travels at CJ velocity relative to its combustion products
($Ma_3 = 1$), which corresponds to maximum mass stream through the wave,
one and only one combustion wave locus can be selected from all possible
loci. We may construct this solution by finding that particular combus-
tion wave locus, where the point of tangency of the straight line
(2)-(3) with the combustion wave locus coincides with the intersection
point of this locus with the $\overleftarrow{S}_r$ locus through point (4).

In Part C we will apply a specific law of heat release, which implies that the mass streams through the combustion waves before and after the interaction are equal. In the p,u-plane this means that we should find that particular combustion wave locus where the slopes of the straight lines through the terminal state points of the $\overrightarrow{CW}$ loci before and after the interaction are equal (e.g. (2*)-(3*)). Here too, a unique solution can be obtained.

We will now give the system of equations that should be solved to obtain a quantitative solution of the problem of the head-on collision of a backward facing shock wave with a forward facing combustion wave.

Case 1: states (1) and (4) are given (see Fig. BII-1)

Rarefaction wave:

$$u_2 = u_1 + \psi_1(p_2)$$

where

$$\psi_1(p_2) = \frac{2c_1}{\gamma-1} \left[\left(\frac{p_2}{p_1}\right)^{\frac{\gamma-1}{2\gamma}} - 1 \right] \qquad\qquad \text{BII-2-1}$$

Combustion wave:

$$u_3 = u_2 - \Omega_2(p_3)$$

where

$$\Omega_2(p_3) = \left\{ \frac{2}{\rho_2} (p_3-p_2) \frac{p_3-p_2-\gamma p_2 (\gamma-1)Q_t/c_2^2}{(\gamma+1)p_3 + (\gamma-1)p_2} \right\}^{\frac{1}{2}} \qquad\qquad \text{BII-2-2}$$

Here, $\rho_2 = \rho_2(p_2)$ and $c_2 = c_2(p_2)$ are given by BI-2-2 to be functions of p_2 and the known state parameters p_1, ρ_1.

Contact region:

$$u_{3'} = u_3 \qquad\qquad\qquad\qquad\qquad\qquad \text{BII-2-3}$$

$$p_{3'} = p_3 \qquad\qquad\qquad\qquad\qquad\qquad \text{BII-2-4}$$

Shock wave:

$$u_{3'} = u_4 - \phi_4(p_{3'})$$

where

$$\phi_4(p_{3'}) = (p_{3'}-p_4) \left(\frac{2}{\rho_4[(\gamma-1)p_4+(\gamma+1)p_{3'}]}\right)^{\frac{1}{2}} \qquad \infty II-2-5$$

Additional condition:

$$\frac{p_2-p_3}{u_2-u_3} = |m| \qquad\qquad BII-2-6$$

where $|m| = (\gamma p_3 \rho_3)^{\frac{1}{2}}$ for CJ conditions behind the combustion wave. Here, $\rho_3 = \rho_3(p_3,p_2)$ given by BI-4-3. Or, $|m| = (p_0-p_4)/(u_0-u_4)$, which will be used for the specific law of heat release, to be discussed in Part C. Eqs. BII-2-1 through BII-2-6 constitute six equations in the six unknowns p_2, u_2, p_3, u_3, $p_{3'}$, $u_{3'}$ and may thus be solved. The number of equations may be reduced by substitutions to a system of two equations in two unknowns. These can be solved by an iterative procedure as the Newton-Raphson method.

BII-§3 Specific examples of the calculation of the resulting waves for case 1

We solved the system of equations that describe the waves which result from the head-on collision of a backward facing shock wave and a forward facing combustion wave for a large number of specific initial conditions. Due to the complexity of the equations we wrote a computer program which performed these calculations. In this section one specific calculation will be discussed in some detail. The results, which are representative for all calculations performed sofar, will be used in Part C.

States (0) and (4) are given by the Von Neumann spike conditions behind the leading shock wave and by the CJ conditions respectively of the detonation in an $C_2H_2+O_2$ mixture at initial pressure of $1.0132 \ 10^5 \ N/m^2$. State (1) is obtained when the shock front of this detonation wave is reflected from a solid wall and prior to the interaction with the combustion wave (see Part C).

The initial state data for the pressure, particle velocity and density have been summarized in Table BII-1. If the combustion wave that results from the interaction was taken to be at CJ conditions ($Ma_3 = 1$), states
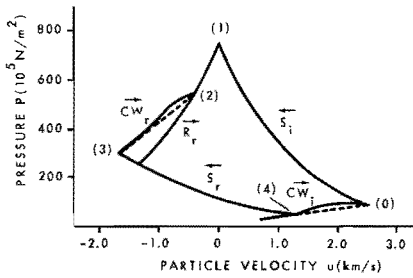
Fig. BII-4   Computed solution of interaction case 1 in the p,u-plane
for a $C_2H_2+O_2$ detonation initially at atmospheric pressure;
initial conditions are given in Table BII-1
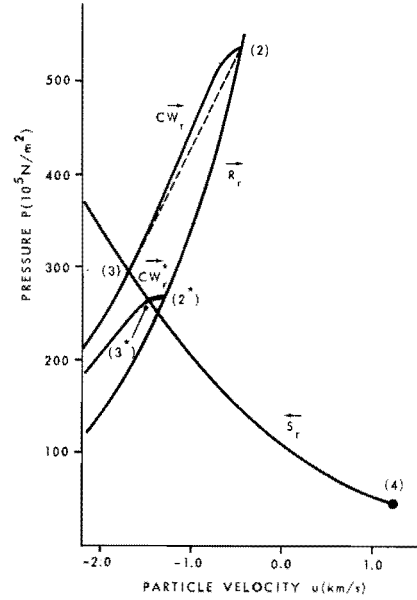
Fig. BII-5   Computed solution of interaction case 1 in the p,u-plane on
a scale different from Fig. BII-4

TABLE BII-1

Computed and initial state points for case 1;
$\gamma = 1.32$ and $Q_t = 56.582 \ 10^5 \ m^2/s^2$.

state	p$[10^5 \ N/m^2]$	u$[m/s]$	$\rho \ [kg/m^3]$
(1)	750.723	0.0	31.618
(4)	44.595	1249.35	2.065
(0)	88.159	2498.70	7.945
(2)	533.914	- 447.77	24.423
(3)	294.789	-1697.11	9.414
(2*)	270.070	-1289.59	14.574
(3*)	263.610	-1474.92	8.212

(2) and (3) resulted. The velocity of this combustion wave with respect
to the tube walls equals 335.91 m/s. Before the interaction the combus-
tion wave velocity was 2937.56 m/s, so that the combustion wave is
slowed down considerably because of the interaction.

If the mass streams through the combustion waves prior to and after the
interaction were taken to be equal, states $(2*)$ and $(3*)$ resulted from
the calculations. In the latter case the combustion wave velocity with
respect to the tube walls after the interaction equals -1050.30 m/s,
while $Ma_3 = 0.206$. Here, the combustion wave that results from the in-
teraction is swept backwards into the tube (it should be remembered
that the wave is still forward facing).

We calculated also the densities behind the transmitted shock waves
(states $(3')$ and $(3*')$) ($\rho_{3'} = 7.291$ kg/m^3 and $\rho_{3*'} = 6.882$ kg/m^3
resp.). Comparison with the densities behind the combustion waves
(states (3) and $(3*)$) shows that a contact region is indeed present be-
tween the transmitted shock wave and the combustion wave.

After solving Equations BII-2-1 through BII-2-6 the computer program
calculated the loci through the state points (0), (1), (2), (3) and
(4) in order to provide a check on the computations and to visualize
the solution in the p,u-plane. Fig. BII-4 shows the computed loci in
the p,u-plane. $\vec{S}_i$ and $\overrightarrow{CW}_i$ loci represent the (incident) waves before
the interaction. It will be seen that the (dashed) straight line (0)-
(4) is tangent to the $\overrightarrow{CW}_i$ locus in state point (4). $\vec{R}_r$, $\vec{S}_r$ and $\overrightarrow{CW}_r$
represent the resulting wave loci. It will be seen that the straight
line (2)-(3) is tangent to $\overrightarrow{CW}_r$ in point (3), where $Ma_3 = 1$.

In Fig. BII-5 we have redrawn part of the computed loci on a somewhat
larger scale. Here, we have also drawn the $\overrightarrow{CW}_r^*$ locus $(2*)-(3*)$ for
constant mass stream. The straight line which connects the terminal
states is not tangent to $\overrightarrow{CW}_r^*$, but intersects the locus at a point,
where $Ma_{3*} < 1$ (see also Chapter AII-§5).

It is of interest to note that the pressure difference across the trans-
mitted shock wave, (p_3-p_4) or $(p_{3*}-p_4)$, turns out to be smaller than
the pressure difference across the incident shock wave, (p_1-p_0). Similar
reduction in strength of the transmitted wave was found in the acousti-
cal approximation analysis by Boa-Teh Chu[47].

Further details of the interaction results will be discussed in Part C.

BII-§4 Analysis of case 2

Referring to Fig. BII-2a, prior to the interaction states (1) and (4) behind the backward facing rarefaction wave and behind the forward facing combustion wave respectively, are connected with a common state (0) in front of both waves. Fig. BII-6 shows schematically an example of the possible locations of the states (0) and (4) in the p,u-plane.
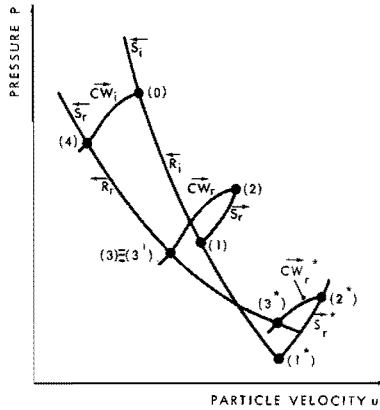
Fig. BII-6   Schematic representation of the case 2 interaction process in the p,u-plane

Through state point (0) we have drawn the $\overleftarrow{R}_i$ locus of all possible states (1) on the right of a backward facing incident rarefaction wave. Through state point (4) we have drawn the $\overleftarrow{R}_r$ locus of all possible states (3) on the right of a backward facing transmitted rarefaction wave. It turns out that these two loci may intersect each other. This is verified by the following arguments.

The $\overleftarrow{R}_i$ locus is given by

$$u_1 = u_0 - \frac{2c_0}{\gamma-1} \left[\left(\frac{p_1}{p_0}\right)^{\frac{\gamma-1}{2\gamma}} - 1 \right]$$ BII-4-1

From this we infer the derivative of this locus in state point (0), i.e. $p_1 = p_0$,

$$\frac{dp_1}{du_1}\bigg|_{(0)} = -\frac{\gamma p_0}{c_0}$$ BII-4-2

Similarly, the $\overleftarrow{R}_r$ locus is given by

$$u_3 = u_4 - \frac{2c_4}{\gamma-1} \left[\left(\frac{p_3}{p_4}\right)^{\frac{\gamma-1}{2\gamma}} -1 \right] \qquad\qquad \text{BII-4-3}$$

so that the derivative of this locus in state point (4) is

$$\frac{dp_3}{du_3}\bigg|_{(4)} = - \frac{\gamma p_4}{c_4} \qquad\qquad \text{BII-4-4}$$

As $p_0 > p_4$ and $c_0 < c_4$ (see Chapter AII-§5), we find that

$$\frac{dp_1}{du_1}\bigg|_{(0)} < \frac{dp_3}{du_3}\bigg|_{(4)} \qquad\qquad \text{BII-4-5}$$

This indicates that the slope of $\overleftarrow{R}_i$ locus in point (0) is steeper than that of the $\overleftarrow{R}_r$ locus in point (4). It is thus quite conceivable that the two loci may intersect at some point.

The state behind the incident rarefaction wave may thus be represented by points like (1) situated on the branch of the $\overleftarrow{R}_i$ locus above the $\overleftarrow{R}_r$ locus or by points like (1*) on the branch of the $\overleftarrow{R}_i$ locus below the $\overleftarrow{R}_r$ locus. In both cases the resulting wave system can be found by a similar construction, i.e. on the reflected forward facing shock locus $\overrightarrow{S}_r$ a state point (2) can be found, from which a combustion wave locus can be constructed that intersects the $\overleftarrow{R}_r$ locus in a point (3), while some additional condition (either CJ or constant mass stream conditions) is fulfilled. We note the formal similarity with the shock tube problem of Fig. BI-8.

To obtain a quantitative solution to the problem of the head-on colli-sion of a backward facing rarefaction wave and a forward facing combus-tion wave, the following system of equations should be solved.

Case 2: (states (1) and (4) are given (see Fig. BII-2)

Shock wave:

$$u_2 = u_1 + \phi_1(p_2)$$

where

$$\phi_1(p_2) = (p_2-p_1) \left(\frac{2}{\rho_1[(\gamma-1)p_1+(\gamma+1)p_2]}\right)^{\frac{1}{2}}$$ BII-4-6

Combustion wave:

$$u_3 = u_2 - \Omega_2(p_3)$$

where

$$\Omega_2(p_3) = \left\{ \frac{2}{\rho_2} (p_3-p_2) \frac{p_3-p_2-\gamma p_2(\gamma-1)Q_t/c_2^2}{(\gamma+1)p_3 + (\gamma-1)p_2} \right\}^{\frac{1}{2}}$$ BII-4-7

Here, $\rho_2 = \rho_2(p_2)$ and $c_2 = c_2(p_2)$ are given by BI-2-2 to be functions of p_2 and the known state parameters p_1, ρ_1.

Contact region:

$$u_{3'} = u_3$$ BII-4-8

$$p_{3'} = p_3$$ BII-4-9

Rarefaction wave:

$$u_{3'} = u_4 - \psi_4(p_{3'})$$

where

$$\psi_4(p_{3'}) = \frac{2c_4}{\gamma-1} \left[\left(\frac{p_{3'}}{p_4}\right)^{\frac{\gamma-1}{2\gamma}} -1 \right]$$ BII-4-10

Additional condition:

$$\frac{p_2-p_3}{u_2-u_3} = |m|$$ BII-4-11

which is supposed to be given as in case 1.

Eqs. BII-4-6 through BII-4-11 constitute a system of six equations in the six unknown variables, p_2, u_2, p_3, u_3, $p_{3'}$, $u_{3'}$, which can be solved by the method described in Chapter BII-§2.

BII-§5 Specific examples of the calculation of the resulting waves
for case 2

As in Chapter BII-§3 we have solved the system of Equations BII-4-6
through BII-4-11 for a number of specific initial conditions. Two
specific examples will be discussed here, which are representative
for all calculations performed. They compare with the two initial state
conditions (1) and (1*) of Fig. BII-6.
In the first example we impose the additional condition of constant
mass stream through the combustion waves prior to and after the inter-
action, while in the second example we impose CJ conditions behind
both waves.
Table BII-2 and Table BII-3 summarize the initial and final state data,
as obtained from the computerized solution of the relevant equations,
for the case of constant mass stream and CJ conditions respectively.
The reason for chosing these initial conditions will become clear in
Part C.
In the case of constant mass stream (Table BII-2) the original veloci-
ty of the combustion wave with respect to the walls of the tube was
-1050.3 m/s. After the interaction the combustion wave velocity was
830.5 m/s. This increase in velocity is due to the accelerating action
of the rarefaction wave as described in Chapter BII-§1. Prior to the
interaction the Mach number Ma_4 = .206, while after the interaction
Ma_3 = .488.
The density ρ_3, behind the transmitted rarefaction wave $\overleftarrow{R}_r$ is 4.074
kg/m^3. Comparison with the density behind the resulting combustion
wave (ρ_3 = 3.708 kg/m^3) shows that a contact region is present between
$\overleftarrow{R}_r$ and $\overrightarrow{CW}_r$.

Similarly, in the case of CJ conditions (Table BII-3) an increase in
combustion wave velocity was obtained from 335.9 m/s to 782.8 m/s. The
density behind $\overleftarrow{R}_r$, ρ_3, = 7.343 kg/m^3 , which demonstrates the presence
of a contact region.
For both cases we have drawn the computed loci through the points (0),
(1), (2), (3) and (4) resulting in Fig. BII-7 and Fig. BII-8 resp.
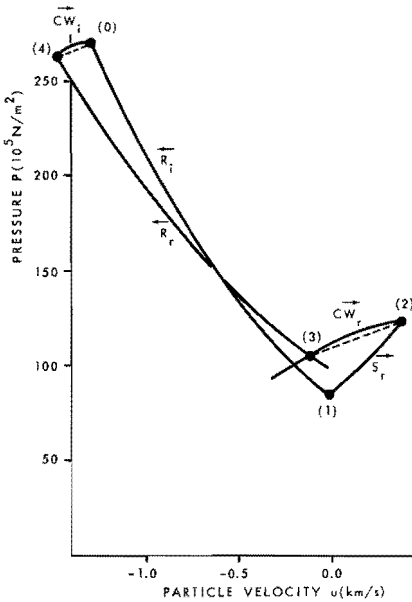
Fig. BII-7 Computed solution of interaction case 2 in the p,u-plane
for constant mass stream conditions; initial conditions are
given in Table BII-2
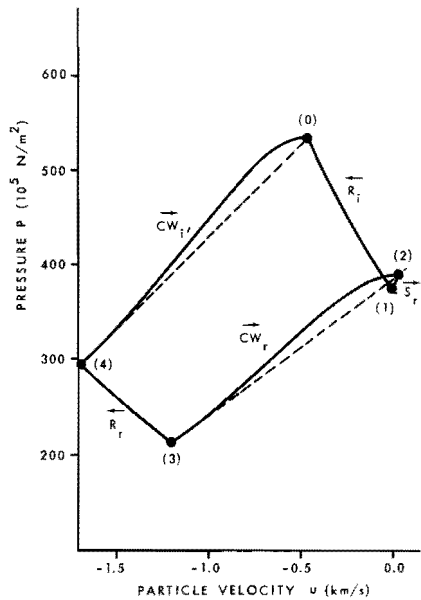
Fig. BII-8 Computed solution of interaction case 2 in the p,u-plane
for CJ conditions; initial conditions are given in Table
BII-3

In Fig. BII-7 it will be seen that the two dashed lines (0)-(4) and
(2)-(3), which represent the absolute values of the mass streams prior
to and after the interaction respectively, have equal slopes and inter-
sect the $\overrightarrow{CW}$ loci in points, where Ma_4 and Ma_3 are smaller than unity.
In Fig. BII-8 the dashed lines are tangent to the $\overrightarrow{CW}$ loci in the point
of intersection of these loci with the $\overleftarrow{R}_r$ locus $(Ma_4 = Ma_3 = 1.0)$.
Finally we note, that in both cases the strength of the transmitted
rarefaction wave, (p_4-p_3), is smaller than the strength of the incident
rarefaction wave, (p_0-p_1), which result was also obtained by Boa-Teh
Chu for the case of the interaction of acoustical waves.

TABLE BII-2

Computed and initial state points for case 2;

additional condition of constant mass streams;

$\gamma = 1.32$ and $Q_t = 56.582 \ 10^5 \ m^2/s^2$.

state	$p[10^5 \ N/m^2]$	$u[m/s]$	$\rho[kg/m^3]$
(1)	84.058	0.0	6.019
(4)	263.611	-1474.92	8.212
(0)	270.073	-1289.59	14.574
(2)	122.037	393.18	7.973
(3)	104.495	- 109.92	3.708

TABLE BII-3

Computed and initial state points for case 2;

additional condition of CJ conditions;

$\gamma = 1.32$ and $Q_t = 56.582 \ 10^5 \ m^2/s^2$.

state	$p[10^5 \ N/m^2]$	$u[m/s]$	$\rho[kg/m^3]$
(1)	374.183	0.0	18.657
(4)	294.789	-1697.11	9.415
(0)	533.914	- 447.77	24.423
(2)	388.826	47.427	19.208
(3)	212.365	-1201.92	7.117

BII-§6 Discussion

Apart from the shock and rarefaction wave loci, which are known from
the theory of non-reactive gasdynamics, we have derived in this PART
the loci of combustion waves, which we introduced in PART A as an ele-
mentary reactive wave, in the p,u-plane. This new approach enabled us
to derive two interaction rules which concern the head-on collision of
a combustion wave with a shock wave, and with a rarefaction wave. In
the subsequent two PARTS of this thesis, which deal with the interaction
of a detonation wave with its surroundings, the import of both the con-
cept of a detonation wave as consisting of a double elementary wave
complex and the interaction rules will be demonstrated.

PART C - THE REFLECTION PROCESS OF A ONE-DIMENSIONAL DETONATION WAVE

In this PART we will study the reflection process of a one-dimensional
gaseous detonation wave against a solid wall. In Chapter C-§1 we pro-
pose three different laminar detonation wave models. Model I and II
are characterized by a constant induction time. In Model I the heat of
explosion is released instantaneously at the end of the induction pe-
riod, while a law of heat release is proposed for Model II, which is
characterized by a heat release "relaxation time". Model III is given
by a temperature and concentration dependent induction time and the law
of heat release employed in Model II. We extrapolated existing induc-
tion time data obtained from laminar reactive flow studies to detonation
wave conditions and compared these data with existing experimental in-
duction times of hydrogen-oxygen detonations.
An interesting example of the application of the interaction rules 1
and 2 is presented by the assumption of a constant induction time,
which is discussed by means of a study in the p,u-plane (Chapter C-§2),
by means of the method of characteristics and by means of the Lax
finite difference scheme (Chapter C-§3 and C-§4). Our experimental re-
sults of reflected pressure measurements by means of pressure bar
transducer I (sensing element 2mm dia x 1 mm) are discussed in Chapter
C-§5.
A more realistic representation of the reflection process is given by
our model III studies of the detonation wave (Chapter C-§6). Some of
our experimental results obtained by means of pressure bar transducer
II (sensing element 10 mm dia x 0.2 mm, rise time about 200 nanoseconds)
are presented in Chapter C-§7.

C-§1 Discussion of different detonation wave models

We will study the interaction of a gaseous detonation wave with a solid
wall by means of three models of a one-dimensional detonation wave, each
of which is less restrictive than the preceding one.
The detonation wave will be assumed to consist, in general, of two re-
gions. Behind the shock front of the wave there is an extended constant
pressure-constant density induction zone. This implies that during

their transition through the shock front and the induction zone the
particles do not release heat. Next there is a region where pressure
and density decrease as heat is released. This part of the detonation
wave is identified as the combustion wave.

The period of time which a particle spends in the induction zone, from
the instant it crosses the shock front until it starts releasing its
heat, or, in terms of gasdynamics, when it is reached by the combustion
wave, is called the induction time τ_{ind}.

When at a specific station, X^o, of a tube we observe the detonation wave,
which passes this station, and we should measure the induction time,
τ^o_{ind}, this time will differ from the local induction time, τ_{ind}, which
is measured along a particle path.
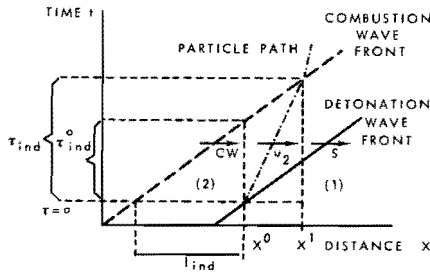
Fig. C-1 Comparison of τ_{ind} and τ^o_{ind} in the X,t-plane

Fig. C-1 depicts the steady induction zone of a detonation wave in the
X,t-plane. The shock wave $\vec{S}$ and the head of the combustion wave $\overrightarrow{CW}$ form
the boundaries of the induction zone. Both waves have the same veloci-
ty, D, with respect to the tube. We also sketched a particle path. The
particle is at rest at station X^o of the tube prior to the arrival of
the detonation wave at this point, $u_1 = 0$. Behind the shock front it
acquires the constant velocity u_2. From Fig. C-1 it is found that

$$x^1 - x^o = D(\tau_{ind} - \tau^o_{ind}) = u_2 \tau_{ind} \qquad\qquad \text{C-1-1}$$

With the equation of conservation of mass across the shock wave,
$\rho_1 D = \rho_2 (D-u_2)$, we derive the equation

$$\tau_{ind} = \frac{D}{D-u_2} \tau^o_{ind} = \frac{\rho_2}{\rho_1} \tau^o_{ind} \qquad\qquad \text{C-1-2}$$

As ρ_2 is generally of the order of five to ten times ρ_1, it follows that $\tau_{ind} > \tau^o_{ind}$. The length of the induction zone is defined as

$$l_{ind} = D\tau^o_{ind} \qquad\qquad\qquad C-1-3$$

Since induction processes generally follow a reciprocal concentration and an exponential temperature dependence[37] we assume that the induction time is given by

$$\tau_{ind}[O_2] = A \exp (E/RT) \qquad\qquad C-1-4$$

where $[O_2]$ is the local oxygen concentration, E the apparent activation energy and A a proportionality constant.

We assume further[37] that the recombination reactions in the combustion wave simply add heat to the flow and are relatively insensitive to the temperature. The law of heat release is taken to be of the form

$$Q = Q_t (1 - \exp(- (\tau-\tau_{ind})/\tau_{rel})) \qquad \tau \geqslant \tau_{ind} \qquad C-1-5$$

where τ is measured along a particle path from the instant it enters the shock wave. Q_t is the total amount of heat that can be added to the flow for the specific detonation wave (see Appendix III). This relation is in accordance with Schott and Getzinger's[48] observations that the recombination process may be adequately described in terms of a single variable β called the extent of recombination. If we define $\beta = Q/Q_t$, then the "relaxation time" τ_{rel} has the significance

$$\frac{1}{\tau_{rel}} = \frac{d\beta}{dt} \bigg|_{\tau = \tau_{ind}} \qquad\qquad C-1-6$$

and determines the rate of heat release. As it would take an infinitely long time to release all heat, we will assume for practical purposes that all heat has been released after a period of time equal to $5 \times \tau_{rel}$. The three models of a detonation wave employed in this study are summarized in Table C-1.

TABLE C-1

Summary of detonation wave models

Model	Induction time	Law of heat release	
I	τ_{ind} = constant	$Q = 0$	$0 \leqslant \tau < \tau_{ind}$
		$Q = Q_t$	$\tau \geqslant \tau_{ind}$
II	τ_{ind} = constant	$Q = 0$	$0 \leqslant \tau < \tau_{ind}$
		Eq. C-1-5	$\tau \geqslant \tau_{ind}$
III	$\tau_{ind} = \dfrac{A}{[O_2]} \exp(E/RT)$	$Q = 0$	$0 \leqslant \tau < \tau_{ind}$
		Eq. C-1-5	$\tau \geqslant \tau_{ind}$

In Model I and II τ_{ind} is constant, i.e. independent of density and temperature. In Model I the heat is released instantaneously after the induction period, while in Model II the heat release law Eq. C-1-5 is employed. In Model III we remove the restriction placed on the induction time and use Eq. C-1-4. In the induction zone of a steady detonation wave pressure, density and temperature are constant and, thus, the induction time has the same value for all three models.

With Fig. C-1 in mind, we consider an interesting property of Models I and II. Here τ_{ind} remains constant and has the same value for all particles. After having crossed the shock front each particle releases its heat a period of time equal to τ_{ind} later, either instantaneously or during a specific period of time, which is also the same for all particles. Moreover, each particle represents a certain amount of mass that is conserved at all times. As far as the combustion wave is concerned, this means that during each unit of time the same amount of mass is transported through the wave, i.e. the mass stream through the combustion wave is constant. When the shock front of the detonation wave collides with a wall, the last particle which is situated at the wall will start to release its heat a period of time equal to τ_{ind} later, or, in other words, the combustion wave reaches the wall.

We will demonstrate below that the application of Models I and II re-

presents a hypothetical experiment in which we are able to show the applicability of both interaction rules of Part B. In applying Model III, however, we will show that, due to the high temperature and density region near the wall upon reflection of the shock front of the detonation wave, the induction time is shortened considerably. As a consequence the gas will be ignited behind the reflected shock wave, so that a second combustion wave originates at the wall.

With the exception of hydrogen-oxygen detonations surprisingly little is known about equivalent one-dimensional reaction zones of gaseous detonation waves, which, in reality, exhibit a propagating transverse wave structure that is quite complex (see Chapter AII-§1). It is therefore of interest to compare the models of a one-dimensional detonation wave with the observed structure of the laminar flow behind a smooth shock wave in an exothermally reactive medium. The density field in such laminar flows has recently been studied by White et al.[49,50] with optical interferometry. Smooth shock waves followed by one-dimensional induction zones may be obtained in a constant area shock tube when one or both reactants are highly dilute, or when the shock wave is in a diverging channel at a low initial pressure. A striking and common feature of most experiments is that the induction zone is a nearly constant density region, where radical concentrations increase exponentially. It is terminated by a region in which the density decreases rather abruptly due to recombination reactions, which are heat releasing reactions, and then, still well above the equilibrium density tends to level off and continue to decrease more slowly toward equilibrium. We found that the law of heat release C-1-5 simulated this behaviour quite well (see Chapter C-§6).

The density structures in H_2-O_2 and $C_2H_2-O_2$ mixtures were found to be qualitatively indistinguishable from each other. Kistiakowsky and Richards[51] demonstrated that the induction periods of acetylene-oxygen reactions at high temperatures are related to those characterizing the hydrogen-oxygen reactions, the inference being that the same rate determining step, $H+O_2 \rightleftharpoons OH+O$, controls the branching process in both oxidations (see also Schott and Kinsey[52], and Soloukhin[28]).

White [50] noted that, although the activation energies are nearly the same for both mixtures, the lengths of the induction periods are not, due to the difference in density and temperature at the same initial pressure. It was confirmed by Kistiakowsky and Kydd[20] by X-ray absorption experiments that the induction periods in acetylene-oxygen mixtures are much shorter than in hydrogen-oxygen mixtures.

Induction times have been measured by a variety of techniques and suffer from a corresponding spread in definition. We have summarized some of the formula's for the calculation of induction time data in Table C-2 and Table C-3 for H_2-O_2 and C_2H_2-O_2 mixtures respectively. Schott and Kinsey measured the absorption of ultraviolet OH line radiation by the incident and reflected shock wave technique[52] in H_2-O_2 mixtures diluted with an excess of argon. The shocked gas temperatures were well within the range of detonation wave temperatures (1100 K < T_2 < 2600 K). The induction times, however, were very much longer due to the dilution. They defined the induction time τ_{ind} as the time at which the OH concentration reached the threshold of detectability. Strehlow and Cohen[53] measured the delay to adiabatic explosion at the back wall of a tube by streak schlieren photographs of the reflected shock region in stoichiometric H_2-O_2 mixtures diluted with argon. This delay time was identified with the induction time.

White and Moore[49,50] studied the density structure behind shock waves in a diverging channel and a constant area shock tube. The induction time was measured from the shock front to the first sign of exothermic reaction, as evidenced by a decrease in the gas density. They also suggested that a better correlation of results is obtained when the product $([O_2][H_2])^{\frac{1}{2}} \tau_{ind}$ is used rather than just $[O_2] \tau_{ind}$ in the formula for the calculation of τ_{ind}.

Kistiakowsky and Richards[51] studied C_2H_2-O_2 reactions by observing the emission of ultraviolet radiation behind shock waves in gas mixtures containing a large excess of argon. The duration of the induction period was defined as the length of time the gas spends behind the shock front before it begins to emit radiation, i.e. the time the photomultiplier current reached a minimum detectable value. Soloukhin[28]

TABLE C-2

Formula for the calculation of induction time data
for hydrogen-oxygen mixtures;
τ_{ind} has units of seconds; concentrations are in moles/litre.

$^{10}\log([O_2]^m[H_2]^{1-m}\tau_{ind})= C+E/RT$				
Source	m	C	E/R	Method
Schott/Kinsey[52]	1	-10.647	18,164/4.58	Absorption UV-radiation
Strehlow/Cohen[53]	1	-10.162	16,328/4.58	Adiabatic explosion delay
White/Moore[49]	1/2	- 9.8	14,198/4.58	Density structure
White[50]	1/3	-10.44	17,200/4.58	Density structure (Lean)

TABLE C-3

Formula for the calculation of induction time data
for acetylene-oxygen mixtures;
τ_{ind} has units of seconds; concentrations are in moles/litre.

$^{10}\log([O_2]^m[C_2H_2]^{1-m}\tau_{ind})= C+E/RT$				
Source	m	C	E/R	Method
Kistiakowsky/Richard[51]	1	-10.57	17,100/4.58	Emission of UV radiation
Soloukhin[28]	1	-11.56	25,000/4.58	Adiabatic explosion delay
White I[50]	1/3	-10.81	17,300/4.58	Density structure (Lean)
Glass[54]	1	-10.56	17,060/4.58	Chemi-ionization
White II[50]	1/2	-10.47	17,400/4.58	Density structure

measured the induction time by the reflection method in argon diluted $C_2H_2-O_2$ mixtures.

Application of the induction time data to the quantitative analysis of the transition to detonation in a gaseous medium[37,55], which is substantially a laminar flow process, has met with considerable success. We have calculated the induction times for detonation waves in stoichiometric hydrogen-oxygen and equimolar acetylene-oxygen mixtures for several initial pressures from the relations given in Tables C-2 and C-3. For this purpose we first computed the Von Neumann spike conditions behind the shock fronts of these waves (see Appendix I, Tables I-4 and I-5). We summarized our computed results in Figs. C-2 and C-3. The defined induction time to the onset of observable exothermic reaction[50,53] is not expected to coincide with the time derived from observations of the growth of [OH][52]. Schott in a private communication[56] indicated that their delays to maximum [OH] were about 1.5 times larger than their appearance delays. Taking this factor into account, Schott and Kinsey's data are within the range of Strehlow's and White and Moore's data. White's data were obtained for very lean mixtures and may not be expected to coincide with the other data on hydrogen-oxygen mixtures (Fig. C-2).

In fig. C-2 we also draw the straight line that represents the best fit to the induction times τ_{ind}^o (observers time) as measured by Jost et al.[57] in stoichiometric H_2-O_2 detonations at low initial pressures. In order to obtain the local induction time τ_{ind} from Jost's data, they have to be multiplied by the density ratio across the shock front, which is of the order of 5.5 (Eq. C-1-2).

We may conclude that the local induction times measured from detonation waves in hydrogen-oxygen mixtures are about a factor of three larger than those obtained from an extrapolation of laminar induction zone experiments. A similar observation was made by Soloukhin[28] from his experiments on $C_2H_2+2.5O_2$ detonations at low initial pressures (< 0.14 10^5 N/m^2). He found that instead of the expected τ_{ind} for a laminar detonation wave, the observed τ_{ind} was more than one order larger. Referring to the three-dimensional structure of a detonation
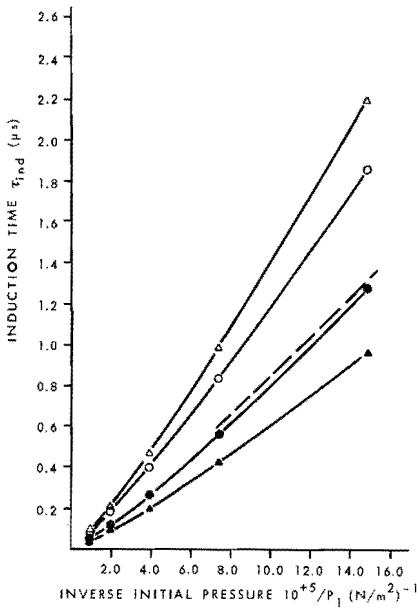
Fig. C-2 Computed induction times as a function of inverse initial
pressure p_1 for $2H_2+O_2$ mixtures according to the formulas
given in Ref. 53 ($\triangle$), Ref. 52 ($\bullet$), Ref. 50 ($\blacktriangle$), and
Ref. 49 (o); dashed line represents experimental τ^o_{ind} data
from Ref. 57 (see Table C-2)
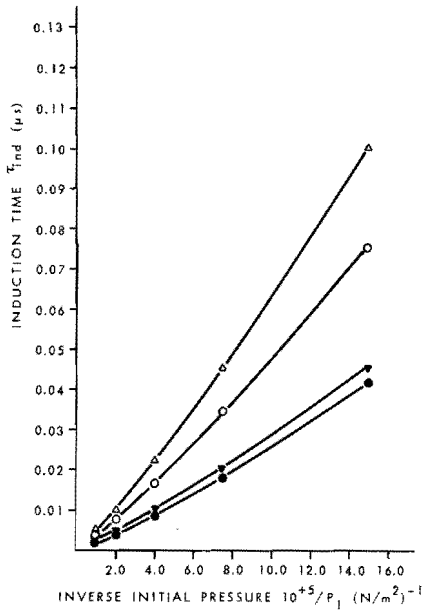
Fig. C-3 Computed induction times as a function of inverse initial
pressure p_1 for $C_2H_2+O_2$ mixtures according to the formulas
given in Ref. 28 ($\bullet$), Ref. 51, 54 (o), Ref. 50II ($\triangle$),
and Ref. 50I ($\blacktriangledown$) (see Table C-3)

wave (Fig. AII-3) it was noted by Soloukhin that waves like 2 and 2'
are unable to ignite the gas fast enough. These regions have been des-
cribed as expanding (non-reactive) blast waves[58] in which temperatures
and densities are lower than would be expected for a one-dimensional
wave. Because of the relatively large size of waves 2 and 2', the over-
all induction period in multiheaded detonations is apparently longer
than expected for the one-dimensional case.

C-§2 Application of detonation wave Models I and II to the reflection
process in the p,u-plane

In this Chapter we will discuss the reflection process of a detonation
wave against a solid wall. The description of this process applies only
to both Model I and II. These models of the detonation wave permit us
to perform an interesting, but hypothetical experiment in which all
features of the interaction process discussed in PART B appear. The
experiment is hypothetical in as far as τ_{ind} is assumed to be constant.
This is a reasonable assumption only as long as temperature and densi-
ty in the induction zone remain nearly constant (see Chapter C-§6).
The following description of the reflection process applies to a deto-
nation wave in the acetylene-oxygen mixture, whose properties we derived
in Appendix III.
The pressure distribution along the tube at a specific instant of time
prior to the interaction of the detonation wave with the wall is shown
schematically in Fig. C-4.

The shock front of the detonation wave is reflected from the wall as a
backward facing shock wave $\overset{\leftarrow}{S}_2$, as shown in Fig. C-4b. Behind this wave
the pressure, density and temperature are raised considerably, while
the particles are at rest between the shock front and the wall. It is
shown in the p,u-plane of Fig. C-5 that a backward facing shock wave
$\overset{\leftarrow}{S}_2$ should result from the reflection of a forward facing shock wave $\vec{S}_1$
against a solid wall. The boundary condition at the wall demands that
the particle velocity $u_4 = 0$. This condition can only be fulfilled by
a backward facing reflected shock wave, as is shown in Fig. C-5 from
the computed $\overset{\leftarrow}{S}_2$ locus through point 2. This locus is given by the re-
lation

$$u_4 = u_2 - (p_4-p_2) \left(\frac{2}{\rho_2[(\gamma-1)p_2+(\gamma+1)p_4]}\right)^{\frac{1}{2}} \qquad \text{C-2-1}$$

and intersects the u = 0 axis at the state point 4. This equation may
be solved for p_4, when $u_4 = 0$ (see Table C-4).
After reflection of the shock front of the detonation wave against the
wall and prior to the interaction of the reflected shock wave with the
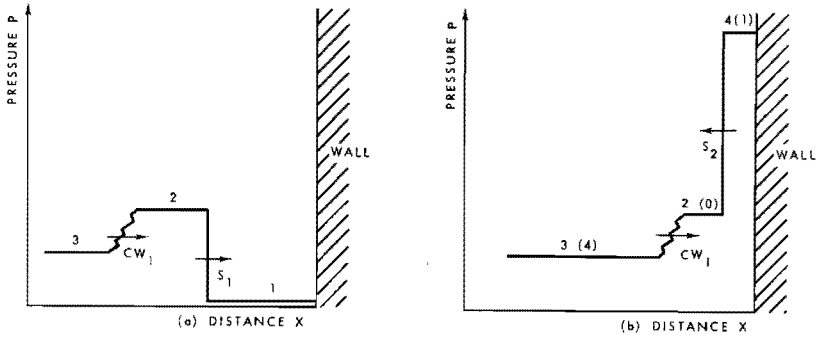
Fig. C-4 Reflection of a detonation wave front against a solid wall
(not to scale); (a) shortly before the interaction; (b) shortly
after the interaction; parenthesized state numbers correspond
to those of Figs. BII-4,5
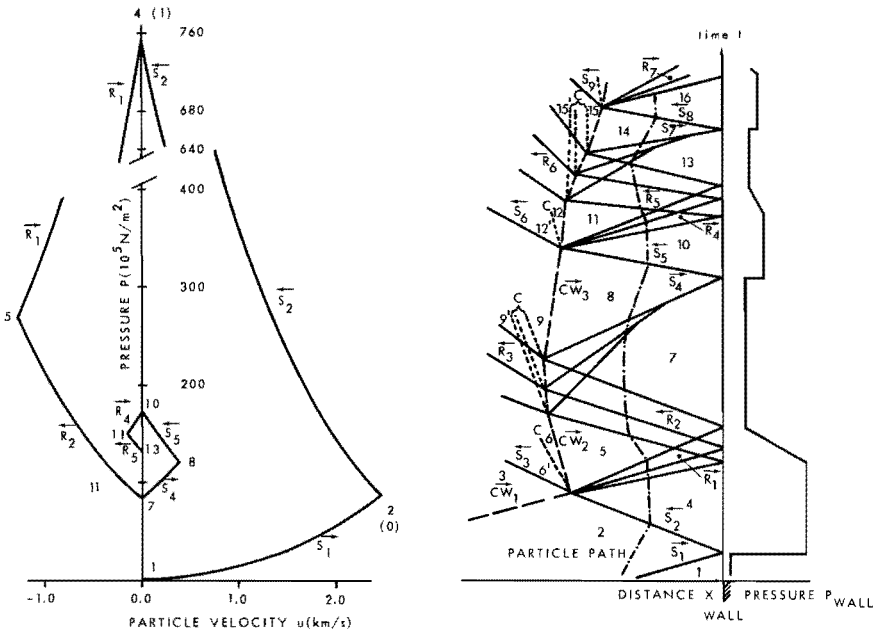
Fig. C-5 Computed p,u-loci connecting the states near the wall (see
Fig. C-6)

Fig. C-6 Sketch of the X,t- and p,t-plane for the interaction of a
detonation wave with a solid wall. Numbers refer to Table C-4;
"C" are contact regions or discontinuities

TABLE C-4

Computed state variables for two complete interaction cycles,
both for constant mass stream and CJ conditions;
Initial conditions are given in Table III-1;
subscripts refer to Fig. C-6.

		FIRST COMPLETE INTER-ACTION CYCLE			SECOND COMPLETE INTER-ACTION CYCLE	
		const. mass stream conditions	CJ conditions		const. mass stream conditions	CJ conditions
p_4	N/m^2	$750.723 \ 10^5$	$750.723 \ 10^5$	p_{10}	$174.314 \ 10^5$	$403.970 \ 10^5$
ρ_4	kg/m^3	31.618	31.618	ρ_{10}	10.432	19.772
u_4	m/s	0.0	0.0	u_{10}	0.0	0.0
p_5	N/m^2	$270.073 \ 10^5$	533.914	p_{11}	$151.128 \ 10^5$	$402.229 \ 10^5$
ρ_5	kg/m^3	14.574	24.423	ρ_{11}	9.363	19.707
u_5	m/s	-1289.59	-447.77	u_{11}	-159.20	-5.371
p_6	N/m^2	$263.611 \ 10^5$	$294.789 \ 10^5$	p_{12}	$138.302 \ 10^5$	$219.939 \ 10^5$
ρ_6	kg/m^3	8.212	9.415	ρ_{12}	4.710	7.333
u_6	m/s	-1474.92	-1697.11	u_{12}	-527.06	-1254.72
$\rho_{6'}$	kg/m^3	6.883	7.291	$\rho_{12'}$	4.582	7.308
U_{CW_2}	m/s	-1050.3	335.91	U_{CW_4}	213.20	735.01
Ma_6		0.206	1.000	Ma_{12}	0.376	1.000
p_7	N/m^2	$84.058 \ 10^5$	$374.183 \ 10^5$	p_{13}	$130.698 \ 10^5$	$400.495 \ 10^5$
ρ_7	kg/m^3	6.019	18.657	ρ_{13}	8.388	19.643
u_7	m/s	0.0	0.0	u_{13}	0.0	0.0
p_8	N/m^2	$122.037 \ 10^5$	$388.826 \ 10^5$	p_{14}	$137.958 \ 10^5$	$400.690 \ 10^5$
ρ_8	kg/m^3	7.973	19.208	ρ_{14}	8.738	19.650
u_8	m/s	393.18	47.43	u_{14}	58.931	0.604
p_9	N/m^2	$104.495 \ 10^5$	$212.365 \ 10^5$	p_{15}	$123.409 \ 10^5$	$219.068 \ 10^5$
ρ_9	kg/m^3	3.708	7.117	ρ_{15}	4.272	7.308
u_9	m/s	-109.92	-1201.92	u_{15}	-358.31	-1248.75
U_{CW_3}	m/s	830.53	782.77	U_{CW_5}	457.96	740.42
Ma_9		0.488	1.000	Ma_{15}	0.418	1.000

combustion wave, the situation is precisely that of case 1, which has
been treated in Chapter BII-§3. In fact, when we replace the unparen-
thesized state numbers of Fig. C-4 by the parenthesized ones, we obtain
Fig. BII-1a.

As a result of the interaction a backward facing shock wave $\overleftarrow{S}_3$ is trans-
mitted through the combustion wave, while a forward facing rarefaction
wave $\overrightarrow{R}_1$ is reflected from the combustion wave. Also, a "new" combustion
wave $\overrightarrow{CW}_2$ is established after the interaction. The computed interaction
results are shown in the p,u-planes of Figs. BII-4 and BII-5 and given
in Table BII-1, where for Models I and II the constant mass stream re-
sults are applicable (see the discussion in Chapter C-§1). The pressure
and particle velocity distributions are sketched in Fig. BII-1b.

For the purpose of clarifying the discussion we have sketched the wave
interaction processes schematically (not to scale) in Fig. C-6, which
shows the X,t-plane close to the wall. On the right hand side of Fig.
C-6 we have also sketched the pressure at the wall, p_w, as a function
of time. Furthermore, we have summarized all relevant computed data in
Table C-4.

The forward facing rarefaction wave $\overrightarrow{R}_1$ will eventually collide with the
wall. At the wall we have the boundary condition $u_w = 0$. As a result of
the collision a backward facing rarefaction wave $\overleftarrow{R}_2$ will be reflected
from the wall. In Fig. C-5 we have drawn the computed forward facing
rarefaction wave locus $\overrightarrow{R}_1$ through point 4. State point 5 behind $\overrightarrow{R}_1$,
which is determined from the first interaction of the shock wave $\overleftarrow{S}_2$
with the combustion wave $\overrightarrow{CW}_1$, is located on this locus. Through point
5 we have drawn the computed backward facing $\overleftarrow{R}_2$ locus, which intersects
the u = 0 axis at point 7. This locus is given by the relation

$$u_7 = u_5 - \frac{2c_5}{\gamma-1} \left[\left(\frac{p_7}{p_5}\right)^{\frac{\gamma-1}{2\gamma}} -1 \right] \qquad\qquad \text{C-2-2}$$

This equation may be solved for p_7, when $u_7 = 0$ (see Table C-4).
In Fig. C-6 it is shown that after the initial high pressure rise at
the wall the pressure drops due to the effect of the rarefaction waves.

After interaction of the rarefaction wave $\vec{R}_1$ with the wall we are confronted with the situation of case 2, where the forward facing combustion wave $\overrightarrow{CW}_2$ will eventually collide with the backward facing rarefaction wave $\overleftarrow{R}_2$. As a result of this interaction a backward facing rarefaction wave $\overleftarrow{R}_3$ is transmitted through the combustion wave, while a forward facing compression wave, which may eventually steepen into a shock wave $\vec{S}_4$, is reflected from the combustion wave.

A "new" combustion wave $\overrightarrow{CW}_3$ is also established. The computed interaction results are shown in the p,u-plane of Fig. BII-7 (for constant mass stream) and given in Table BII-2. The computational results have been summarized in Table C-4 (see also Fig. C-6).

The transmitted rarefaction wave $\overleftarrow{R}_3$, which travels at sonic speed with respect to the gas, will eventually overtake the shock wave $\overleftarrow{S}_3$, which was transmitted through the combustion wave some time earlier. This will cause the shock strength of $\overleftarrow{S}_3$ to decay.

We have now arrived at a situation, which is at least qualitatively similar to the situation prior to the arrival of the detonation wave at the wall. A shock wave (or compression wave) followed by a combustion wave is running in the direction of the wall. This shock wave (or compression wave) $\vec{S}_4$ will reflect from the wall as a backward facing shock wave (compression wave) $\overleftarrow{S}_5$, causing the pressure at the wall to rise again. The reflected shock wave will collide with the combustion wave (case 1), etc. We have computed this second cycle of interactions, too. All results are summarized in Table C-4, where the subscripts refer to Fig. C-6. For the purpose of comparison we have also given in the same Table the computed values of the parameters, that would have been obtained, if CJ conditions would have been postulated behind the combustion waves. The first cycle of interactions for these conditions was discussed in Chapter BII.

It may be clear that the interaction processes with the combustion waves will not continue infinitely. From the instant the detonation wave front reaches the wall, the last particle located at the wall will start to release its heat, i.e. the combustion wave will reach the wall, at a period of time equal to τ_{ind} later. From this time on

the case 1 and case 2 type interactions are over. Furthermore, as we have seen above, the strengths of the transmitted waves will decay some period of time thereafter, and, thus, a steady state flow will finally be established.

We note, that, as τ_{ind} is taken increasingly smaller, the complete interaction process will be finished correspondingly sooner. Moreover, compression waves that are reflected from the combustion waves may not steepen into shock waves before they interact again with a combustion wave. To be able to verify the basic findings of the above analysis, we have written a computer program that simulates the complete flow process. This will be discussed in the next chapters.

Finally we note, that in the course of time the strengths of the waves involved in the interaction processes become increasingly smaller. As mentioned in Chapter BII, it looks as if the combustion waves tend to "quench" the waves that interact with them. This effect is shown in Fig. C-5, where the computed loci of the waves that interact with the wall form sort of a spiral, that appears to converge towards some point on the $u = 0$ axis. Although the pressure rise due to the arrival of $\vec{S}_4$ at the wall may still be considerable, the subsequent interactions with the wall produce much smaller rises and decays.

C-§3 Finite difference method for the solution of the equations of motion

The gasdynamical equations of conservation of mass, momentum and energy for plane one-dimensional time dependent flows may be expressed in the Eulerian or Lagrangian form. These equations can be solved by finite difference methods for appropriate initial and boundary conditions[59,60].

In plane geometry, the Lagrangian form has much to commend it, as it gives more information: it describes the motion of particular particles of the fluid, which is convenient in the case of reactive flows, where particles release heat.

The equations are valid for smooth flows, i.e. the dependent variables and/or their derivatives are all continuous over the whole flow field.

In general, however, the flow variables and/or their derivatives may
have discontinuous values. Across the head and tail of a rarefaction
wave only derivatives of the flow variables change discontinuously.
Across a contact discontinuity p and u are continuous, but ρ and e are
not. Across shock waves all flow variables change discontinuously. Es-
pecially the presence of shock waves complicates the solution of the
equations of motion, which must be supplemented by the Rankine-Hugoniot
conditions for the shock wave transition.

In order to avoid the difficulty of shock fitting, Von Neumann and
Richtmeyer[61] introduced a pseudo-viscosity term "q" added to the
pressure term in the Lagrangian equations of motion, which would auto-
matically account for the Rankine-Hugoniot conditions in the presence
of shock waves. This "q-term" is zero, if $\partial u/\partial x \geqslant 0$, and proportional
to $\rho(\partial u/\partial x)^2$, if $\partial u/\partial x < 0$. With this method, which acts only in the
shock region, the shock is no longer a discontinuity; the shock tran-
sition (or other extreme changes) is smooth and extends over a small
number (3 to 5) of mesh intervals. Nevertheless, it has very nearly
the correct jump and travels at very nearly the correct speed through
the gas[59].

The variable profiles taken at specific times along the X-axis, ob-
tained with the "q-method" always show oscillations behind the shock
front. The sharper the shock transition, the more severe are the spu-
rious oscillations, so there must be a compromise between a smooth
profile behind the shock and a sharp transition[59].

If an error made at some point in the calculation tends to increase as
it spreads over the points of the finite difference network, we say
that the difference equations are unstable. If, on the other hand,
this small error decreases or remains the same, the equations are said
to be stable. The stability of finite difference schemes for smooth
flow regions requires the Courant condition[59]

$$\nu = \frac{\rho c \Delta t}{\rho_0 \Delta X} = \frac{c \Delta t}{\Delta X} \leqslant 1 \qquad\qquad C-3-1$$

where $\nu = c\Delta t/\Delta X$ is the Courant number. Here, c is the local sound
speed and $\Delta X/\Delta t$ may be interpreted as the mesh speed, which is the

maximum speed at which a disturbance can propagate from place to place in the space-time network. The Courant condition for stability thus states: "the mesh speed must always be greater than the sound speed". In difference schemes employing the "q-method" the pseudo-viscosity term reduces the permissible time increment Δt by about a factor of three[59]. In studies involving chemical reactions, where reaction rates may depend exponentially on temperature, the spurious fluctuations inherent in the "q-method" render the method almost useless. Zovko and Macek[62], therefore, abandoned the "q-method" in their study of the transition from deflagration to detonation in solid high explosives.

Another method for handling the problem of discontinuities in flows was devised by Lax[63]. While the "q-method" involves a quasi-physical concept and a modification of the equations of motion, the Lax method does neither. Rather, it handles discontinuities by the nature of its differencing scheme. The Lax method has been applied by many investigators to the subject of computation of the initiation of detonation in high explosives[38].

The Lax scheme requires that all differential equations of motion are in the "conservative" Lagrangian from[62,63]

$$\frac{\partial f}{\partial t} = \frac{\partial g}{\partial y} \qquad\qquad C-3-2$$

where the vectors $f = (V,u,E)$ and $g = (u,-p,-pu)$, $E = e+\frac{1}{2}u^2+Q$ for reactive flow problems, and where y is defined by $dy = \rho_0 dx = \rho dX$ with dimension $[kg/m^2]$. The pressure p for the ideal gas equation of state can then be found from

$$p = \frac{\gamma-1}{V} (E-\tfrac{1}{2}u^2-Q) \qquad\qquad C-3-3$$

Lax approximated these equations by a difference scheme of first order accuracy, which enables central space differences and forward time differences to be used,

$$\frac{1}{\Delta t} \{f_j^{n+1} - \tfrac{1}{2}(f_{j+1}^n + f_{j-1}^n)\} = \frac{1}{2\Delta y} (g_{j+1}^n - g_{j-1}^n) \qquad\qquad C-3-4$$

where f_j^n is the value of f at the point $(j\Delta y, n\Delta t)$ in the space-time network. The Lax method is stable if the Courant condition C-3-1 applies[63]. The solution of problems with discontinuities in the flow variables may be obtained without the addition of explicit dissipation terms. In fact, this scheme introduces a diffusion term, which we see by rearranging C-3-4 in the form

$$\frac{1}{\Delta t}(f_j^{n+1}-f_j^n) - \frac{1}{2\Delta y}(g_{j+1}^n-g_{j-1}^n) = \frac{1}{2\Delta t}(f_{j+1}^n-2f_j^n+f_{j-1}^n)$$

which is an approximation to the differential equation

$$\frac{\partial f}{\partial t} - \frac{\partial g}{\partial y} = k\frac{\partial^2 f}{\partial y^2} \qquad \text{where } k = \frac{(\Delta y)^2}{2\Delta t}$$

which is a diffusion equation for the function f. In smooth regions of the flow $\partial^2 f/\partial y^2$ is small and we obtain the ordinary forward difference scheme

$$\frac{1}{\Delta t}(f_j^{n+1}-f_j^n) = \frac{1}{2\Delta y}(g_{j+1}^n-g_{j-1}^n) \qquad\qquad \text{C-3-5}$$

In regions where $\partial^2 f/\partial y^2$ is large, this equation is not valid and the Lax scheme comes into effect. It causes any discontinuities to be replaced by a steep but smooth change without oscillations behind the discontinuities.

The calculation is performed in a staggered manner as follows.

If $f(y,0)$ is known, we can determine $f(y,t)$ for all values of t which are integer multiples of Δt; in particular the values of $f(y,0)$ at the lattice points $y = j\Delta y$, $j = 0, 2, 4 \ldots$ determine $f(y,t)$ at all points of the staggered network $t = n\Delta t$, $n = 0, 1, 2 \ldots$; $y = j\Delta y$, $j+(-1)^n = 0, 2, 4 \ldots$

In Fig. C-7 we indicated by arrows how the staggering calculation is performed; for example, point $(j\Delta y, n\Delta t)$ is determined from points $((j-1)\Delta y, (n-1)\Delta t)$ and $((j+1)\Delta y, (n+1)\Delta t)$.

Calculations carried out by the Lax scheme have the general feature that the width of the transition across a shock depends on the magni-
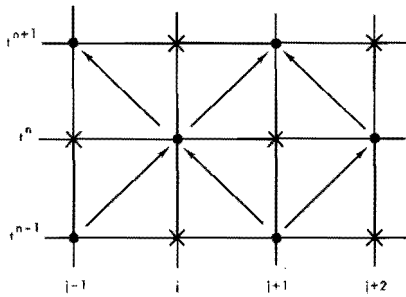
Fig. C-7 Space-time mesh for the Lax method; (●) calculated mesh
points; (x) non-calculated mesh points

tude of $\Delta t/\Delta y$; it is narrower if $\Delta t/\Delta y$ is taken as large as possible[63].
Lax and Wendroff[64] devised a finite difference method which is of
second order accuracy. To check the performance of the Lax scheme against
the Lax-Wendroff scheme[64] we performed several explorative calculations.
Examples of this endeavour are given in Appendix IV. The results show
that the Lax scheme gives quite a good approximation to the actual ana-
lytical calculations. The Lax method is free from spurious oscillations,
which can hardly be suppressed in the Lax-Wendroff scheme. These facts
gave us confidence in the Lax method when it is applied to more compli-
cated flow problems. Moreover, the Lax scheme proved to be 5 to 6 times
"faster" than the Lax-Wendroff (with q) scheme.

Finally, taking into consideration the fact that a complex three-dimen-
sional detonation wave structure is modelled by a simplified one-dimen-
sional wave, it is only reasonable to employ a simple difference
scheme to obtain at least some qualitative understanding of complicated
flow problems. Summing up, the Lax method was chosen to perform the
calculations of the detonation wave reflection problem.

C-§4 Computational results of Model I and Model II studies

For the purpose of simulating the reflection process of a gaseous de-
tonation wave against a solid wall we wrote a computer program based
on the finite difference scheme of Lax. A flow diagram of the program
is given in Appendix V. For most cases investigated the distance co-

ordinate axis X was divided in about 500 zones, i.e. $j = 1, ..., 500$, with the back wall located at $j = 500$. The initial spacing of the zones was typically $\Delta X(x,0) = 0.2$ mm or smaller. The region covered by the computation was thus confined to about ten cm or less in front of the back wall. We found that variation of the mesh width had essentially no effect on the results.

Experimentally, detonation waves are generated in tubes of several meters length. The decrease of pressure, density etc. in the Taylor expansion wave behind the CJ surface is then almost negligeable in our region of interest (see Chapter AII-§4). Computationally, the steady state reaction zone is generated by applying a piston to the flow with a velocity-time history determined by conditions on the Rayleigh line. After establishment of the steady state region the piston velocity is maintained at the CJ particle velocity.

We performed calculations for a number of constant gamma-constant molecular weight mixtures, which closely resemble acetylene- and hydrogen-oxygen detonations for a range of initial pressures, from $p_1 = 1.0132 \ 10^5$ N/m^2 down to $p_1 = 0.1358 \ 10^5$ N/m^2.

We will first discuss some results of the Model I and Model II studies. Representative for all calculations performed is the example of the detonation wave reflection discussed in the preceding sections. Computed pressure-distance profiles of the reflection process for this example are shown in Fig. C-8a and C-8b (Model I: $\tau_{ind} = 7.0$ µs, $\tau_{rel} = 0.0$ µs). When the computer program was started, the time t was set equal to zero. Since only time differences are relevant here, we changed the actual times into the ones indicated in the Figures for reasons of convenience. In the finite difference scheme, where the shock discontinuity is replaced by a smooth transition spread over a few zones, the particle "clocks" were started at $\tau = 0$, when the pressure of the particle reached half the peak pressure in the shock front. About one time increment later, at $\tau \simeq \Delta t$, the peak pressure was attained.

Comparison with the results of Chapter C-§2 shows that the predictions made as to the reflection process for Model I are confirmed. When the detonation wave front collides with the wall, the pressure at the wall
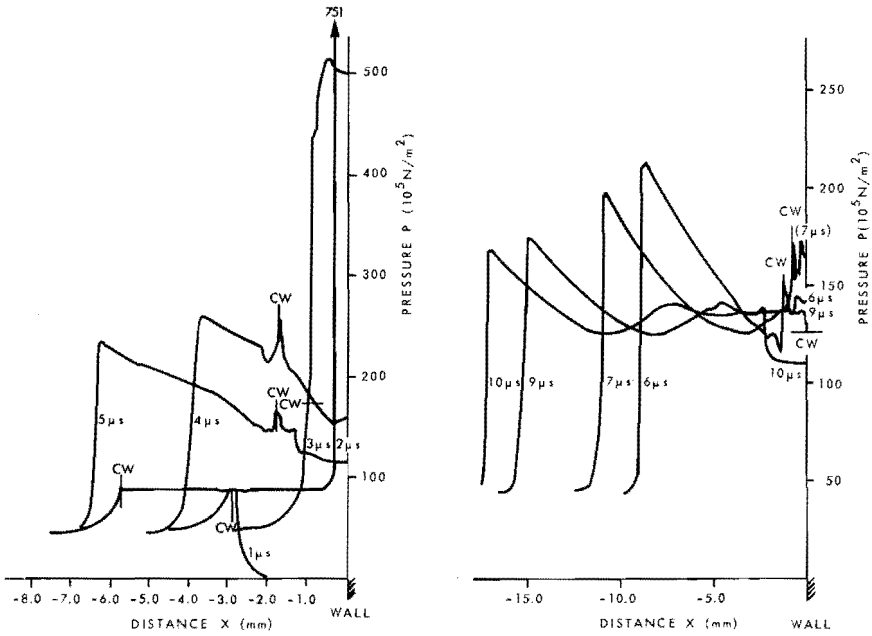
Fig. C-8a   Computed pressure-distance profiles for the reflection pro-
blem; Model I (τ_{ind} = 7.0 μs) of an acetylene-oxygen detona-
tion wave initially at atmospheric pressure; "CW" denotes
position of combustion wave

Fig. C-8b   see Fig. C-8a (continued)

rises steeply; this is followed by a steep decay of the pressure at the
wall due to the effect of the rarefaction waves $\vec{R}_1$ and $\overleftarrow{R}_2$. The head-on
collision of the rarefaction wave $\overleftarrow{R}_2$ with the combustion wave produces
a compression wave which causes the pressure to rise again at the wall.
It is of interest to note, that when we analyse the reflection of a CJ
model of a detonation wave (no reaction zone, CJ conditions immediately
behind the shock front), we obtain as a result for the pressure of the
steady state behind the reflected shock wave resulting from the inter-
action, p_w = 110 10^5 N/m^2. This is very nearly the value of the pressure
attained by the Lax scheme when the combustion wave finally collides
with the wall.

Fig. C-9   Computed pressure at wall p_w as a function of time for a
Model I (τ_{ind} = 9.0 µs) acetylene-oxygen detonation initially
at atmospheric pressure; solid line:from computer solution;
dashed line: from solution by the method of characteristics
(see also Fig. C-10)

Fig. C-10 Reflection process in the X,t-plane as calculated by the
method of characteristics for a Model I (τ_{ind} = 9.0 µs)
acetylene-oxygen detonation initially at atmospheric pres-
sure;
A, B, C and D correspond with those of Fig. C-9; symbols
refer to those of Fig. C-6

The pressure at the wall, p_w, as a function of time for a slightly
longer induction delay time, τ_{ind} = 9.0 µs, is shown in Fig. C-9. The
time scale was chosen in such a way that t = 0.0 µs at the instant the
detonation wave front collided with the wall.

A major disadvantage of the computerized integration of the equations of motion by a difference scheme is, that the computer program merely produces the variable distributions as functions of distance and time. Especially in complicated flow problems it is sometimes difficult to discover the connections between the variable distributions and their causes. The method of characteristics is preferable to finite difference schemes from the point of view of making these causal connections. Since we were particularly interested in the cause of the steep pressure decay and subsequent rise at the wall, we performed a few calculations with the method of characteristics (see Chapter AI-§1) up to the point where the head of the first reflected compression wave reached the wall. In order to keep the number of calculations within reasonable bounds (except for the interaction of the first Q waves with the combustion wave, which was computerized, the calculations were performed on a desk calculator), the rarefaction wave $\vec{R}_1$ was approximated by a family of seven P characteristics. The computed results for Model I (τ_{ind} = 9.0 μs) are shown in the X,t-plane of Fig. C-10. For a comparison with the computer simulation we inserted the pressure profile at the wall, which results from the solution by the method of characteristics, in Fig. C-9 (dashed curve). This shows satisfactory agreement and in particular demonstrates the causal connections of the pressure profile at the wall with the wave interaction process.

The application of Model II, which represents a more realistic law of heat release, did not introduce any new features of the reflection process, with the exception that with increasing value of τ_{rel} the pressure profile at the wall became smoother. This effect is shown in Figs. C-11a and C-11b. We obtained analogous results for the hydrogen-oxygen detonations.

Sofar we have not paid any attention to a realistic value of the induction delay time, which, in fact, was taken arbitrarely large in the examples discussed in order to illustrate the interaction processes clearly. In reality the induction times are much smaller (see Chapter
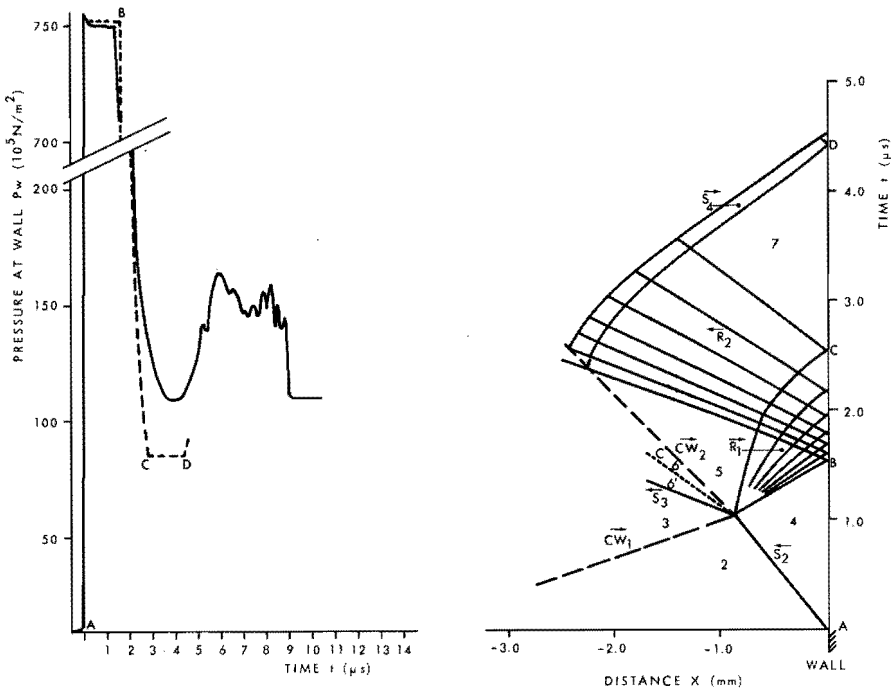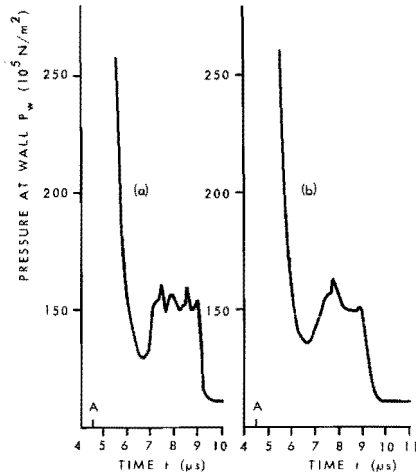
Fig. C-11 Computed pressure profiles at wall as a function of time
for a Model II acetylene-oxygen detonation initially at
atmospheric pressure; (a) τ_{ind} = 4.5 μs; τ_{rel} = 0.1 μs;
(b) τ_{ind} = 4.5 μs; τ_{rel} = 0.25 μs

C-§1), and hence the time scales of the p_w-t records should be taken
correspondingly smaller. However, apart from their value for the anal-
ysis of the interaction rules, the examples treated above offer con-
clusive evidence of the non-validity of previous assumptions made with
regard to observations of the pressure-time history at the back wall
of a tube.

Edwards, Williams and Breeze[25] observed the pressure at the back wall
upon reflection of hydrogen-oxygen mixtures at 1.01 10^5 N/m² initial
pressure with a pressure bar transducer (see Appendix II). They found
that upon collision of the detonation wave with the wall the pressure
rose steeply which was followed by a decay. At approximately 12 μs
after the beginning of the first rise a second steep pressure rise,
which thereafter decayed to the expected reflected CJ pressure, was
observed. For a qualitative explanation of this observation Edwards
c.s. employed essentially a Model I (τ_{ind} = const.) description of the
detonation wave. They assumed that at the point in the tube, where the

first reflected shock wave interacted with - in our terms - the combustion wave, the particle velocity could be taken equal to zero. Reasoning from this hypothesis a shock wave was needed to get consistency with the particle flow in the area between the combustion wave and the wall. Upon collision with the wall this shock wave would then produce the observed second pressure "hump". Although his assumption was erroneous as our calculations show (Chapter C-§2) he did arrive at analogous results as our Model I and Model II studies do with regard to the second pressure "hump". However, in order to obtain quantitative agreement with experimental observations, more particularly as far as the arrival time of the second "hump" at the wall is concerned, our calculations show that then the induction times should be taken unrealistically large. Our own pressure recordings, which will be discussed in the next section, provide us with some more evidence on this subject.

C-§5 Discussion of experimental results

We developed two different types of pressure transducers (see Appendix II). Gauge I (2 mm dia x 1 mm sensing element) is meant as a side-on transducer, but has also been utilised for reflection measurements. Gauge II (10 mm dia x 0.2 mm sensing element) is a high resolution transducer specially developed for reflection measurements. The rise time of this gauge is about 200 nanoseconds.

Fig. C-12 gives an oscilloscope record of the reflected pressure of a $2H_2+O_2$ detonation at initial pressure of $1.01 \cdot 10^5 \, N/m^2$. We clearly discern a second shock wave after the first pressure rise and decay. At about double the time interval between these first two waves a third pressure rise is observed and again a fourth rise at about the same spacing. At lower initial pressures ($< 0.5 \cdot 10^5 \, N/m^2$) the second and following pressure rises became less distinct due to the fact that oscillations became more pronounced. This is presumably due to the transverse wave structure of the detonation waves which apparently became more pronounced at these initial pressures.

In equimolar acetylene-oxygen mixtures similar observations were made (Fig. C-13). In these mixtures the pressure rises, and in particular the second shock waves were quite distinct at all initial pressures em-
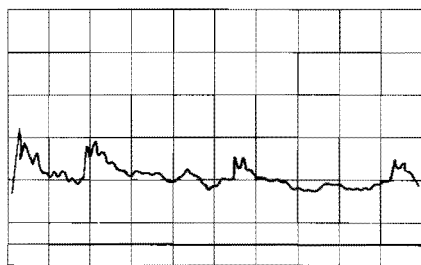
Fig. C-12   Oscillogram of the reflected pressure obtained from gauge I;
$2H_2+O_2$ mixture; $p_1 = 1.01 \ 10^5$ N/m²; time scale 5 μs/div.
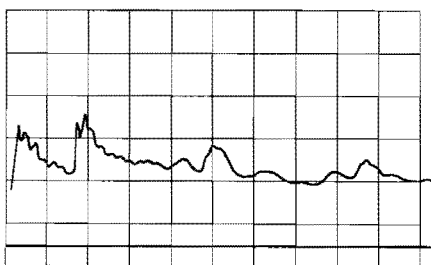
Fig. C-13   Oscillogram of the reflected pressure obtained from gauge I;
$C_2H_2+O_2$ mixture; $p_1 = 0.25 \ 10^5$ N/m²; time scale 5 μs/div.
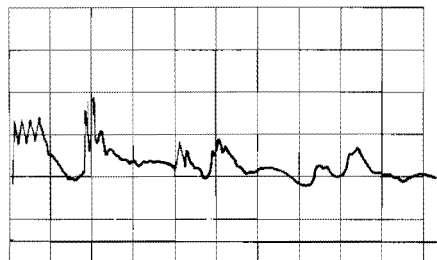
Fig. C-14   Oscillogram of the reflected pressure obtained from gauge I;
$C_2H_2+O_2$ mixture; $p_1 = 0.51 \ 10^5$ N/m²; time scale 5 μs/div.
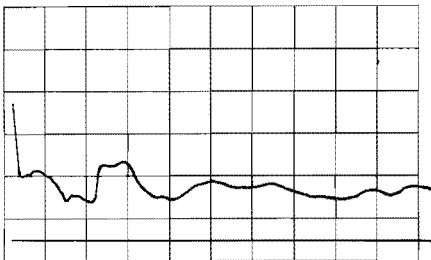
Fig. C-15   Oscillogram of the reflected pressure obtained from gauge II;
$C_2H_2+O_2$ mixture; $p_1 \approx 0.14 \ 10^5$ N/m²; time scale 5 μs/div.

ployed in this work. In some of our experiments it appeared that the
third and fourth pressure "humps" occurred in closely spaced pairs (see
Fig. C-14). Fig. C-15 gives an oscilloscope record made with gauge II.
The second shock wave is quite distinct. Notice the pressure peak at
the start of the record. We will discuss this phenomenon in the follow-
ing sections.
The observed time intervals between the arrival of the first and second
shock wave at the wall turned out to be only slightly dependent on

initial pressure. For acetylene-oxygen mixtures we measured $(7.0\pm0.5)\mu s$, (9.5 ± 0.5) μs and (10.0 ± 0.5) μs at initial pressures of 0.51 10^5 N/m^2, 0.25 10^5 N/m^2 and 0.14 10^5 N/m^2 respectively. For hydrogen-oxygen mixtures we found this time interval to be equal to $(11.0\pm1)\mu s$ at an initial pressure of 1.01 10^5 N/m^2. At lower initial pressures about the same time interval was observed in so far as the second shock wave could be discerned on the records.

Since the induction delay times are approximately inversely proportional to the initial pressure and since the spacings between the first and second shock waves appeared to be almost independent of initial pressure, it may be clear that the results of our experiments lead again to our previous conclusion that the second pressure rise is presumably not connected with the reflection of the reaction zone off the end wall. This is particularly evident from the results of the acetylene-oxygen experiments. Here the induction delay times are extremely small (see Chapter C-§1) and do not seem to have any correlation with the relatively long time intervals that were measured between the first and second shock arrival at the wall.
The observed third and fourth pressure rises at about double the first time interval also do not fit into the picture presented by the Model I and II studies.

Edwards, Jones and Price[66] took streak schlieren photographs through narrow vertical windows placed perpendicular to the detonation tube axis of detonation waves in hydrogen-oxygen mixtures at initial pressure of 1.01 10^5 N/m^2. These photographs revealed a wave pattern of oblique shocks behind the detonation front which was stationary with respect to the front. Similar observations have been made by Fay and Opel[67], and Fay[68] in acetylene-oxygen mixtures. Edwards c.s. identified the pressure peaks on their pressure records as arising from the reflection of these oblique waves at the end wall as observed on the schlieren records.
Fay and Opel suggested that these waves originated from boundary layer effects at the tube wall near the reaction zone. Fig. C-16 gives a
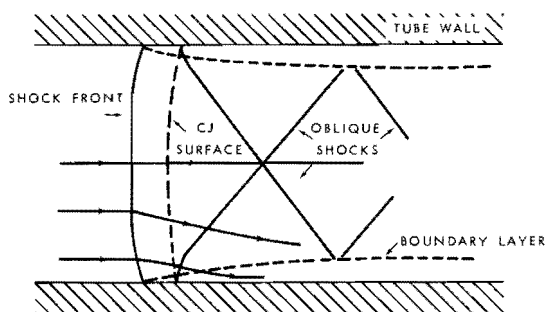
Fig. C-16 Reconstruction of schlieren records taken by Edwards[66] which
shows the oblique shock waves and the divergence of the stream
lines

sketch of the two-dimensional flow behind the detonation wave as re-
constructed from the schlieren photographs[66] . The boundary layer
causes a slight divergence of the flow behind the detonation front and
a slight curvature of the front itself, which is then convex toward
the oncoming flow. As a consequence of the continued growth of the
presumably turbulent boundary layer the continued divergence of the
streamlines causes the flow, that is subsonic in the reaction zone and
that becomes sonic at the CJ surface, to become supersonic behind the
CJ surface. Fay and Opel indicated that in this respect the flow is
analogous to that of reacting mixtures through converging-diverging
nozzles. By analogy with supersonic nozzle flow, oblique shock waves
are established at the interaction point formed by the CJ surface and
the boundary layer. Successive reflections of these waves at the tube
end wall will then give rise to the observed pressure "humps".
This also explains our observations of the apparent independency of
initial pressure of the time spacings between these pressure "humps".
When the oblique shocks are assumed to be sufficiently weak to be re-
garded as Mach waves, the slope of the waves with respect to the tube
axis is entirely determined by the flow Mach number behind the CJ sur-
face[66] . Regardless of the initial pressure the Mach number behind the
CJ surface, where Ma = 1, should be of the same order of magnitude,
which according to Edwards and Fay is about 1.10 to 1.15. Our own ob-

servations of the third and fourth pressure "humps" at about double
the time interval between the first two waves fit in this picture too.

Although the mechanism whereby these oblique waves arise is not yet
completely clear, and in the author's opinion may acquire elucidation
in the future in the light of the present knowledge on the three-dimen-
sional structure of detonation waves, it has been established beyond
question that the flow at the rear of the reaction zone is slightly
supersonic. White[33] came to the same conclusion on the basis of his
turbulent-structure model of detonation waves (see Chapter AII-§1).
It is of interest to note that one of the consequences of the super-
sonic character of the flow behind the CJ surface would be that the
Taylor rarefaction wave (see Chapter AII-§4) of which the head travels
at sonic speed with respect to the gas, cannot be attached directly to
the CJ surface. Like Edwards[25], we observed a pressure plateau behind
the Von Neumann spike which extended to about 20 µs behind the shock
front (see Appendix II).

C-§6 Computational results of Model III studies

The application of a temperature and density dependent induction time
instead of the constant induction time applied for the Model I and II
studies gave results that differed essentially from those discussed in
the preceding sections.
When the detonation wave front collides with the wall a high temper-
ature and high density region is established behind the reflected shock
wave. It turned out that under these conditions the induction delay
times were shortened by a factor of 20 or more. As a consequence the
gas at the end wall is ignited and exothermic reactions start even be-
fore the reflected shock wave has collided with the combustion wave.
Thus behind the reflected shock wave a new combustion wave originates,
which travels in the same direction as the reflected shock wave.
The resultant situation is essentially analogous to that observed in
the initiation of detonation studies behind reflected shock waves,
which are made to determine induction delay times (see Chapter C-§1).

In our case the time scale is much smaller due to the very much higher temperatures and densities than customarily employed in the reflected-shock experiments. It is of interest to dwell upon this subject in order to understand the complicated wave patterns that occur behind the reflected shock wave. Strehlow and Cohen[69] and Soloukhin[8] among others observed the initiation of detonation in gaseous mixtures upon reflection of a shock wave against the end wall of a conventional shock tube. Fig. C-17 shows a sketch of the behaviour they observed for strong shock waves in the X,t-plane.
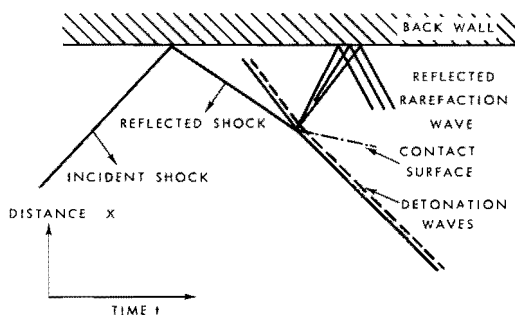
Fig. C-17 The initiation of detonation behind a reflected shock wave[69]

An adiabatic explosion starts a certain space of time, equal to the local induction time, after the reflection of the incident shock wave at the back wall of the tube. This exothermic reaction generates an accelerating pressure wave, which may develop into a detonation wave before reaching the reflected shock wave. This wave then interacts with the reflected shock wave producing a new detonation wave, a contact surface and a reflected strong rarefaction wave. The latter wave will reflect against the end wall and interact with the contact surface and the detonation wave, giving rise to further wave developments.
The analysis of the subsequent wave development has not been investigated thoroughly, because the main interest of these studies lies in the determination of the delay to adiabatic explosion.
Before proceeding with the discussion we will present some of our computational results obtained from the study of the Model III behaviour of the detonation wave.

For Model III it is assumed that the induction delay time is a function of temperature and density (Eq. C-1-4) and that the heat release process is given by Eq. C-1-5. A complete description of the reflection process is only possible for the hydrogen-oxygen mixtures, which system is the only one for which both theoretical and experimental data are known to some extent nowadays. We made the following assumptions as to the values of τ_{ind} and τ_{rel}.

According to the discussion in Chapter C-§1 the induction times measured from detonation waves in hydrogen-oxygen mixtures[27] are about a factor of 3 to 4 larger than those obtained from laminar reactive flow experiments (see Fig. C-2, data from Strehlow and White et al.). However, since the measured τ^o_{ind} data of Jost et al. closely follow the τ_{ind} results of Schott and Kinsey, we decided to employ Schott and Kinsey's formula (see Table C-2) with the exception that the preexponential factor A of Eq. C-1-4 was multiplied by a constant which was equal to the theoretical density ratio across the shock front of the detonation wave (about a factor of 5.5 depending on the initial pressure). Although Jost et al. performed their experiments at relatively low initial pressures ($< 0.2 \ 10^5 \ N/m^2$) we thought it reasonable to extrapolate their data up to $1.0 \ 10^5 \ N/m^2$ by means of Schott and Kinsey's formula for the induction period.

Secondly, reasonable values of τ_{rel} had to be found. To this end we employed the recently compiled data on reaction zone lengths of stoichiometric hydrogen-oxygen detonations by Lu, Dabora and Nicholls[70] (Fig. C-18). The procedure was to adjust the value of τ_{rel} in such a way that the computed length of the reaction zone fell somewhere in the range of experimentally obtained values. To give an example, at $0.14 \ 10^5 \ N/m^2$ τ_{rel} equals 0.5 µs. With this procedure we obtained computed reaction zone lengths indicated by the triangles in Fig. C-18, while τ_{rel} turned out to be slightly more than inversely proportional to the initial pressure. These values of τ_{rel} were applied only to the primary detonation wave. Because of the extreme conditions behind the reflected shock wave τ_{rel} was arbitrarily set equal to zero in this region.
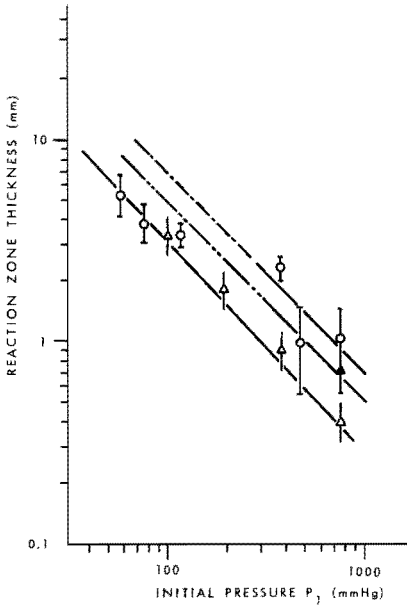
Fig. C-18   Reaction zone thickness as a function of initial pressure for
            $2H_2+O_2$ detonation waves[70];
            ▲ laser schlieren; −·− self emission; −··− time resolved
            schlieren; ⌀ spark schlieren; ⌀ this work (computed)
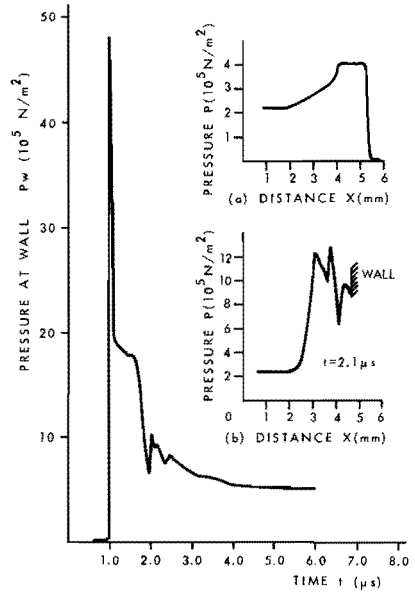
Fig. C-19   Computed pressure at wall as function of time for Model III
            $2H_2+O_2$ detonation at initial pressure of $0.1358 \cdot 10^5$ N/m²;
            $\gamma = 1.23$; $Q_t = 70 \cdot 10^5$ m²/s²; $Q_{tr} = 30 \cdot 10^5$ m²/s²;
            (a) detonation wave prior to collision with the wall;
            (b) pressure profile at t = 2.1 μs

The final assumption was made with regard to the total amount of heat,
Q_{tr}, that would be released behind the reflected shock wave. This
quantity is dependent on thermodynamic conditions behind the shock
wave. One may assume that the reflected detonation wave prior to at-
taining a steady state velocity is close to CJ conditions. We there-
fore assumed that the total amount of heat that is released in the re-
flected detonation wave could be taken as constant and equal to the
amount of heat released in a CJ detonation wave. To obtain this quan-

tity we computed the CJ conditions behind such a wave with the accurate method outlined in Appendix I, while the initial conditions were those of the Von Neumann spike values of the incident detonation wave. The calculations are summarized in Table I-6 of Appendix I. We also computed the Von Neumann spike values of the reflected detonation wave which are given in the same Table. Subsequently the quantity Q_{tr} was then obtained by the method outlined in Appendix III.

The above assumptions were inserted in the computer program. A typical example of the computed pressure at the wall, p_w, as a function of time is given in Fig. C-19 for a $2H_2 + O_2$ mixture at $0.1358 \ 10^5 \ N/m^2$ initial pressure. The pressure distribution in the detonation wave prior to the collision with the end wall is also shown. The p_w, t-profile is explained as follows.

The very high and narrow pressure peak is caused by the wave interaction process sketched in Fig. C-17. Almost immediately upon collision of the shock front of the incident detonation wave with the wall, combustion occurs of the particles near the wall behind the reflected shock wave. This causes the pressure to rise steeply. When the resulting secondary detonation wave overtakes the reflected shock wave, a strong rarefaction wave is reflected towards the wall which causes the rapid decay of the pressure. After this decay a quasi-steady state is established near the wall. When the reflected detonation wave collides with the combustion wave of the incident detonation wave the subsequent wave development can be explained by interaction rule No. 1. The interaction of the shock front of the reflected detonation wave with the incident combustion wave causes a reflected forward facing rarefaction wave. This rarefaction wave is transmitted through the combustion wave of the reflected detonation wave (interaction rule No. 2), which causes the pressure at the wall to decrease further when it collides with the wall.

When finally the combustion waves of the incident and reflected detonation waves collide and when all particles have released their heat, a contact discontinuity is established in the region of interaction separating the particles that were processed by the two combustion

waves. The small pressure rise that is observed is presumably due to a small compression wave which originates from the interaction of the rarefaction wave with this contact region. After that the pressure will continue to decay to the steady (reflected CJ) value.

It is shown that at $t = 2.1$ μs a complicated wave pattern exists in the region in front of the wall. It will also be seen that the very high and narrow pressure peak has decayed rapidly in travelling away from the wall.

In view of these results it seems to be an oversimplification to assume that immediately upon reflection of the shock front of the incident detonation wave a CJ detonation wave is reflected. Both Denisov[71] and Droppleman[72] in their study of the reflection of a detonation wave with a solid wall made this assumption. Denisov's analysis of the process is too concise to be of much value here. Droppleman's thesis is of interest since he performed pressure measurements with a so-called Baganoff pressure transducer (see Appendix II), which has a rise time of 0.1 μs, although the total recording time is limited to less than 5 μs.

Our theoretical calculations of the parameters of this reflected CJ detonation wave (see Appendix I, Table IV and VI) show that behind this wave the product particle velocity is not equal to zero as assumed by these two authors, but that the particles have a finite velocity directed towards the wall. Since the boundary conditions at the wall require the particle velocity at the wall to be zero, adjustment of the flow behind the assumed CJ detonation wave is required. This may be accomplished by a shock wave or by a shock wave followed by a rarefaction wave moving in the product gas behind the CJ detonation wave travelling away from the wall. Although the reflected detonation wave might attain CJ conditions even prior to collision with the combustion wave of the incident detonation wave, it may be clear from the above comments that the flow behind the reflected detonation wave is much more complicated than previously assumed.

From his measurements of the reflected pressure in hydrogen-oxygen mixtures Droppleman obtained the time interval, t_{75}, from first response of

the transducer, due to the collision of the shock front of the incident detonation wave, to 75% decrease of the pressure toward the steady pressure level. His t_{75} data are given as a function of inverse initial pressure in Fig. C-20 by triangles. The solid line is the best fit to his data. We determined t_{75} from our theoretical p_w,t records. For this calculation we disregarded the high and narrow peak, to which no present gauge is able to respond to, and took the peak pressure as the quasi-steady state pressure which occurs prior to the arrival of the reflected rarefaction wave from the interaction of the reflected detonation wave with the incident combustion wave. Our t_{75} results for
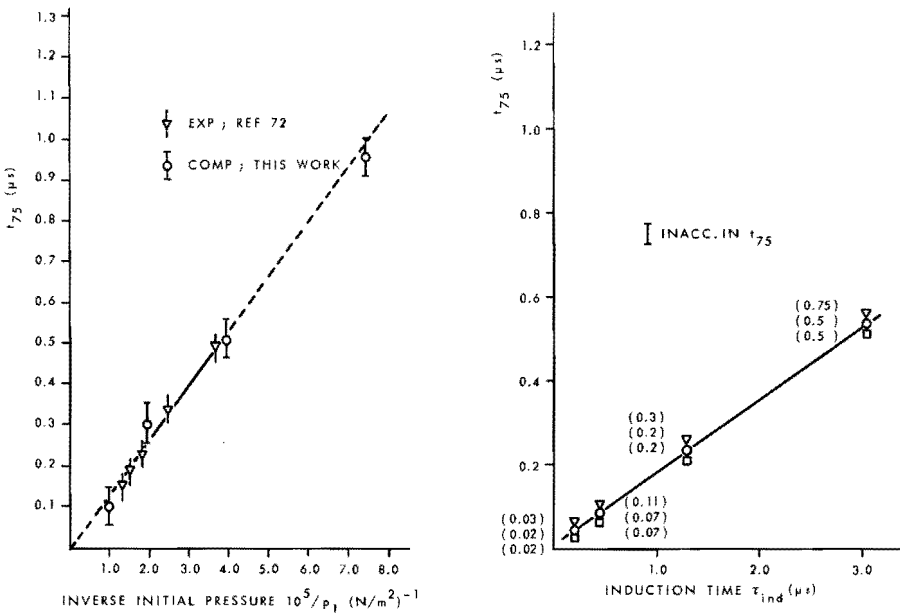
Fig. C-20 t_{75} as a function of inverse initial pressure for $2H_2+O_2$ detonations

Fig. C-21   Computed t_{75} as a function of τ_{ind} for $C_2H_2+O_2$ detonation initially at $p_1 = 0.1358 \cdot 10^5$ N/m^2; numbers in brackets give the value of τ_{rel} in µs; ∇ and x: $Q_{tr} = Q_{ti}/5$; o : $Q_{tr} = Q_{ti}/2$

several initial pressures are shown in the Figure by open circles. The inaccuracy in the determination is also indicated.

The agreement found between Droppleman's extrapolated data and our theoretical values is encouraging but may seem somewhat fortuitous in view of the assumptions previously made.

In order to evaluate the influence of the various parameters that are incorporated in the Model III study of the detonation wave, we decided to perform some calculations on equimolar acetylene-oxygen mixtures, for which system even the induction time data are uncertain. This parameter study was done at an initial pressure of $0.1358 \cdot 10^5$ N/m^2. The parameters, that were varied, were the total amount of heat Q_{tr} added to the reflected combustion wave, the heat release "relaxation time" τ_{rel} and the induction delay time of the incident detonation wave. The results are given in Fig. C-21. It is evident that both a change in Q_{tr}, which has a small effect on the peak pressure of the quasi-steady state, and a change in τ_{rel} have a small effect on the t_{75} data. The dominant parameter appears to be the induction time. It is seen that over the range of variation of τ_{ind}, t_{75} is linearly dependent on τ_{ind}. If at this initial pressure an induction time of the order of 0.2 μs is assumed, which is one order larger than the one obtained from laminar reactive flow experiments[28], it appears that t_{75} is then of the order of 0.05 μs - 0.1 μs. Since the rise time of presently existing pressure transducers is of the same order, we may not expect to be able to measure t_{75} of these mixtures reliably in this pressure range.

C-§7 Experiments

Although the rise time of gauge II (0.2 μs, see Appendix II) is not sufficiently small to resolve t_{75} reliably from our records of the reflected pressure, we would like to present a few typical oscillograms of the reflected pressure made with this gauge. Three oscillograms of the reflected pressure of a stoichiometric hydrogen-oxygen mixture are given in Figs. C-22a, 22b and 22c for the initial pressures of $0.25 \cdot 10^5$ N/m^2, $0.33 \cdot 10^5$ N/m^2 and $0.53 \cdot 10^5$ N/m^2 respectively. The gauge response clearly exhibits qualitatively the predicted pressure
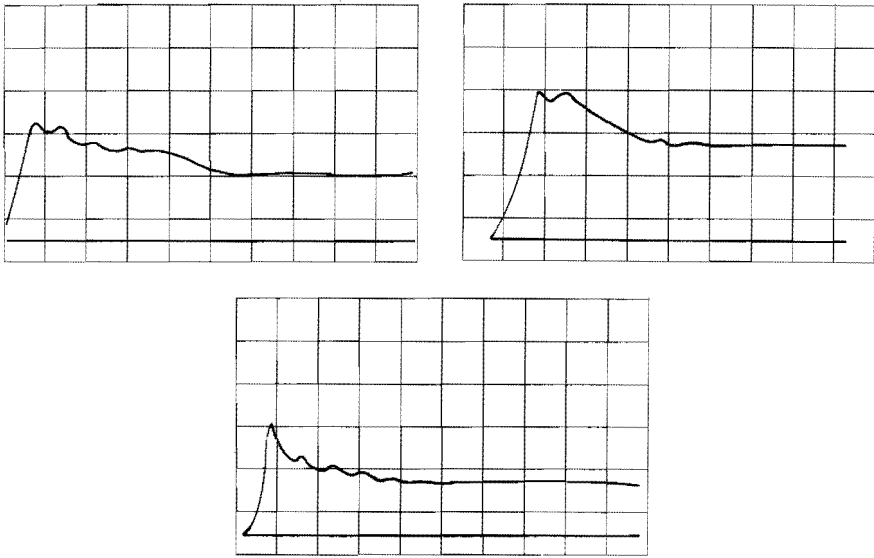
Fig. C-22 Oscillograms of the reflected pressure obtained from gauge II;
$2H_2+O_2$ mixture; (a) $p_1 = 0.25 \ 10^5 \ N/m^2$; (b) $p_1 = 0.33 \ 10^5 \ N/m^2$,
(c) $p_1 = 0.53 \ 10^5 \ N/m^2$; all time scales 0.2 $\mu s/div$.
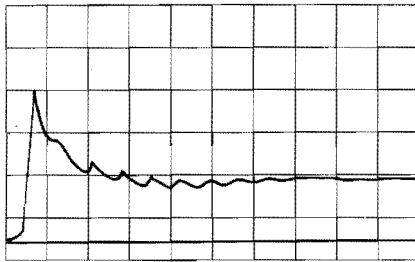
Fig. C-23 Oscillogram of the reflected pressure obtained from gauge II;
$C_2H_2+O_2$ mixture; $p_1 = 0.14 \ 10^5 \ N/m^2$; time scale 0.2 $\mu s/div$.

peak and pressure decay. It may also be seen that the order of magni-
tude of the duration of the pressure peak is in qualitative agreement
with theory and that it becomes smaller with increasing initial pres-
sure.
It was also observed that the gauge signal became less reproducable
and showed a lower peak pressure than would be expected from the rise

time of the gauge at initial pressures smaller than $0.3 \cdot 10^5$ N/m^2. This is presumably due to the pronounced transverse structure of the detonation wave in these mixtures at low initial pressures. The equimolar acetylene-oxygen mixtures, however, still showed a reproducable high pressure peak at the lowest initial pressure employed in this work, which may be seen from the oscillogram of Fig. C-23. This fact provides additional evidence that the induction delay times of acetylene-oxygen mixtures are much smaller than those of hydrogen-oxygen mixtures at the same initial pressures.

It seems feasible to construct a piezoelectric gauge of the type II which has a rise time comparable with that of the Baganoff gauge by reducing the thickness of the sensing element to 0.1 mm. Improved gauge construction would then provide a gauge which is superior to the Baganoff gauge as it has a relatively long recording time combined with a small rise time.

C-§8 General discussion

The primary purpose of PART C is to illustrate the applicability of the interaction rules 1 and 2 which were developed in PART B. It was shown that these rules govern the reflection process of a gaseous detonation wave with a solid wall. From Model I and II computer studies, which may be regarded as a hypothetical experiment in view of the assumed constancy of the induction time, a typical pressure profile at the wall is obtained which shows some qualitative resemblance with experimentally observed pressure profiles. Further experimental and theoretical evidence was provided which shows conclusively that the second and following pressure "humps" cannot be correlated with the reflection process of the reaction zone. These humps are apparently caused by the reflection of previously observed oblique shock waves that travel behind the incident detonation wave.

The Model III studies, in which a temperature and density dependent induction time is applied, give a more realistic representation of the reflection process than the preceding models. It is made plausible that the interaction rules 1 and 2 govern the experimentally observable decay of the pressure at the wall. Employing realistic induction times

and reaction zone lengths,we obtained reasonable agreement with exist-
ing experimental observations of the characteristic decay time, t_{75},
in hydrogen-oxygen mixtures.

Our results were obtained assuming that a three-dimensional multiheaded
detonation wave can be modelled by a one-dimensional laminar wave con-
sisting of a shock and combustion wave. The chain branching reactions,
which in reality govern the induction zone structure of this wave,
were modelled by a temperature and density dependent induction delay
time relation, while the heat releasing recombination reactions were
modelled by an exponential heat release law, the rate of heat release
being given by a characteristic "relaxation time". These models have
been successfully applied to the initiation to detonation studies in
laminar reactive flows. Our survey of induction delay times indicates
that (laminar) induction times of hydrogen-oxygen mixtures when extra-
polated to detonation wave conditions are significantly smaller than
experimentally observed ones. A similar observation was made by
Soloukhin[28] for stoichiometric acetylene-oxygen mixtures, which he
explained by referring to the expanding (nonreactive) blast wave struc-
ture of the detonation wave.

In view of the fact that a first order accurate finite difference
scheme was used for the calculations, and in view of the assumptions
made as to the equation of state (constant gamma-constant molecular
weight gas), the amount of heat released and as to the models, these
calculations may be considered as exploratory as they were meant to
be. The author believes that refined calculations may not even be jus-
tified because the results will still have significance only on the
average, as long as the primary assumption will remain that a complex
three-dimensional detonation wave structure is modelled by a laminar
one, which, in fact, is the best we can do at the present state of
knowledge.

PART D - ON THE DETERMINATION OF THE REACTION ZONE LENGTH OF HIGH
        EXPLOSIVES BY THE PLATE-VELOCITY METHOD

Measurements of detonation pressures and reaction zone lengths of high
explosives are important to the physical understanding of the detona-
tion mechanism and its applications. The plate-velocity technique,
where the free-surface velocities of thin metal plates in contact with
an explosive are observed, provides such information. In Chapter D-§1
the method is discussed in particular with regard to the determination
of the reaction zone length. In Chapter D-§2 it is suggested that the
interaction rules developed in PART B provide an explanation for the ob-
served discrepancies in reaction zone lengths.

D-§1 Introduction

Goranson[80,81] is credited with the suggestion that the reaction zone
profile of detonating high explosives could be determined by studying
the free-surface velocity imparted to thin metal plates in contact with
the explosive as a function of plate thickness. Duff and Houston[80] and
Deal[81] measured the CJ pressures and reaction zone lengths of several
high explosives, like Composition B (64/36 RDX/TNT) and TNT, by this
plate-velocity method. The initial free-surface velocity, u_{fs}, imparted
to the plates was found to change with plate thickness as shown schemat-
ically by the solid curve in Fig. D-1.
The observed behaviour of the u_{fs} vs d curve, which is regarded as a
confirmation of the ZND model of a detonation wave, was explained as
follows. When a plane detonation wave impinges normally on an inert
plate, a shock wave is transmitted followed by a steep rarefaction wave
corresponding to the pressure decay in the reaction zone of the explo-
sive. This, in turn, is followed by a more gradual rarefaction corres-
ponding to the Taylor wave pressure distribution of the explosive. The
strength of the transmitted shock wave will first decrease relatively
quickly because of the small thickness of the reaction zone (of the
order of 1 mm for solid high explosives) and then much slower due to
the effect of the transmitted Taylor rarefaction wave. The shock impe-
dance (see Appendix VI) discontinuity at the interface also causes a
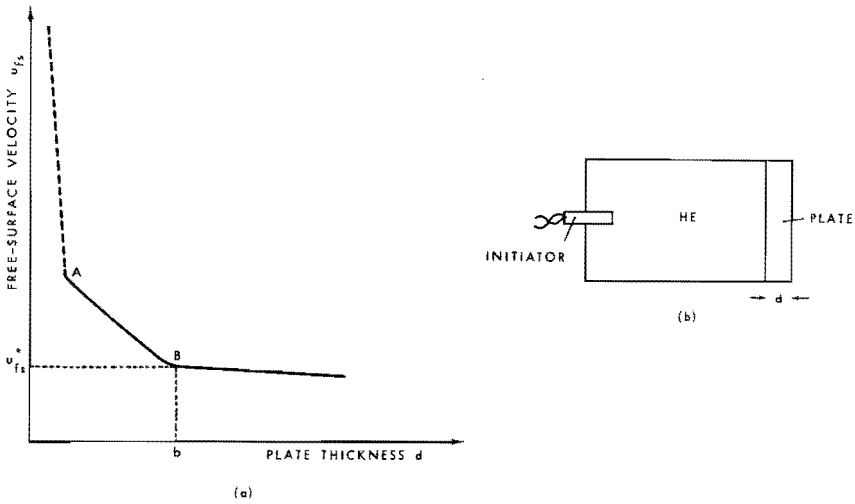
Fig. D-1 (a) Free-surface velocity u_{fs} of an inert plate as a function
of plate thickness d; solid curve as measured by Duff/Houston;
dotted curve as measured by Hauver and Craig.
(b) Schematic view of experimental set-up

shock or rarefaction wave, depending on the direction of change of im-
pedance, to be reflected back into the explosive. The effect of this
reflected wave on subsequent wave developments and reaction kinetics is
assumed to be negligible.

The following expression can be derived (see Appendix VI) relating the
CJ pressure p_{CJ} of the explosive to the transmitted pressure p_{2m} in a
metal plate

$$\frac{p_{CJ}}{p_{2m}^*} = \frac{\rho_1 D + \rho_{1m} U_{1m}^*}{2\rho_{1m} U_{1m}^*}$$

D-1-1

where D is the detonation velocity, ρ_1 the density of the undetonated
explosive, ρ_{1m} the density of the unshocked metal, p_{2m} the shocked
pressure in the metal and U_{1m} the shock velocity in the metal. Super-
script $*$ refers to the conditions in the metal at the break B of the
u_{fs} vs d curve.

For the materials employed in the plate-velocity method experimental
relations between the shock velocity U_{1m} and shock particle velocity
u_{2m} have been determined[82]. In the region of interest $(p_{2m} > 100 \text{ kbar})$
these relations are, to a good approximation, given by the linear equa-
tion

$$U_{1m} = a + cu_{2m} \qquad\qquad D-1-2$$

where a and c are constants.
The following relation (see Appendix VI) gives the pressure behind the
(strong) shock wave into the material at rest

$$p_{2m} = \rho_{1m}u_{2m}U_{1m} \qquad\qquad D-1-3$$

It has been shown[82,83] that, to a very good approximation, the shock
particle velocity of an inert plate is one-half the initial free-surface
velocity

$$u_{2m} = \tfrac{1}{2}u_{fs} \qquad\qquad D-1-4$$

Combination of D-1-2 through D-1-4 gives

$$p_{2m} = \tfrac{1}{2}\rho_{1m}u_{fs}(a+\tfrac{c}{2}u_{fs}) \qquad\qquad D-1-5$$

which shows that p_{2m}^{*} and thus p_{CJ} can be determined from the measured
free-surface velocity and the known properties of the high explosive
(ρ_1,D) and the material (ρ_{1m}).

Craig[84] performed free-surface velocity measurements on very thin
plates adjacent to the explosive to obtain the structure of the reac-
tion zone of condensed explosives. He observed two distinct changes in
the slope of the initial free-surface velocity versus plate thickness
curve. This is indicated in Fig. D-1a by the dotted line and break
points A and B. It is not generally known that the region of rapidly
falling velocity was first noted by Hauver and Eichelberger[85] by means
of the promising technique of shock-induced polarization of Plexiglas'
disks adjacent to the monitor plate.

Craig's conclusion was that the structure of a detonation wave consists of three zones: 1) a reaction zone, 2) a decay zone, 3) a zone of relatively slowly falling pressure. The region of rapidly falling pressure (dotted line) is due to the reaction zone. A decay zone follows the reaction zone, which in turn is followed by the Taylor wave. The pressure corresponding to the *first* break in the curve was called the CJ pressure. Craig, however, gave no explanation for the presence of a decay zone. This interpretation leads to CJ pressures which are about 15% higher than theoretical pressures derived from thermo-gasdynamics calculations and than CJ values measured more directly[86,87]. It turns out that the value of the CJ pressure derived from the second break B in the curve is in agreement with these values. Nevertheless Craig argued that their discrepancy in the pressure invalidates the ZND theory for condensed explosives.

The anomaly of the "observed" decay zone was recently removed by Petrone[87], who, on the basis of ad hoc assumptions about reaction kinetics, made numerical computer calculations of the flow resulting from a detonating charge in contact with metal plates of varying thicknesses. He was thus able to reproduce one of Craig's curves. Petrone suggested from his computer results that the first break A in the curve represented the "image" of the point of inflection in the pressure profile of the detonation wave, where there is a maximum in the pressure gradient, since the pressure distance profile must be concave downward (due to kinetics) at the shock front and concave upward at the CJ plane (due to continuity). This necessitates the inflection point somewhere in between. The CJ point was thus again identified with the second break B in the u_{fs} vs d curve.

Duff and Houston[80] also developed a relation to calculate the reaction zone thickness from a knowledge of the free-surface velocity versus thickness of the plate and other characteristics of the explosive and of the inert plate material. The equation for the reaction zone length "l" was developed from a geometric analysis of the distance-time representation of the interactions between the Von Neumann spike of the explosive and the plate (see Fig. D-2).
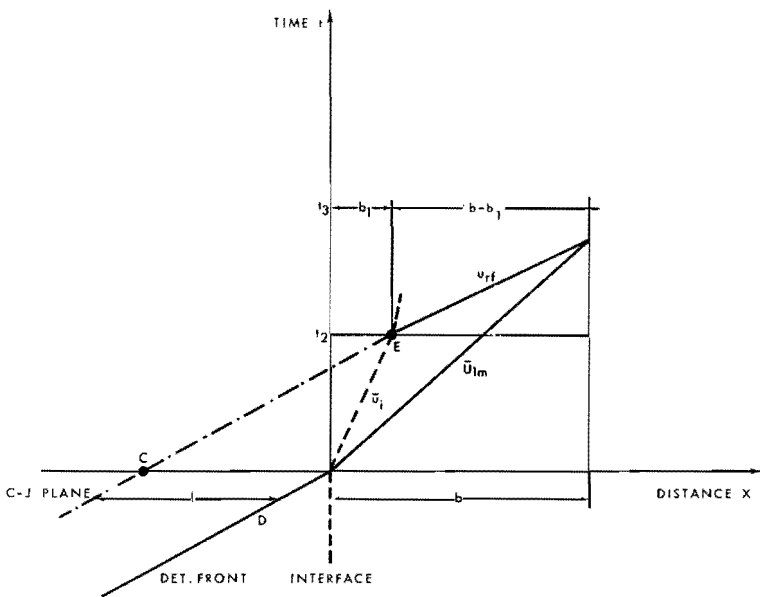
Fig. D-2 Distance-time representation of the interaction between the
Von Neumann spike in the explosive and the plate

For this analysis it was assumed that reflected waves could be neglect-
ed (perfect impedance match). An estimate of the reaction zone length
can be made from a determination of the distance required for the tail
of the rarefaction wave corresponding to the CJ plane to overtake the
shock wave in the inert material. The interface is initially assumed to
be at X = 0. A detonation wave comes in from the left with a velocity
D. The average velocity of the interface is $\bar{u}_i$, the average shock velo-
city in the material is $\bar{U}_{1m}$ and the velocity of the tail of the rare-
faction wave is u_{rf}. As the interaction proceeds the interface and
shock velocity in the material will vary. The appropriate average to
be used is the inverse average, i.e.

$$\bar{U}_{1m} = \left(\frac{1}{b} \int_0^b \frac{dX}{U_{1m}(X)} \right)^{-1} \qquad\qquad D-1-6$$

Likewise $\bar{u}_i$ is determined from a similar inverse average. In order to show the crucial point in the reasoning we will perform the analysis as follows. From Fig. D-2 we find

$$t_3 = t_2 + (t_3 - t_2) \qquad\qquad \text{D-1-7}$$

where

$$t_3 = \frac{b}{\bar{U}_{1m}} \ , \quad t_2 = \frac{b_1}{\bar{u}_i} \quad \text{and} \quad (t_3 - t_2) = \frac{b - b_1}{u_{rf}} \ .$$

This gives

$$\frac{b}{\bar{U}_{1m}} = \frac{b_1}{\bar{u}_i} + \frac{b - b_1}{u_{rf}} \qquad\qquad \text{D-1-8}$$

Secondly we find from the distance-time plane

$$\frac{b_1}{1} = \frac{\dfrac{b_1}{\bar{u}_i} - \dfrac{1}{D}}{\dfrac{1}{D}} \qquad\qquad \text{D-1-9}$$

which is based essentially on the straightness of the line CE. Elimination of b_1 from D-1-8 and D-1-9 gives the following expression for the reaction zone length

$$1 = b \ \frac{(D - \bar{u}_i) \ (u_{rf} - \bar{U}_{1m})}{\bar{U}_{1m}(u_{rf} - \bar{u}_i)} \qquad\qquad \text{D-1-10}$$

We note that this derivation is strictly valid only if we assume that all heat release occurs instantaneously and completely at the CJ plane (Model I of a detonation wave). In general, however, even assuming a perfect impedance match, when the heat release occurs gradually during the entire length of the reaction zone, that part of the reaction zone which has already collided with the interface will produce a transmitted rarefaction wave *and* a reflected rarefaction wave running backwards through the remaining part of the reaction zone. This point seems to have been overlooked in literature, but is clearly demonstrated by the shock/combustion wave theory of a detonation wave (see Fig. D-3).
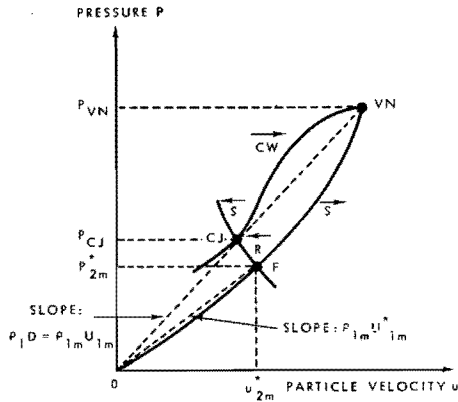
Fig. D-3 Schematic representation of the interaction in the p,u-plane
in the case of a perfect impedance match
O-F-VN : Shock locus of undetonated explosive and inert mate-
rial coincide;
CJ-F : locus of states behind reflected wave into explosive
products (at CJ conditions)

In the case of a perfect impedance match the shock locus of the inert
material and the undetonated high explosive coincide in the region of
pressures given by point VN (curve O-VN). In this way no wave is re-
flected back into the explosive at the first instant when the shock
front of the detonation wave interacts with the interface. It is not
unreasonable to assume that these shock loci will remain coincident in
the entire region of interest given by the pressure range P_{CJ} to P_{VN}.
The slope of the straight line O-CJ-VN represents the value of the de-
tonation velocity and the initial velocity of the shock wave transmit-
ted into the inert material. From the analysis of the shock/combustion
wave complex (see PART A) we know that the CJ point is located on the
combustion wave locus VN-CJ on the left hand side of the shock locus.
If the explosive products are assumed to be at CJ conditions (neglect-
ing the Taylor wave), the final state in the inert material, when all
transient wave phenomena due to the presence of the Von Neumann spike
have died down, is given by point F. This can be seen by considering

the interaction of a CJ model of a detonation wave (negligible reaction zone) with the inert material. By drawing the loci of all possible states on the right of the backwards reflected wave into the CJ products (curve CJ-F) it is seen that this wave is a rarefaction wave. The final velocity of the shock wave in the inert material is then represented by the slope of the line 0-F.

It may be clear that this reflected rarefaction wave will be generated as soon as the front part of the combustion wave starts to interact with the interface. Consequently, the tail part of the combustion wave collides head-on with the front part of the generated rarefaction wave. This will cause the line CE of Fig. D-2 to become curved and relation D-1-10 no longer applies rigorously, even in the case of a "perfect" impedance match. It is also clear that a mismatch between the explosive and the inert material will produce a reflected shock or rarefaction wave immediately upon interaction of the detonation shock front with the interface. These waves also will change the velocity of the CJ plane, thus invalidating Equation D-1-10.

Recently Jameson and Hawkins[88] published effective reaction zone lengths, l_{eff}, which were obtained by applying Eq. D-1-10 to the results of the plate velocity method for TNT with four impedance combinations: a shock wave would be reflected back into the TNT reaction zone from the monitor materials brass (result: l_{eff} = 0.4 mm) and aluminum (result: l_{eff} = 0.3 mm), while a rarefaction wave would be reflected from Plexiglas (result: l_{eff} = 0.7 mm). A magnesium monitor is nearly a "perfect" match for TNT and there would be no reflection (result: l_{eff} = 0.6 mm). These results for TNT reaction zones differ widely. Jameson and Hawkins suggested that the reaction could be slowed as the pressure in the reaction zone dropped by a reflected rarefaction wave and, conversely, accelerated when the pressure was increased by a shock wave. This would then account for the observed behaviour of l_{eff} of TNT with the four impedance combinations.

We would like to reconsider the effect of a reflected shock or rarefaction wave on the apparent length of the reaction zone of high explo-

sives in the light of the interaction rules developed in PART B. Intuitively we may expect that a reflected shock wave colliding with the combustion wave part of the detonation wave will generate a forward facing rarefaction wave (interaction rule No. 1), which after being transmitted through the interface will cause the free-surface velocity to decrease more steeply than as a result of the decrease caused by the rarefaction wave corresponding to the reaction zone-interface interaction alone. Conversely, if a backward facing rarefaction wave is generated at first interaction of the shock front of the detonation wave with the interface, this will cause a forward facing compression wave (interaction rule No. 2) after collision with the combustion wave. This compression wave upon transmission through the interface may cause a slower decay of the u_{fs} vs d curve than in the case of a perfect impedance match. In the former case the transmitted rarefaction wave may thus effect the calculated reaction zone length to appear shorter, while in the latter case because of the compressive action this length would appear to be longer than in the case of a perfect impedance match. This will be the subject of the next Chapter.

D-§2 Discussion of computational results

To obtain the solution to the flow resulting from a detonating high explosive charge in contact with inert plates of various thicknesses we performed a series of numerical computations.
The calculation method involved the solution by the finite difference scheme of Lax of the one-dimensional Lagrangian gasdynamics equations, the equations of state and a law for the explosive decomposition.
The Lax method has been discussed in Chapter C-§3. About 300 zones were available for the high explosive, while the original mesh width was generally equal to 0.05 mm. As in previous calculations variation of the mesh width was found to have essentially no effect on the results. The inert material comprised about 500 zones. The equations of state of both the high explosive and the inert material were taken to be the constant gamma ideal gas relation. For the former medium this is a good approximation for the product gases in the pressure range of interest with the isentropic exponent equal to about three[91].

For both the undetonated explosive and the inert material it would have
been more realistic to employ a solid state equation of state, like the
Grüneisen equation of state. Since the emphasis was not on quantitative
agreement with experimental details but rather on the qualitative ef-
fect of the waves reflected from the shock impedance discontinuity, any
equation of state would do. The initial conditions for the high explo-
sive for the specific examples to be discussed here are given in Table
D-1.

TABLE D-1

Initial conditions for the high explosive.

	Initial conditions	CJ conditions	VN spike conditions
p $[10^{+11}$ N/m$^2]$	$1.013 \ 10^{-6}$	0.210	0.419
V $[10^{-3}$ m^3/kg$]$	1/1.6	0.469	0.313
u [m/s]	0.0	1810	3620
$Q_t = 32.8 \ 10^5$ m^2/s^2; $\gamma_1 = 3.0$			

Following earlier theoretical work[38] the decomposition of an heteroge-
neous condensed explosive is assumed to obey the so-called two-thirds-
power rate law given by the grain-burning model of Eyring

$$\frac{d\beta}{dt} = A(1-\beta)^{2/3} \qquad\qquad\qquad D-2-1$$

Factor A is in general a function of pressure and temperature. In order
to rule out any effect of chemical kinetics it was assumed for this
work that A is a constant. When we replace A by $1/\tau_{rel}$, it can be seen
that τ_{rel} is the rate determining factor of the decomposition, which is
completed at $\tau = \tau_{ind} + 3\tau_{rel}$, where τ is taken from the instant a
particle crosses the shock front of the detonation wave. For the same
reason τ_{ind} was taken to be a constant.
The steady state reaction zone is generated by applying a piston with
a velocity-time history determined by conditions on the Rayleigh line.
The piston velocity is maintained at the CJ particle velocity after

establishment of the steady state region. In this way the effect of the Taylor wave is eliminated.

Like Petrone[87], instead of calculating u_{fs} for each different plate thickness, a single run was made in which the shock attenuated as it travelled through the plate material. To find the value of u_{fs} for any plate thickness the approximation $u_{fs} = 2u_{2m}$ was made, where u_{2m} is the calculated shock particle velocity at that point.

Typical pressure-distance profiles are shown in the inserts of Figs. D-4 and D-5. Two typical examples of the calculated free-surface velocity versus plate thickness d for inert materials with the same shock impedance as the explosive, therefore producing no reflected wave at the first instant of interaction, are shown in Fig. D-4.
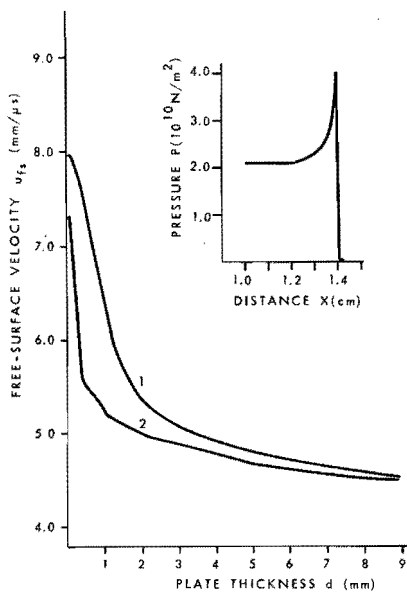
Fig. D-4 Calculated free-surface velocity of inert plates (ρ_{1m} = 1.6 g/cm^3, γ_m = 3.0) as a function of thickness d;
Curve 1: τ_{ind} = 0.05 μs; τ_{rel} = 0.1 μs; curve 2: τ_{ind} = 0.01 μs; τ_{rel} = 0.1 μs.
The insert shows the pressure-distance profile of the detonation wave (2)

The first part of the u_{fs} vs d curve shows a rapid decay, while the second part shows a much slower decay, which is essentially in quali-tative agreement with Craig's observations (see Fig. D-1), although a decay zone is not needed to obtain these results. At first sight these curves also appear to confirm Petrone's suggestion that the profile of u_{fs} vs d curve is the image of the reaction zone profile. We would like to suggest that a mechanism different from a mere transmission of the reaction zone into the inert material attributes to the rather abrupt changes in slope and the relatively long decay distance to steady state values.

In the previous section it was made plausible that, even in the case of a perfect impedance match, a rarefaction wave is reflected back into the tail part of the reaction zone when the front part interacts with the interface. This has an interesting consequence for the subsequent flow in the inert material. According to interaction rule No. 2 the front part of the reflected rarefaction wave in running backwards through the tail part of the reaction zone will generate a forward facing com-pression wave. We suggest that the delayed arrival of the forward fa-cing compressive action on the flow superimposed on the transmitted rarefaction wave which corresponds to the interaction of the reaction zone with the interface causes the rather abrupt change in slope of the u_{fs} vs d curve and the relatively long period to decay to steady state conditions.

In order to test the validity of Eq. D-1-10 of the reaction zone length we evaluated several results completely. A typical example is shown in fig. D-5 for three different shock impedance combinations. Curve 1 corresponds to a lower shock impedance than the explosive one (reflected rarefaction wave at first instant of interaction), curve 2 to a perfect impedance match (no reflected wave) and curve 3 to a higher shock im-pedance than the explosive (reflected shock wave). The parameters $\bar{U}_{1m}$ and $\bar{u}_i$ were computed by means of Eq. D-1-6. Computed results are shown in Table D-2. The calculations were based on the value of b obtained by determining the point where the shock velocity in the inert material has reached its final value within 5% of the difference between its ini-tial and final value.
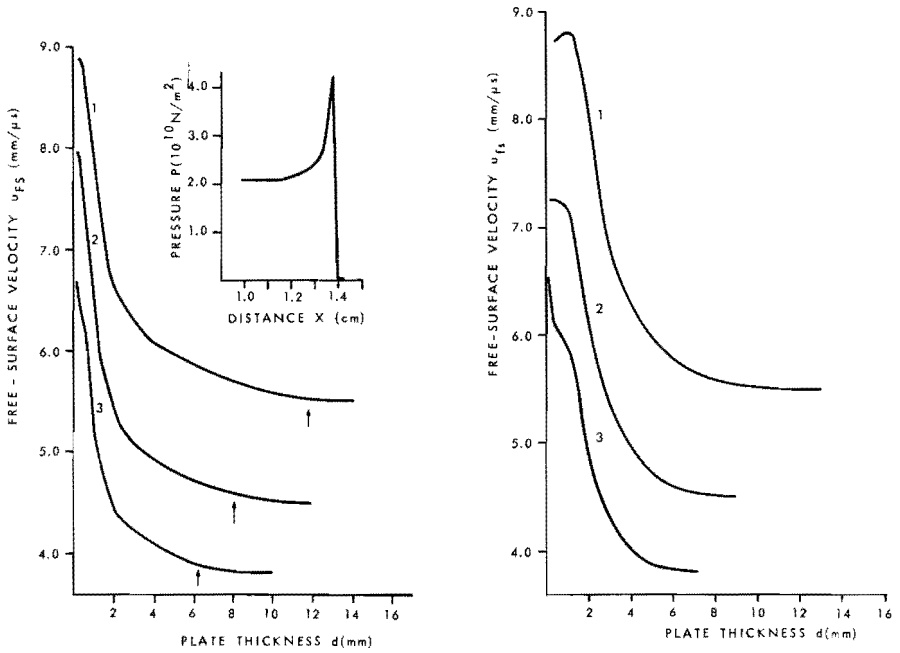
Fig. D-5 Calculated free-surface velocity of inert plates ($\gamma_m = 3.0$)
as a function of thickness d;
Curve 1: $\rho_{1m} = 0.8$ g/cm^3; curve 2: $\rho_{1m} = 1.6$ g/cm^3; curve 3:
$\rho_{1m} = 2.7$ g/cm^3. Arrows indicate the value of b.
The insert shows the pressure-distance profile of the detona-
tion wave ($\tau_{ind} = 0.05$ μs; $\tau_{rel} = 0.1$ μs)

Fig. D-6 Calculated free-surface velocity of inert plates ($\gamma_m = 3.0$)
as a function of thickness d; same densities as in Fig. D-5;
detonation wave: $\tau_{ind} = 0.1$ μs, $\tau_{rel} = 0.02$ μs

An error analysis of these calculations (including a variation in b up
to the 99% limit and a change in mesh width of $\pm$ 30%) showed that the
l_{eff} values were accurate within $\pm$ 0.04 mm.
The p_{CJ} values were obtained from Eq. D-1-1 and are in good agreement
with the actual value of p_{CJ} (Table D-1). It is of interest to note
that Eq. D-1-1 was derived for a reflected shock wave. In all cases of
Table D-2 in the final state a rarefaction wave is reflected since ρ_{1m}

TABLE D-2

Computed parameters for the
calculation of l_{eff} from D-1-10

		Curve 1	Curve 2	Curve 3
ρ_{1m}	$[g/cm^3]$	0.8	1.6	2.7
$\bar{U}_{1m}$	$[mm/\mu s]$	6.21	5.18	4.48
b	$[mm]$	11.7	8.0	6.2
$\bar{u}_i$	$[mm/\mu s]$	3.00	2.51	2.10
u_{rf}	$[mm/\mu s]$	7.47	6.15	5.21
l_{eff}	$[mm]$	2.25	1.95	1.67
p_{CJcalc}	$[10^{+11}\ N/m^2]$	0.215±0.05	0.211±0.05	0.209±0.05

$\gamma_m = 3.0$; $l_{real} = (1.90\pm0.02)$ mm

is smaller than $2\rho_1$ (see Appendix VI). However, in the region near the CJ point in the p,u-plane the shock and rarefaction wave loci coincide to a good approximation (see Chapter BI-§2) so that Eq. D-1-1 will still apply with some reliability.

The l_{eff} data show a similar trend as the ones observed by Jameson and Hawkins, i.e. a larger shock impedance than the explosive gives a smaller value of l_{eff} than in the case of a perfect impedance match, while conversely a smaller shock impedance than the explosive gives a larger value of l_{eff} than for a perfect impedance match.

From the u_{fs} vs d curves for the different cases it is seen that specially the first part of the curves is rather different for each one. Curve 1 shows an initial decay which is much smaller than that of curve 2 and 3. The cause of these differences in decay can be seen more clearly when we expand the distance-time scale somewhat by taking τ_{ind} larger. Fig. D-6 shows the three cases of shock impedances. Curve 1 (reflected rarefaction wave at first instant of interaction) exhibits a small rise in u_{fs} before it starts to decay. Curve 2 is initially

flat (no reflected wave), while curve 3 (reflected shock wave) starts
to decay immediately. This behaviour proves our earlier suggestion
(Chapter D-§1) that a backward facing reflected rarefaction wave run-
ning through the combustion wave produces a forward facing compression
wave, while a reflected shock wave running back through the reaction
zone generates a forward facing rarefaction wave. We therefore suggest
that the effect of the forward facing waves, ultimately caused by the
shock impedance discontinuity, superimposed on the transmitted rarefac-
tion wave generated by the interaction of the reaction zone with the
interface, causes the apparent differences in l_{eff}. This value is
smaller when the "reaction zone" rarefaction wave is superimposed on a
rarefaction wave (higher shock impedance) and larger when it is super-
imposed on a compression wave (smaller shock impedance).
Although any effect of reflected waves on the induction period and heat
release law has been avoided in this work in order to demonstrate purely
the effect of reflected waves on the u_{fs} vs d curves, we believe that
Jameson and Hawkins suggestion as to the explanation of the observed
l_{eff} behaviour may only enhance the tendency of l_{eff} for mismatched
materials to deviate from the one for the matched case.

Future work on this subject may be done by incorporating the chemical
kinetics effects, accurate equations of state and a more accurate dif-
ference scheme than the one used here. This, however, is beyond the
scope of this Chapter, which has the primary objective to demonstrate
the applicability of the interaction rules to a subject which is
holding the attention of many investigators in the field of high ex-
plosive research.

Appendix I Thermodynamic states behind detonation waves in H_2-O_2
and equimolar $C_2H_2-O_2$ mixtures

Due to the lack of data on the thermo and gasdynamical states based
on modern thermochemical properties of the species involved behind
CJ detonations in H_2-O_2 and equimolar $C_2H_2-O_2$ mixtures at low initial
pressures, we wrote a computer program for these calculations.
An approach slightly different from Eisen et al.[92] was taken here and
a brief analysis is presented. Consider the steady wave system

(3)	(1)
←	←
p_3, ρ_3, T_3, v_3	p_1, ρ_1, T_1, v_1
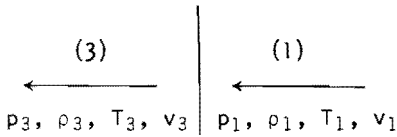
The class of reactions

Following Eisen's notation

$$a_0 H_2 + a_1 O_2 \rightarrow b_2 H_2 O + b_4 O_2 + b_6 OH + b_8 O + b_9 H + b_{11} H_2$$
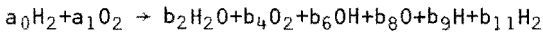
a_i is the number of moles of ith reactant; $a_0 = 1$
b_i is the number of moles of ith product.

Conservation of momentum

$$p_1 + \rho_1 v_1^2 = p_3 + \rho_3 v_3^2 \qquad\qquad \text{I-1}$$

where

$$\bar{m}_1 = \frac{\Sigma a_i m_i}{\Sigma a_i} \quad ; \quad \bar{m}_3 = \frac{\Sigma b_i m_i}{\Sigma b_i}$$

$$Ma_1^2 = \frac{\bar{m}_1 v_1^2}{\gamma_1 R T_1} \quad ; \quad Ma_3^2 = \frac{\bar{m}_3 v_3^2}{\gamma_3 R T_3}$$

$$\gamma_1 = \frac{\Sigma a_i c_{p_i}}{\Sigma a_i (c_{p_i} - R)}$$

$$\gamma_3 = \frac{\Sigma b_i c_{p_i}}{\Sigma b_i (c_{p_i} - R)}$$

$$\frac{p}{\rho} = \frac{RT}{\bar{m}}$$

or $\quad \dfrac{p_1}{p_3} = \dfrac{1+\gamma_3 Ma_3^2}{1+\gamma_1 Ma_1^2}$ $\qquad\qquad$ I-2

Conservation of mass

$$\rho_1 v_1 = \rho_3 v_3$$

or

$$\frac{v_3}{v_1} = \frac{\bar{m}_1}{\bar{m}_3}\; \frac{p_1}{p_3}\; \frac{T_3}{T_1} \qquad\qquad \text{I-3}$$

Conservation of atoms

$$2 = 2b_2 + b_6 + b_9 + 2b_{11}$$

$$a_1 = \tfrac{1}{2}b_2 + b_4 + \tfrac{1}{2}b_6 + \tfrac{1}{2}b_8 \qquad\qquad \text{I-4}$$

Conservation of energy

$$\tfrac{1}{2}\sum_{i=0}^{1}(a_i m_i)v_1^2 + \sum_{i=0}^{1} a_i h_i(T_1) = \tfrac{1}{2}\sum_{i=2}^{11}(b_i m_i)v_3^2 + \sum_{i=2}^{11} b_i h_i(T_3)$$

The enthalpy per mole h_i can be expressed as

$$h_i = h_i(298.15) + \int_{298.15}^{T} c_{p_i}\, dT$$

where the reference temperature is taken as 298.15 K. This may be written as

$$h_i = h_i(298.15) + [H_T - H_{298.15}]$$

Defining the heat of formation of the ith species at T = 298.15 K

$$h_i(298.15) \equiv \Delta H_i^o$$

and the enthalpy difference due to temperature as

$$\Delta H_i^T \equiv H_T - H_{298.15}$$

the energy equation may be written as

$$\tfrac{1}{2}\Sigma\,(a_i m_i)v_1^2 + a_0\,(\Delta H_{H_2}^0 + \Delta H_{H_2}^{T_1}) + a_1\,(\Delta H_{O_2}^0 + \Delta H_{O_2}^{T_1}) = \tfrac{1}{2}\Sigma\,(b_i m_i)v_3^2 +$$

$$+\, b_2\,(\Delta H_{H_2O}^0 + \Delta H_{H_2O}^{T_3}) + b_4\,(\Delta H_{O_2}^0 + \Delta H_{O_2}^{T_3}) + b_6\,(\Delta H_{OH}^0 + \Delta H_{OH}^{T_3}) +$$

$$+\, b_8\,(\Delta H_0^0 + \Delta H_0^{T_3}) + b_9\,(\Delta H_H^0 + \Delta H_H^{T_3}) + b_{11}\,(\Delta H_{H_2}^0 + \Delta H_{H_2}^{T_3}) \qquad\qquad \text{I-5}$$

Equilibrium equations

$$H_2 + \tfrac{1}{2}O_2 \rightleftharpoons H_2O$$
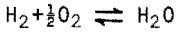
$$k_{H_2O}(T_3) = \frac{p_{H_2O}}{p_{H_2}(p_{O_2})^{\frac{1}{2}}} = \frac{b_2}{b_{11}}\,\left(\frac{\Sigma b_i}{b_4 p_3}\right)^{\frac{1}{2}}$$

$$\tfrac{1}{2}O_2 \rightleftharpoons O$$

$$k_0(T_3) = \frac{p_0}{(p_{O_2})^{\frac{1}{2}}} = b_8\,\left(\frac{p_3}{\Sigma b_i b_4}\right)^{\frac{1}{2}}$$

$$\tfrac{1}{2}H_2 \rightleftharpoons H$$
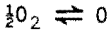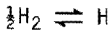
$$k_H(T_3) = \frac{p_H}{(p_{H_2})^{\frac{1}{2}}} = b_9\,\left(\frac{p_3}{\Sigma b_i b_{11}}\right)^{\frac{1}{2}}$$

$$\tfrac{1}{2}H_2 + \tfrac{1}{2}O_2 \rightleftharpoons OH$$
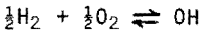
$$k_{OH}(T_3) = \frac{p_{OH}}{(p_{H_2}p_{O_2})^{\frac{1}{2}}} = \frac{b_6}{(b_4 b_{11})^{\frac{1}{2}}} \qquad\qquad \text{I-6}$$

Solution of the equations

Defining the following variables

$$y_i \equiv e^{x_i} \equiv \frac{b_i}{\Sigma b_i} \qquad\qquad \text{I-7}$$

we may derive the following system of equations

$$x_6 = \frac{1}{2} x_2 + \frac{1}{4} x_4 + \ln k_{OH} - \frac{1}{2} \ln k_{H_2O} - \frac{1}{4} \ln p_3$$

$$x_8 = \frac{1}{2} x_4 - \frac{1}{2} \ln p_3 + \ln k_O$$

$$x_9 = \frac{1}{2} x_2 - \frac{1}{4} x_4 - \frac{1}{2} \ln k_{H_2O} + \ln k_H - \frac{3}{4} \ln p_3$$

$$x_{11} = x_2 - \frac{1}{2} x_4 - \frac{1}{2} \ln p_3 - \ln k_{H_2O} \qquad \text{I-8}$$

$$1 - \sum_{i=2}^{11} e^{x_i} = 0 \qquad \text{I-9}$$

$$a_1 (e^{x_2} + \tfrac{1}{2} e^{x_6} + \tfrac{1}{2} e^{x_9} + e^{x_{11}}) - \tfrac{1}{2} e^{x_2} - e^{x_4} - \tfrac{1}{2} e^{x_6} - \tfrac{1}{2} e^{x_8} = 0 \qquad \text{I-10}$$

$$\frac{1}{2\Sigma b_i} (\Sigma a_i m_i) v_1^2 - \tfrac{1}{2} v_1^2 \frac{\overline{m_1}^2}{\overline{m_3}} (\frac{p_1 T_3}{p_3 T_1})^2 + \frac{a_0}{\Sigma b_i} (\Delta H_{H_2}^0 + \Delta H_{H_2}^{T_1}) +$$

$$+ \frac{a_1}{\Sigma b_i} (\Delta H_{O_2}^0 + \Delta H_{O_2}^{T_1}) - e^{x_3} (\Delta H_{H_2O}^0 + \Delta H_{H_2O}^{T_3}) - e^{x_4} (\Delta H_{O_2}^0 + \Delta H_{O_2}^{T_3}) +$$

$$- e^{x_6} (\Delta H_{OH}^0 + \Delta H_{OH}^{T_3}) - e^{x_8} (\Delta H_{O}^0 + \Delta H_{O}^{T_3}) - e^{x_9} (\Delta H_{H}^0 + \Delta H_{H}^{T_3}) +$$

$$- e^{x_{11}} (\Delta H_{H_2}^0 + \Delta H_{H_2}^{T_3}) = 0 \qquad \text{I-11}$$

where

$$\frac{1}{\Sigma b_i} = (\tfrac{1}{2} e^{x_2} + e^{x_4} + \tfrac{1}{2} e^{x_6} + \tfrac{1}{2} e^{x_8})/a_1 \qquad \text{I-12}$$

and

$$\overline{m}_3 = \Sigma m_i e^{x_i} \qquad \text{I-13}$$

and

$$v_1^2 = \frac{p_3/p_1 - 1}{\frac{\overline{m_1}}{RT_1} (1 - \frac{T_3 p_1 \overline{m_1}}{T_1 p_3 \overline{m_3}})} \qquad \text{I-14}$$

The computational procedure is to specify a value of T_3 and calculate x_2, x_4 and p_3 with the Newton-Raphson method for simultaneous equations. Then T_3 is assigned a new value until v_1 is minimized.

Theory dictates that at the CJ point $Ma_3 = 1$. This then provides an excellent check on the accuracy of the computations. Great care must be taken, however, in computing Ma_3. The Mach number Ma_3 is defined as v_3/c_3, where c_3 is the speed of propagation of small disturbances in the gas at state 3. There has been a long discussion in literature on the definition of the sound speed[92].

We must distinguish between the equilibrium sound speed, c_e (velocity of sound at zero frequency or infinite chemical reaction rates) defined by

$$c_e^2 \equiv (\frac{\partial p}{\partial \rho})_{S,b_i} + \Sigma (\frac{\partial p}{\partial b_i})_{\rho,S} \cdot (\frac{\partial b_{ie}}{\partial \rho})_S \qquad I-15$$

where b_i has to be taken equal to the equilibrium value b_{ie} after performing the differentiation, and the velocity of sound at any other frequency up to frequencies that are very high and correspond to very slow chemical reaction rates. The sound speed in a mixture of fixed chemical composition is referred to as the frozen sound speed and defined as

$$c_f^2 \equiv (\frac{\partial p}{\partial \rho})_{S,b_i} \qquad I-16$$

It will also be confirmed from the computations that it is the equilibrium sound speed which must be employed to compute Ma_3 so that at the CJ point $Ma_3 = 1$. In fact, by minimizing v_1, it will turn out that $Ma_3 = 1$.

Calculation of the equilibrium sound speed

We will set up a system of equations consisting of the atom balance equations, the ideal gas law, the equations for chemical equilibrium and the equation for the entropy change, that describe small variations in the thermochemical properties of the products.

Class of reactions

$$b_2H_2O + b_4O_2 + b_6OH + b_8O + b_9H + b_{11}H_2 \rightarrow (b_2+\delta b_2)H_2O +$$

$$+ (b_4+\delta b_4)O_2 + (b_6+\delta b_6) \ OH + (b_8+\delta b_8)O + (b_9+\delta b_9)H + (b_{11}+\delta b_{11})H_2$$
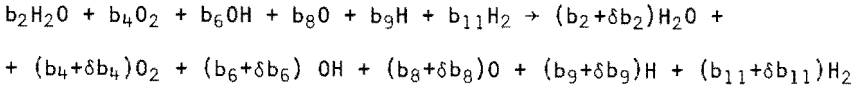
The *atom balance* gives

$$2\delta b_2 + \delta b_6 + \delta b_9 + 2\delta b_{11} = 0$$

$$\delta b_2 + 2\delta b_4 + \delta b_6 + \delta b_8 = 0 \qquad\qquad\qquad I-17$$

From the ideal gas law we obtain

$$\frac{RT_3}{\bar{m}_3 p_3} \delta \rho_3 + \frac{1}{T_3} \delta T_3 - \frac{1}{p_3} \delta p_3 - \frac{1}{\bar{m}_3} \delta \bar{m}_3 = 0 \qquad\qquad I-18$$

The change in $\bar{m}_3$ is defined as

$$\Sigma b_i \delta \bar{m}_3 + \Sigma (\bar{m}_3 - m_i) \delta b_i = 0 \qquad\qquad\qquad I-19$$

Applying van 't Hoff's law to the equilibrium equations

$$van \ 't \ Hoff \qquad \frac{d\ln k_i}{dT} = \frac{\Delta H_i}{RT^2}$$

we obtain the following set of equations

$$- 2 \frac{\Delta H_{H_2O}}{RT_3^2} \delta T_3 - 2 \frac{\delta b_{11}}{b_{11}} - \frac{\delta p_3}{p_3} - \frac{\delta b_4}{b_4} + \frac{\Sigma \delta b_i}{\Sigma b_i} + 2 \frac{\delta b_2}{b_2} = 0$$

$$- 2 \frac{\Delta H_H}{RT_3^2} \delta T_3 + 2 \frac{\delta b_9}{b_9} - \frac{\delta b_{11}}{b_{11}} - \frac{\Sigma \delta b_i}{\Sigma b_i} + \frac{\delta p_3}{p_3} = 0$$

$$- 2 \frac{\Delta H_O}{RT_3^2} \delta T_3 + 2 \frac{\delta b_8}{b_8} - \frac{\delta b_4}{b_4} - \frac{\Sigma \delta b_i}{\Sigma b_i} + \frac{\delta p_3}{p_3} = 0$$

$$- 2 \frac{\Delta H_{OH}}{RT_3^2} \delta T_3 - \frac{\delta b_4}{b_4} + 2 \frac{\delta b_6}{b_6} - \frac{\delta b_{11}}{b_{11}} = 0 \qquad\qquad I-20$$

The entropy change is set equal to zero

$$\Sigma\Delta H_i \delta b_i - \frac{RT_3}{p_3} \Sigma b_i \delta p_3 + (\Sigma b_i c_{p_i}) \delta T_3 = 0 \qquad I-21$$

Eqs. I-17 through I-21 constitute a system of 9 equations from which the ratio $\delta p/\delta \rho$ is determined uniquely.

Determination of the thermochemical properties of the species

For the calculations we need to know the thermochemical properties of the products of combustion as continuous functions of temperature. These properties were taken from the 1965 JANAF THERMOCHEMICAL TABLES and fitted by the method of least squares to 5th degree polynomials. The heat capacity at constant pressure, c_p, the standard heat of formation at temperature T, ΔH_i, and the enthalpy at temperature T less the enthalpy at 298.15 K, $H_T - H_{298.15}$, were fitted by polynomials given by the following equation

$$z = c_0 + c_1 T + c_2 T^2 + c_3 T^3 + c_4 T^4 + c_5 T^5 \qquad I-22$$

The logarithms of the equilibrium constants were fitted by polynomials

$$z = c_0 + \frac{c_1}{T} + \frac{c_2}{T^2} + \frac{c_3}{T^3} + \frac{c_4}{T^4} + \frac{c_5}{T^5} \qquad I-23$$

The results for the coefficients are shown in Table I-1.

The results for the computations for a stoichiometric hydrogen and oxygen detonation are summarized for several initial pressures in Table I-2.

We have also calculated the properties of equimolar $C_2H_2 + O_2$ detonations. It is well known from literature[58] that here we have to consider only the products of combustion CO, H and H_2. Lee[58] performed similar calculations, but he took the wrong formula for the ratio's of specific heats. The results are shown in Table I-3.

It is clear from these calculations that the minimum detonation velocity corresponds to equilibrium conditions ($Ma_{3e} = 1$). The Mach number for frozen conditions is smaller than unity ($Ma_{3f} < 1$). These conditions show that the calculations are quite good.

TABLE I-1

Coefficients c_i of 5th degree polynomials fitted to the JANAF THERMOCHEMICAL DATA 1965. The letter "E" stands for the ten's exponent. Since specific heats have dimension [cal/mole K] and enthalpies have dimension [kcal/mole] in the JANAF Tables, values of c_p have to be multiplied by J, while values of enthalpies have to be multiplied by 10^3 J.

z	c_0	c_1	c_2	c_3	c_4	c_5
H_T-H_{298} H2O	-.15597801E01	.52170268E-02	.30835018E-05	-.59171548E-09	.61367774E-13	-.26161944E-17
ΔH H2O	-.56689210E02	-.39645167E-02	.17646707E-05	-.40380828E-09	.43586981E-13	-.18679092E-17
c_p H2O	.49737535E01	.66474945E-02	-.21245515E-05	.36345540E-09	-.31750660E-13	.11170529E-17
10 logk H2O	-.31874554E01	.14306429E05	-.35952774E07	.57780669E10	-.47412857E13	.15017886E16
H_T-H_{298} O2	-.26754005E01	.77919281E-02	.29084536E-06	.20613262E-10	-.62985635E-14	.33977141E-18
c_p O2	.71762386E01	.16509584E-02	-.62609684E-06	.18217215E-09	-.27887261E-13	.16119636E-17
H_T-H_{298} OH	-.14555349E01	.54179738E-02	.12213072E-05	-.22431544E-09	.22712876E-13	-.94577753E-18
ΔH OH	.98677537E01	-.10823039E-02	.47686905E-06	-.13171715E-09	.14845391E-13	-.62597670E-18
c_p OH	.56320926E01	.21187265E-02	-.47321750E-06	.33280270E-10	.31088604E-14	-.40626163E-18
10 logk OH	.53709964E00	-.47333478E03	-.45201745E07	.71224955E10	-.56172576E13	.17334970E16
H_T-H_{298} O	-.14634845E01	.50301045E-02	-.94806611E-08	-.86497879E-11	.33738518E-14	-.24392750E-18
ΔH O	.59428938E02	.11420444E-02	-.16019330E-06	-.17316342E-10	.62855508E-14	-.40085976E-18
c_p O	.49943162E01	.55684074E-04	-.82280140E-07	.32977458E-10	-.43487830E-14	.18891165E-18
10 logk O	.35488880E01	-.13594914E05	.35443199E06	-.20205209E09	.15307400E12	-.66519505E14
H_T-H_{298} H	-.14804509E01	.49675227E-02	-.11810847E-09	.19108688E-12	-.48701230E-16	.37662431E-20
ΔH H	.51284262E02	.23282512E-02	-.58851334E-06	.99633840E-10	-.10538742E-13	.46314758E-18
10 logk H	.32523925E01	-.12313617E05	.32589884E06	.55816056E09	-.73419681E12	.26532651E15
H_T-H_{298} H2	-.13223675E01	.52692437E-02	.11845260E-05	-.20166277E-09	.21429733E-13	-.94575671E-18
c_p H2	.59971616E01	.11321784E-02	.17186595E-06	-.14243469E-09	.26935956E-13	-.16760293E-17

TABLE I-2

Results for $2H_2+O_2$ CJ detonation. Initial temperature 298 K.

p_1 [N/m²]	1.0132×10^5	0.5066×10^5	0.2533×10^5	0.1358×10^5	0.6790×10^4	0.2716×10^4
ρ_1 [kg/m³]	0.491135	0.245568	0.122784	0.064623	0.0323115	0.0129246
γ_1	1.40168	1.40168	1.40168	1.40168	1.40168	1.40168
$\bar{m}_1$ [kg/mole]	12.0107×10^{-3}	12.0107×10^{-3}	12.0107×10^{-3}	12.0107×10^{-3}	12.0107×10^{-3}	12.0107×10^{-3}
Y_2	0.529208	0.516129	0.504447	0.494757	0.485398	0.474588
Y_4	0.0486622	0.0596568	0.0525852	0.0543179	0.0561371	0.0584674
Y_6	0.138389	0.136543	0.134115	0.131443	0.128182	0.123415
Y_8	0.0383563	0.0413320	0.0441528	0.04661469	0.0491007	0.0521043
Y_9	0.0810198	0.0888452	0.0966360	0.103792	0.111430	0.121357
Y_{11}	0.164364	0.166494	0.168063	0.169076	0.169751	0.170068
T_3 [K]	3680.37	3551.79	3429.02	3320.56	3208.96	3070.01
p_3 [N/m²]	19.09375×10^5	9.31436×10^5	4.54248×10^5	2.33611×10^5	1.13911×10^5	0.440824×10^5
Ma_1	5.28331	5.21199	5.14106	5.07600	5.00663	4.91667
v_1 [m/s]	2841.04	2802.69	2764.55	2729.56	2692.26	2643.89
v_3 [m/s]	1545.26	1522.95	1500.95	1480.76	1459.43	1431.87
$\bar{m}_3$ [kg/mole]	14.4718×10^{-3}	14.3284×10^{-3}	14.1945×10^{-3}	14.0786×10^{-3}	13.9616×10^{-3}	13.81900×10^{-3}
Ma_{3f}	0.962698	0.959563	0.956545	0.953753	0.950874	0.947170
γ_{3f}	1.218455	1.222169	1.225819	1.229139	1.232658	1.237204
Σb_i	1.24490	1.25736	1.26922	1.27967	1.29040	1.30371
γ_{3e}	1.12942	1.12560	1.12183	1.11841	1.11482	1.11026
c_{3e} [m/s]	1545.38	1523.14	1501.10	1480.98	1459.62	1432.08
Ma_{3e}	0.999923	0.999880	0.999897	0.999852	0.999866	0.999854
p_{31}	18.8450	18.3860	17.9332	17.5231	17.0890	16.5331
$v_{31} = \rho_{13}$	0.543906	0.543390	0.542927	0.542491	0.542082	0.541577
T_{31}	12.3502	11.9188	11.5068	11.1428	10.7683	10.3020

TABLE I-3

Results for the class of reactions $C_2H_2+O_2 \rightarrow b_1CO+b_2H+b_3H_2$. Initial temperature 298 K.

p_1 [N/m²]	1.0132×10^5	0.5066×10^5	0.2533×10^5	0.1358×10^5	0.6790×10^4	0.2716×10^4
ρ_1 [kg/m³]	1.18663	0.593316	0.296658	0.156136	0.0780679	0.0312272
γ_1	1.29258	1.29258	1.29258	1.29258	1.29258	1.29258
$\bar{m}_1$ [kg/mole]	29.0190×10^{-3}	29.0190×10^{-3}	29.0190×10^{-3}	29.0190×10^{-3}	29.0190×10^{-3}	29.0190×10^{-3}
Y_1	0.5927172	0.586883	0.581450	0.576768	0.572084	0.566445
Y_2	0.221848	0.239352	0.255652	0.269695	0.283747	0.300664
Y_3	0.185435	0.173765	0.162899	0.153537	0.144169	0.132891
p_3 [N/m²]	46.7751×10^5	22.7511×10^5	11.0559×10^5	5.66588×10^5	2.75155×10^5	1.05876×10^5
T_3 [K]	4512.61	4335.85	4165.60	4014.73	3859.41	3666.50
Ma_1	8.84545	8.70823	8.57030	8.44303	8.30702	8.13073
v_1 [m/s]	2938.58	2892.999	2847.18	2804.90	2759.71	2701.14
v_3 [m/s]	1626.23	1597.05	1568.21	1541.59	1513.51	1477.54
$\bar{m}_3$ [kg/mole]	17.200×10^{-3}	17.0308×10^{-3}	16.8731×10^{-3}	16.7372×10^{-3}	16.6013×10^{-3}	16.4377×10^{-3}
Ma_{3f}	0.95924	0.95444	0.94997	0.94585	0.94171	0.93662
γ_{3f}	1.31755	1.322669	1.32757	1.33190	1.33634	1.34183
Σb_i	3.37429	3.40784	3.43968	3.46760	3.49600	3.53079
γ_{3e}	1.21187	1.20484	1.1979	1.19163	1.18508	1.17683
c_{3e} [m/s]	1625.92	1597.01	1568.10	1541.63	1513.51	1477.35
Ma_{3e}	1.0002	1.0000	1.0000	1.0000	1.0000	1.0000
p_{31}	46.1657	44.9092	43.6476	42.4997	41.2783	39.7087
$v_{31} = \rho_{13}$	0.553406	0.552039	0.550794	0.549608	0.548431	0.547006
T_{31}	15.14298	14.5498	13.9785	13.4722	12.9510	12.3037

148

TABLE I-4

Results for Von Neumann spike parameters for $2H_2+O_2$ detonations.
Initial temperature 298 K.

p_1 [N/m²]	1.0132×10^5	0.5066×10^5	0.2533×10^5	0.1358×10^5	0.6790×10^5	0.2716×10^4
v_1 [m/s]	2841.04	2802.69	2764.55	2729.56	2692.26	2643.89
T_2 [K]	1768.84	1731.19	1695.58	1662.57	1627.72	1583.05
p_2 [N/m²]	33.549×10^5	16.315×10^5	7.932×10^5	4.068×10^5	1.978×10^5	0.762×10^5
ρ_2 [kg/m³]	2.7398	1.3608	0.6758	0.3534	0.1755	0.06955
Ma_2	0.40130	0.40253	0.40378	0.40500	0.40625	0.40797
v_2 [m/s]	509.291	505.784	502.300	499.107	495.707	491.305
γ_2	1.31533	1.31685	1.31838	1.31980	1.32133	1.32335
P_{21}	33.112	32.205	31.316	30.512	29.666	28.587
T_{21}	5.9357	5.8118	5.6900	5.5791	5.4622	5.3123
ρ_{21}	5.5784	5.5413	5.5038	5.4689	5.4312	5.3814

TABLE I-5

Results for Von Neumann spike parameters for $C_2H_2+O_2$ detonations.
Initial temperature 298 K.

p_1 [N/m²]	1.0132×10^5	0.5066×10^5	0.2533×10^5	0.1358×10^5	0.6790×10^5	0.2716×10^4
v_1 [m/s]	2938.58	2893.00	2847.18	2804.90	2759.71	2701.14
T_2 [K]	2589.77	2527.98	2466.62	2410.66	2351.57	2276.05
p_2 [N/m²]	93.870×10^5	45.471×10^5	22.011×10^5	11.238×10^5	5.4371×10^5	2.0822×10^5
ρ_2 [kg/m³]	12.650	6.2776	3.1144	1.6271	0.80695	0.31929
Ma_2	0.29785	0.29896	0.30011	0.30120	0.30241	0.30403
v_2 [m/s]	275.645	273.427	271.205	269.162	266.987	264.179
γ_2	1.15422	1.15486	1.15552	1.15615	1.15684	1.15778
P_{21}	92.647	89.756	86.896	84.299	81.567	78.093
T_{21}	8.6905	8.4832	8.2773	8.0895	7.8912	7.6378
ρ_{21}	10.6608	10.5805	10.4982	10.4208	10.3365	10.2247

TABLE I-6

Reflected detonation wave properties for $2H_2+O_2$ detonations as
calculated with the method outlined in this section. Initial
conditions (1) refer to the Von Neumann spike conditions of
the incident detonation wave as given in Table II-4.

p_1 [N/m²]	33.549×10^5	16.315×10^5	7.932×10^5	4.068×10^5
T_3 [K]	4254.1	4078.2	3912.1	3766.9
p_3 [N/m²]	111.12×10^5	53.48×10^5	25.73×10^5	13.07×10^5
Ma_1	2.171	2.154	2.137	2.121
v_1 [m/s]	2755.3	2706.6	2658.3	2614.3
v_3 [m/s]	1708.2	1678.2	1648.6	1621.8
$\overline{m}_3$ [kg/mole]	13.88	13.73	13.60	13.48
γ_{3f}	1.225	1.229	1.233	1.237
Ma_{3f}	0.967	0.963	0.960	0.957
γ_{3e}	1.145	1.141	1.136	1.132
c_{3e} [m/s]	1708.4	1678.5	1648.9	1622.0
Ma_{3e}	1.000	1.000	1.000	1.000
P_{21}	5.271	5.188	5.106	5.030
T_{21}	1.640	1.632	1.624	1.616
ρ_{21}	3.214	3.179	3.145	3.113
v_2 [m/s]	857.3	851.3	845.5	839.9
γ_2	1.282	1.283	1.285	1.287
Ma_2	0.534	0.537	0.540	0.543

Appendix II Details of experimentation

1. Detonation tube

The measurements reported in this presentation were carried out in a
steel pipe of 7.5 cm internal diameter. The flanged pipe was made in
two equal sections of 1.2 m length, bolted together with flanges.
To ensure air-tight connections, groves were machined in the flanges
into which fitted "0" ring seals. The side walls of the tube is in-
strumentated with pressure transducers for pressure measurements and
with ionization probes for velocity measurements. The probes are spaced
10 cm apart, starting 50 cm from the ignition end of the tube. In total
12 measurement stations were available.
The ends of the tube were closed by plates on either end bolted to the
flanges. In one plate the ignition assembly was mounted; in the other
plate provisions were made for the mounting of a pressure gauge. For
side-on velocity and pressure measurements this end of the tube was
connected to a steel tank of approximately 40 dm^3 to allow the detona-
tion wave to expand before emerging into the open. A mylar diaphragm
was then clamped between the flanges of the steel tank and the tube.
The tube was provided with valves for evacuating the tube and for
filling it with the detonable mixture.

2. Test gases

Stoichiometric hydrogen-oxygen and equimolar acetylene-oxygen mixtures
were used throughout the present experiments. These mixtures may be
readily detonated with relatively short induction distances. The gases
were of commercial purity and were used for mixing without further
purification. The mixtures were prepared in 40 dm^3 capacity high pres-
sure steel tanks by the method of partial pressures.
After evacuating the tanks, they were filled to a pressure of $3 \ 10^5 \ N/m^2$.
The acetylene-oxygen mixtures were allowed to mix by diffusion for at
least 24 hours before use, which resulted in adequate mixing. The hydro-
gen-oxygen mixtures were stirred by means of a magnetic stirrer device
for 12 hours before use.

The errors involved in the mixing procedures are small, since detonation velocities measured in the same mixture prepared on different occasions are repeatable within ± 0.5%. The detonation waves were always fully developed at the first measurement station located at 50 cm from the ignition end of the tube.

3. Ignition methods

The detonation wave was ignited in three different ways: 1. by a high intensity spark discharge; 2. by an exploding wire; 3. by the detonation of a small pellet (100 mg) of pressed lead azide, which is an extremely sensitive high explosive. It can be readily detonated by means of a glow wire (6 V DC).

For spark ignition a capacitor was charged to 10 kV and then discharged across two brass electrodes with a spark gap of about 5 mm. This method has been used for relatively few experiments.

For exploding wire ignition, a thin Nichrome wire of about 2 cm length and 0.1 mm thick is exploded by discharging a capacitor charged to 10 kV through the wire.

The detonation wave velocity and pressure measurements proved to be independent of the type of ignition, as could be expected for steady state detonation waves.

The lead azide detonation ignition turned out to be the most convenient way of igniting the mixture. Both the spark and exploding wire methods sometimes gave random electromagnetic interference which spoiled the trigger events. Nevertheless, a large part of the measurements have been performed by the exploding wire method before the pressed lead azide pellets became available.

4. Test procedure

Prior to an experiment the detonation tube was first evacuated to pressures lower than 0.1 mm Hg. The evacuated tube was then filled with the desired mixture. After filling all valves were closed and the lines to the mixture tanks were removed to prevent any accidental detonation feedback. All experiments were performed at room temperature (19°C - 22°C).

5. *Ionization probes*

We developed ionization probes for the measurement of detonation wave
velocities. The electrodes, or pins, consist of two steel needles set
1.2 mm apart in a Teflon plug. The assembly is secured by epoxy resin
in the center of the plug. The probe is mounted flush with the inside
wall of the detonation tube, the pins extending about 4 mm into the
tube. The plug was held in place by two pins and by a bolt screwed to
a steel box welded to the pipe wall (see Fig. II-1).
The signal circuit is similar to that used by Knight and Duff[73] and
consisted of a 120 pF capacitor charged to 300-500 V and a 5600 ohm
resistor in series with the pins. Fig. II-2 shows the pin circuit.
When the detonation wave arrives at the pins, current flows due to the
conductivity behind the wave front in the pin circuit and a signal ap-
pears across the resistor. For this work we used on an average 5 such
pins in parallel. Only one signal resistor is needed and diodes prevent
early pins from shorting later ones. The resulting pulses are fed by
a coaxial cable to a pulse transformer, which shaped the pulse into
a square pulse and thus improved the rise time of the event pulses.
In general we required a total recording time of 100 μs to 200 μs with
a time resolution of less than 0.1 μs. This is beyond that obtainable
from a linear oscilloscope trace. To convert an oscilloscope into a
time-measuring device a calibrated extended sweep is necessary.
For this purpose we designed a raster-oscilloscope technique. A
Tektronix type 454 oscilloscope was chosen as the basic display unit,
because it has a high frequency response, it is easy to photograph at
high sweep speeds and provides an X-Y-Z-type operation. The block dia-
gram of the circuit is shown in Fig. II-3.
The circuit was triggered by an additional pin circuit located in front
of the signal pins. The triggered unit was a Model 9030 Beckman Function
Generator which provided the 454 oscilloscope with an adjustable burst
of sawtooth waves and the 545 oscilloscope with a simultaneous burst of
square waves. The 545 oscilloscope in single sweep operation produced
a single sawtooth, and a single square wave (gate-out), which was
amplified by a DC amplifier and fed into the Z-axis of the 454 oscillo-
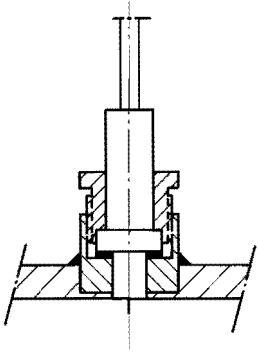
Fig. II-1   Ionization probe mounted in tube wall
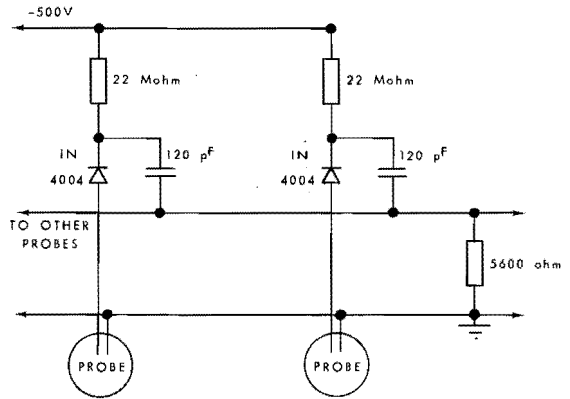
Fig. II-2   The ionization probe circuit
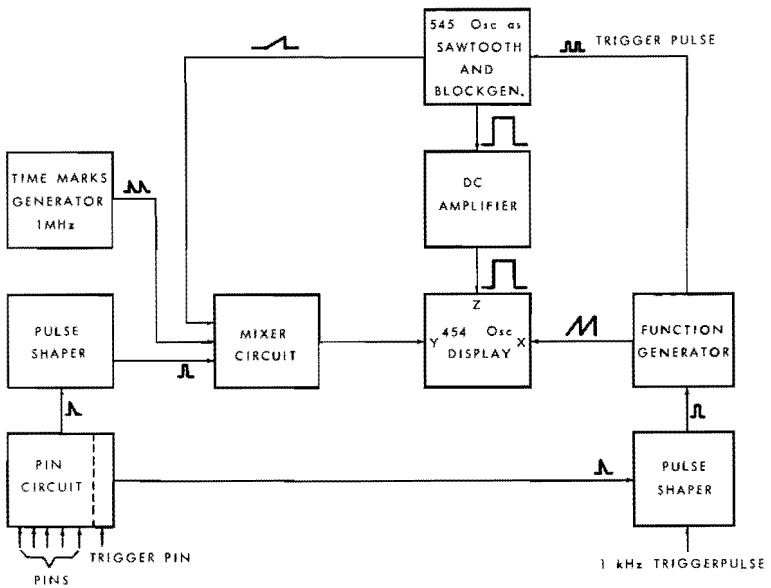
Fig. II-3   Block diagram of raster-oscilloscope technique

scope which caused the beam to brighten. The duration of these single waves was adjustable between 100 μs to 200 μs depending on the required recording time. The event pulses were transformed by a pulse shaper, which was fed into a mixer circuit, where they were superposed together with 1 μs timing marks on the sawtooth wave provided by the Tektronix 545 oscilloscope. These combined signals were fed into the vertical (Y-axis) amplifier of the display oscilloscope. The complete system could be set in continuous operation for adjustments by applying a repetitive trigger pulse of 1 kHz to the Function Generator.
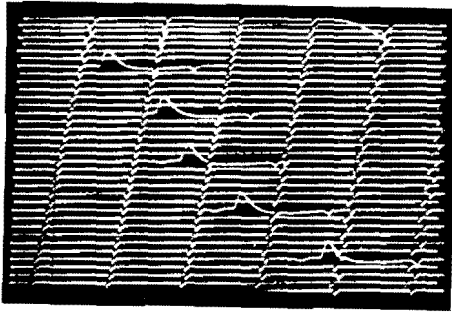
Fig. II-4   Typical oscilloscope record by raster technique;
distance between time marks: 1 μs

For detonation wave measurements at least six experiments were performed with the same initial conditions. Fig. II-4 shows an oscilloscope record with 5 event pulses obtained with this technique of a detonation wave in an equimolar acetylene-oxygen mixture at initial pressure of $0.5 \cdot 10^5$ N/m^2. If the pin-to-pin spacing is known from travelling microscope measurements and the relative contact time is known then the velocity can be calculated. The photographs were projected on a screen by an episcope and measured.

The accuracy of the ionization probe technique is within ± 0.5 % with the probe spacing of 10 cm. Limitation of the precision of velocity measurements is not the system itself, but rather other experimental variables such as initial compositions, mixture uniformity, initial temperature etc.

6. Pressure transducers

The measurements of rapid pressure variations over a wideband frequen-
cy range from zero to above 1 MHz and for relatively long times require
pressure transducers with sensing elements of very small dimensions.
Piezoelectric elements have been the most successful devices for this
purpose. A reliable reproduction of the pressure in the high frequency
range is difficult to achieve because of spurious elastic waves in the
sensing element. These waves can be eliminated to some extent by appro-
priate design of the transducer.

Edwards[25,74,75] utilised a quartz disk sandwiched between Duralumin
rods, one of which is exposed to the pressure source. Longitudinal
stress waves travelling along the bar traverse the disk and generate a
charge. The acoustic impedances of the piezoelectric element and the
rods are matched, so that reflected waves off the interface are mini-
mized.

These pressure transducers have a poor rise time, which is a function
of the distance of the sensing element off the side which is exposed to
the pressure source. Moreover, the signal exhibits overshoot and damped
oscillations.

Soloukhin[8] placed the piezoelectric element directly on the front face
of an acoustically matched backup rod. The Soviet design utilizes a
1 mm diameter barium titanate disk which is soldered to a zinc rod and
potted in Siberian bees'wax. Ragland[76] followed the same design ap-
proach, but utilised a lead metaniobate element soldered to a tin rod.
The element was 3.18 mm diam. and 1.27 mm thick. The rod assembly was
potted in silicone rubber.

Lee[77,78] designed a transducer which is essentially a combination of
the Soloukhin and the Ragland designs. His gauge consisted of a barium
titanate piezoelectric element of 3.2 mm diameter and 2 mm thick. The
element was backed by a zinc rod of the same diameter. The assembly
was potted in Siberian bees' wax to damp the transverse waves accruing
when the element is subjected to axial loads. He found that rubber
alone as in Ragland's design was not entirely satisfactory in this res-
pect. On the other hand Siberian bees' wax was found to be a poor me-
chanical damper, whereas rubber was ideal. Consequently, the entire

assembly of element, rod and bees' wax was encased in a thin copper
tube and this tube was then located coaxially within another brass
sleeve with silastic rubber in between the two tubes for shock damping.
This gauge had an excellent performance.

We followed essentially the same approach as Lee. Dutch bees' wax was
found to be entirely satisfactory. The pressure sensing element is a
2 mm dia x 1 mm lead zirconate titanate piezoelectric disk (obtained
from Quartz & Silice, France). The acoustic absorbing rod is tin. The
rod was made 21 cm long to give a theoretical "ring free" time of about
165 µs. We found that a minimum overshoot of the gauge signal to a
pressure step function was achieved by reducing the clearance between
the brass and the pressure sensing element to a minimum. Fig. II-5
shows the assembled transducer (Gauge I).
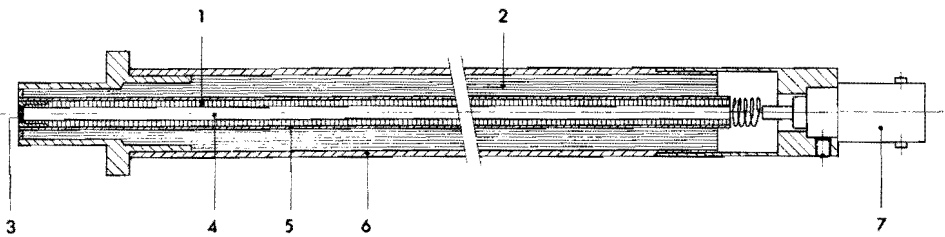
Fig. II-5 Pressure bar transducer I;
           1) bees' wax, 2) silicone rubber, 3) piezoelectric element,
           4) tin bar, 5) inner brass tube, 6) outer brass tube,
           7) connector
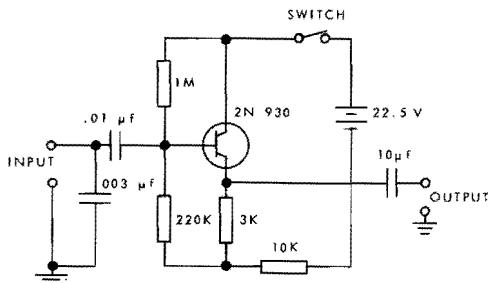
Fig. II-6 Emitter follower for pressure transducers

Fig. II-7 Typical oscillogram of the response of transducer I mounted
in the side wall of a conventional shock tube; time scale
5 μs/div.

Fig. II-8 Typical oscillogram of the response of transducer I mounted
in the side wall of the detonation tube; $C_2H_2+O_2$ mixture;
$p_1 = 0.25 \ 10^5$ N/m^2; time scale 5.0 μs/div.; vert. 50 mV/div.
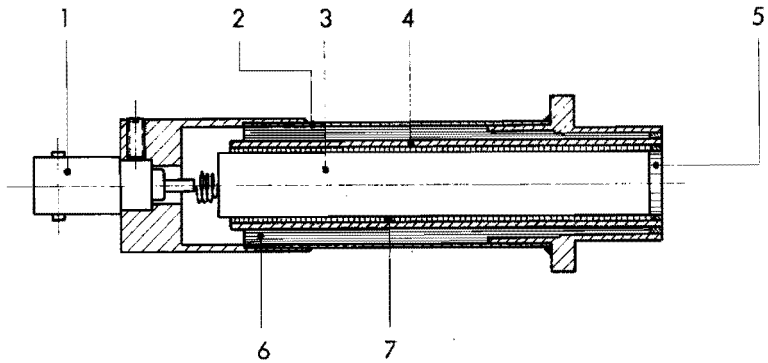
Fig. II-9 Pressure bar transducer II;
1) connector, 2) outer brass tube, 3) tin bar, 4) inner brass
tube, 5) piezoelectric element (10 mm dia x 0.2 mm thick),
6) silicone rubber, 7) epoxy compound

The pressure transducer is connected to an emitter follower with a
gain of approximately unity. The circuit is shown in Fig. II-6 (cour-
tesy of Dr. Lee). The pressure gauge was calibrated in a conventional
shock tube. A typical oscillogram obtained from the gauge mounted in
the side wall of the shock tube is shown in Fig. II-7. The rise time
of the signal is associated primarily with the time for the shock to
traverse the face of the sensing element. These gauges have a sensiti-
vity of $(7.85 \pm 0.40) \, 10^{-5} \, mV/N/m^2$.

A typical oscillogram obtained from the gauge mounted in the side wall
of the detonation tube is shown in Fig. II-8. Note the partial res-
ponse to the Von Neumann spike.

When for the measurement of reflected pressures a high time resolution
is required, the rise time, defined as the time taken for the output
signal to increase from 10% to 90% of its steady value in responding
to a step pressure function, should be of the order of 0.1 µs or less.
For this purpose Baganoff[30] developed a pressure transducer, which
employs closely spaced capacitor plates as its pressure sensitive ele-
ment. When constructed of polycarbonate plastic or pyrex[29,72], the
gauge exhibits a response time of 0.1 µs, although reliable recording
of the pressure is limited to a period of 5 µs.

In pursuing smaller rise times, Jones[79] followed the pressure bar
approach of Edwards c.s., in which a piezoelectric disk is sandwiched
between two bars. He constructed a pressure bar from a beryllium bar of
3 mm dia and 20 cm length. The bar was cut into two equal lengths and
a lead zirconate titanate disk of 0.5 mm thickness was cemented between
the two pieces. The experimentally observed rise time of the gauge was
0.54 µs, which was substantially faster than any other gauge of this
type hitherto reported.

In view of the success of the Soloukhin-Ragland-Lee design where the
pressure sensing element is placed on the front face of a bar, we pur-
sued this approach to thinner sensing disks. Philips, Elonco provided
us with specially made lead zirconate titanate disks of 10 mm dia x
0.2 mm. A major problem was encountered in soldering the disk to a
10 mm dia tin bar. If the joint is bad, severe oscillations of the
signal output occurs. Instead of the previously used bees' wax it was
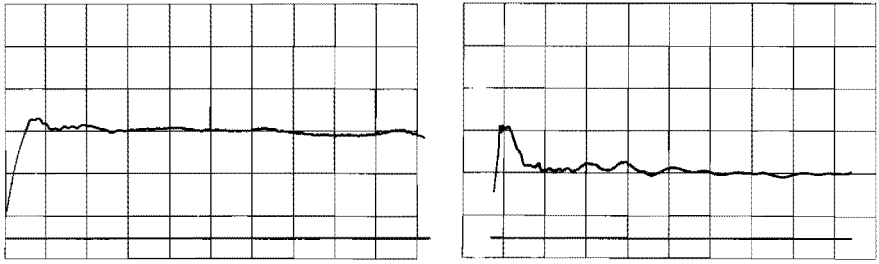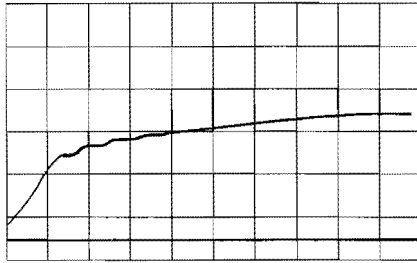
Fig. II-10   Typical oscillogram of the response of transducer II mounted
              in the end wall of a conventional shock tube; time scale
              0.2 μs/div.

found that a better response in terms of overshoot and spurious oscil-
lations was obtained by potting the assembly in an epoxy compound. A
sketch of the assembled gauge is shown in Fig. II-9. A typical oscillo-
gram obtained from the gauge mounted in the end wall of a conventional
shock tube is shown in Fig. II-10. It will be seen that the rise time
of this gauge II is about 0.2 μs, which is a substantial improvement
over Jones'[79] design. After the first 0.2 μs of the gauge response a
relatively slow increase of the signal is observed which we were unable
to eliminate. It may be noted that spurious oscillations are almost
negligible.

Appendix III Detonation wave equations

We will derive some equations in dimensionless form that have been used
to calculate the state (3) of the combustion products behind a steady
detonation wave proceeding into a constant gamma gas of state (1).
The system of conservation equations across the complete detonation wave
is written as

mass: $\rho_3 v_3 = \rho_1 v_1$ III-1

momentum: $p_3 + \rho_3 v_3^2 = p_1 + \rho_1 v_1^2$ III-2

energy: $\dfrac{\gamma}{\gamma-1} \dfrac{p_3}{\rho_3} + \tfrac{1}{2}v_3^2 = \dfrac{\gamma}{\gamma-1} \dfrac{p_1}{\rho_1} + \tfrac{1}{2}v_1^2 + Q_t$ III-3

where $v_1 = u_1 - D$ and $v_3 = u_3 - D$.

From III-1 we find

$$\rho_3 = \rho_1 \frac{v_1}{v_3} \qquad\qquad \text{III-4}$$

Substitution of III-4 into III-2 gives

$$p_3 = p_1 + \rho_1 v_1^2 - \rho_1 v_1 v_3 \qquad\qquad \text{III-5}$$

Substitution of III-4 and III-5 into III-3 gives after some manipulations

$$\frac{v_3}{v_1} = \frac{1}{\gamma+1} \left(\gamma + \frac{1}{Ma_1^2}\right) (1 \pm \alpha) \qquad\qquad \text{III-6}$$

where $Ma_1 = v_1/c_1$, and

$$\alpha^2 = 1 - \frac{(\gamma^2-1)\left(1 + \dfrac{2}{\gamma-1}\dfrac{1}{Ma_1^2} + \dfrac{2Q_t}{c_1^2 Ma_1^2}\right)}{\left(\gamma + \dfrac{1}{Ma_1^2}\right)^2} \qquad\qquad \text{III-7}$$

Substitution of III-6 into III-4 gives

$$\frac{\rho_3}{\rho_1} = \frac{\gamma+1}{\left(\gamma + \dfrac{1}{Ma_1^2}\right)(1 \pm \alpha)} \qquad\qquad \text{III-8}$$

Substitution of III-6 into III-5 gives

$$\frac{p_3}{\rho_1 v_1^2} = \left(1 + \frac{1}{\gamma Ma_1^2}\right)\left(\frac{1 \mp \gamma \alpha}{\gamma+1}\right) \qquad\qquad \text{III-9}$$

The above equations are analogous to those given by Sedov[42].

It will be seen that for each given detonation wave Mach number Ma_1 two possible solutions are obtained. These solutions correspond to weak detonations (top sign proceeding α terms) and strong detonations (lower sign proceeding α terms). For $\alpha = 0$ the unique CJ detonation properties

are obtained. For most detonations it is found that Ma_1 is of the order
of 5 to 10. Hence, neglecting terms of the order of $1/Ma_1^2$ as compared
to unity - which is tantamount to neglecting the initial pressure p_1 -
we find the following relations for CJ detonations for a wave moving
into a gas at rest ($u_1 = 0$).

$$\frac{u_3}{D} = \frac{p_3}{\rho_1 D^2} = \frac{1}{\gamma}\frac{\rho_1}{\rho_3} = \frac{1}{\gamma+1} \qquad \text{III-10}$$

From this we may derive

$$c_3 = \left(\frac{\gamma p_3}{\rho_3}\right)^{\frac{1}{2}} = \gamma u_3 \qquad \text{III-11}$$

When the initial conditions in front of the detonation wave, p_1, ρ_1 and
$u_1 = 0$, and the velocity of the combustion products u_3, which is also
the velocity of the piston behind the wave, are given, we may find for
a particular value of gamma the Mach number Ma_1 for a CJ detonation
($\alpha = 0$) from Eq. III-6. Subsequently, we may derive from Eqs. III-7,
III-8 and III-9 the values of the heat of explosion Q_t, the density ρ_3
and the pressure p_3 of the combustion products respectively. The ratio
of the specific heats γ may be chosen in such a way that these variables
closely correspond to the values obtained from exact calculations, as
performed in Appendix I. With these initial conditions and the Mach
number Ma_1 known, we may calculate the variables of the Von Neumann

TABLE III-1

Detonation wave properties for $C_2H_2+O_2$ mixture

	state (1)	state (2)	state (3)
p [10^5 N/m^2]	1.0132	88.159	44.595
ρ [kg/m^3]	1.187	7.945	2.065
u [m/s]	0.0	2498.70	1249.35
$\gamma = 1.32$; D = 2937.56 m/s; Ma_1 = 8.671; Q_t = 56.582 10^5 m^2/s^2			

spike (state 2) of the detonation wave from the shock wave equations (Chapter AI-§2).

In Table III-1 we have summarized the computed values of the variables of a detonation wave in an $C_2H_2+O_2$ mixture to which is frequently referred in this thesis.

Appendix IV Comparison of the Lax and Lax-Wendroff method

Like the Lax method[63] the Lax-Wendroff method[64] starts with the Lagrangian differential equations of motion in conservative form

$$\frac{\partial f}{\partial t} = \frac{\partial g}{\partial y} \qquad\qquad\qquad \text{IV-1}$$

where f and g are vectors defined as

$$f = \begin{bmatrix} V \\ u \\ E \end{bmatrix} \quad ; \quad g = \begin{bmatrix} u \\ -p \\ -pu \end{bmatrix} \qquad\qquad \text{IV-2}$$

Employing the ideal gas law, the pressure p may be obtained from

$$p = \frac{\gamma-1}{V}\left(E-\tfrac{1}{2}u^2\right) \qquad\qquad\qquad \text{IV-3}$$

We define the matrix $A = A(f)$ such, that $A = \partial g/\partial f$. Thus,

$$\frac{\partial g}{\partial t} = A\frac{\partial f}{\partial t} \qquad\qquad\qquad \text{IV-4}$$

Explicitly, A may be written as

$$\begin{bmatrix} 0 & 1 & 0 \\ \dfrac{p}{V} & \dfrac{(\gamma-1)}{V}u & -\dfrac{(\gamma-1)}{V} \\ \dfrac{pu}{V}-\dfrac{(\gamma-1)}{V}\left(E-\tfrac{3}{2}u^2\right) & -\dfrac{(\gamma-1)}{V}u \end{bmatrix} \qquad\qquad \text{IV-5}$$

The Lax-Wendroff equations start from a Taylor's series of f in t,

$$f(t+\Delta t) = f(t) + \Delta t \frac{\partial f}{\partial t} + \tfrac{1}{2}(\Delta t)^2 \frac{\partial^2 f}{\partial t^2} + \ldots \qquad \text{IV-6}$$

The t-derivatives in IV-6 are replaced by the y-derivatives by means of IV-1 and

$$\frac{\partial^2 f}{\partial t^2} = \frac{\partial}{\partial t} \left(\frac{\partial g}{\partial y}\right) = \frac{\partial}{\partial y} \left(\frac{\partial g}{\partial t}\right) = \frac{\partial}{\partial y} \left(A \frac{\partial f}{\partial t}\right) = \frac{\partial}{\partial y} \left(A \frac{\partial g}{\partial y}\right) \qquad \text{IV-7}$$

Thus, we obtain

$$f(t+\Delta t) = f(t) + \Delta t \frac{\partial g}{\partial y} + \tfrac{1}{2}(\Delta t)^2 \frac{\partial}{\partial y} \left(A \frac{\partial g}{\partial y}\right) + \ldots \qquad \text{IV-8}$$

We discretize the y and t coordinates, such that

$$f_j^n = f(j\Delta y, n\Delta t) \text{ and } g_j^n = g(j\Delta y, n\Delta t), \quad n = 0, 1, 2 \ldots, j = 0, 1, 2$$

From IV-8 we may obtain the difference scheme

$$f_j^{n+1} = f_j^n + \tfrac{1}{2}\frac{\Delta t}{\Delta y} (g_{j+1}^n - g_{j-1}^n) +$$

$$+ \tfrac{1}{2}\left(\frac{\Delta t}{\Delta y}\right)^2 \left[A_{j+\frac{1}{2}}^n (g_{j+1}^n - g_j^n) - A_{j-\frac{1}{2}}^n (g_j^n - g_{j-1}^n) \right] \qquad \text{IV-9}$$

where $A_{j+\frac{1}{2}}^n$ denotes $A(\tfrac{1}{2}f_{j+1}^n + \tfrac{1}{2}f_j^n) = \tfrac{1}{2}A(f_{j+1}^n) + \tfrac{1}{2}A(f_j^n) = \tfrac{1}{2}(A_{j+1}^n + A_j^n)$.

When we define the vector w_j^n, such that

$$w_j^n = \tfrac{1}{2}(g_j^n + g_{j-1}^n) + \tfrac{1}{2}\frac{\Delta t}{\Delta y} \frac{A_j^n + A_{j-1}^n}{2} (g_j^n - g_{j-1}^n) \qquad \text{IV-10}$$

IV-9 may be written as

$$f_j^{n+1} = f_j^n + \frac{\Delta t}{\Delta y} (w_{j+1}^n - w_j^n) \qquad \text{IV-11}$$

It can be shown[59] that the stability of the Lax-Wendroff scheme is given by the Courant condition

$$\nu = \frac{c\Delta t}{\Delta X} \leqslant 1 \qquad\qquad\qquad IV\text{-}12$$

We applied the Lax-Wendroff difference scheme in the computation of the generation of a shock wave by a piston, moving at the constant speed of 1.0 km/s. The initial conditions of the gas are $p_1 = 1.0 \ 10^5 \ N/m^2$, $\rho_1 = 1.0 \ kg/m^3$, $\gamma = 1.4$. The position of the particles at $t = 0$ is given by $X(j\Delta x, 0)$, $j = 0, 1, 2 \ldots$, where $\Delta x = 1.0$ mm. The time increment Δt was chosen to be constant and equal to 0.3 μs.

The pressure distribution as a function of X at a specific instant of time is shown in Fig. IV-1a. It will be seen that, as in the "q-method" of Von Neumann and Richtmyer, spurious oscillations occur behind the shock.
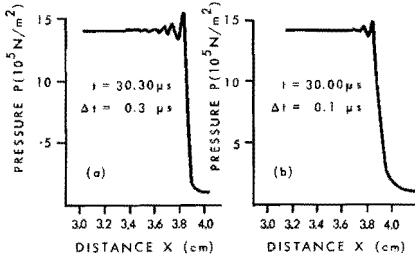
Fig. IV-1 Computed piston driven shock wave solution obtained from Lax-Wendroff scheme, a) no artificial viscosity term, b) with artificial viscosity term
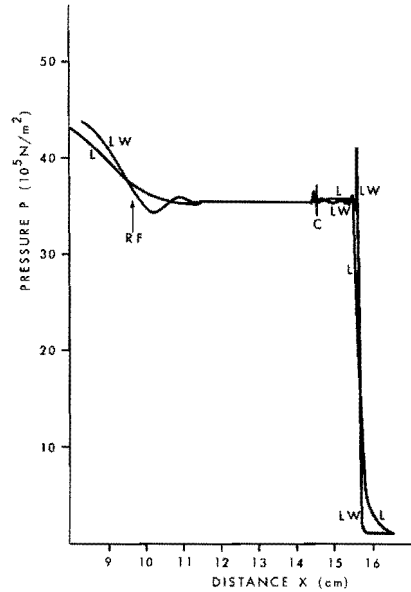
Fig. IV-2 Shock tube problem; computed pressure versus distance profile at 30.4 μs after breaking of the diaphragm; L) Lax method; LW) Lax-Wendroff method

Nevertheless, the values of all variables in the "steady" part of the
flow agree within 1% of the analytically calculated values ($p_2 = 14.092$
10^5 N/m^2, shock speed U = 1308.2 m/s). The shock transition occurs
within 3 mesh widths.

In order to suppress the oscillations, it is possible to introduce a
pseudo-viscosity term similar to the "q-term" of Von Neumann-Richtmyer[65].
This may be done by using $w_j^n + q_j^n$ instead of w_j^n in IV-11, where the
vector q = (q1, q2, q3) is given by

$$q1_j^n = 0$$

$$q2_j^n = - \frac{(u_{j-1}^n - u_j^n + |u_{j-1}^n - u_j^n|)^2}{\frac{1}{2}(V_j^n + V_{j-1}^n)} \quad \frac{\sigma}{(2\Delta y)^2}$$

$$q3_j^n = \frac{1}{2}(u_{j-1}^n + u_j^n) \; q2_j^n \qquad\qquad\qquad \text{IV-13}$$

where σ is a constant of dimension $(\Delta y)^2$. The above piston problem has
been performed with this "q-term". A result is shown in Fig. IV-1b. A
50% decrease of overshoot in the shock front is obtained, and the oscil-
lations are damped sooner by a judicious choice of Δt and σ. The shock
transition, however, is less steep than in Fig. IV-1a, while the time
increment Δt is 1/3 smaller to keep the system stable. This implies
that the computer "run time" is at least three times longer.

In order to check the performance of the Lax method, which is of first
order accuracy, against the Lax-Wendroff method, which is of second or-
der accuracy, we thought it worthwhile to investigate both methods
for the shock tube problem, which involves a shock and rarefaction wave
and a contact discontinuity (see Chapter BI-§3). Fig. IV-2 gives a re-
sult for both methods. The Lax method gives a somewhat wider shock
transition, but without oscillations. The Lax-Wendroff method also
gives oscillations near the tail of the rarefaction wave. A small os-
cillation is visible near the contact discontinuity for the Lax method.
For both methods the results agree within 1% of the analytically cal-
culated values (analytical: $p_2 = 35.46 \; 10^5$ N/m^2, $u_2 = 1525.0$ m/s,
U = 1894.1 m/s). The analytically calculated position of the tail of

the rarefaction wave is indicated in the Figure by the arrow RF. The initial conditions are given in Table IV -1.

TABLE IV-1

Initial conditions for shock tube problem. At $t = 0$, diaphragm at $X = 100$ mm. The time increment Δt was calculated at every cycle of the computation and was taken to be 0.95 times the maximum allowable value determined by the Courant condition.

$p_1 = 1.0132 \times 10^5$ N/m^2	$p_{41} = 43.576$
$\rho_1 = 1.193$ kg/m^3	$\rho_4 = 2.052$ kg/m^3
$u_1 = 0.0$ m/s	$u_4 = 1249.4$ m/s
$\gamma_1 = 1.40$	$\gamma_4 = 1.3166$

Appendix V Flow diagram of computer program for the simulation of the reflection process

```
┌─────────────────────────────────┐
│      Start                      │
│ read constants,                 │
│ number of zones, etc.           │
└─────────────────────────────────┘
            │
┌─────────────────────────────────┐
│      Store                      │
│ initial and boundary conditions │
│ for all zones: p,V,u,E,X,τ,t = 0│
└─────────────────────────────────┘
            │
┌─────────────────────────────────┐
│ Calculate maximum time increment│
│ from stability condition        │
│ Δt = 0.95xdy/(ρc)               │
└─────────────────────────────────┘
            │
┌─────────────────────────────────┐
│ Calculate and store new values  │
│ p,V,u,E,Q,X,τ,t with Lax scheme,│
│ eq. of state, and heat release  │
│ subroutines                     │
└─────────────────────────────────┘
            │
┌─────────────────────────────────┐
│ Evaluate boundary values with   │
│ piston subroutine               │
└─────────────────────────────────┘
            │
┌──────────────┐
│   Print?     │ ── yes ──→ ┌──────────────┐
└──────────────┘            │ print results│
       │                    └──────────────┘
      no ──────────────────────────────→
                                    ┌────────┐
                                 no │ Stop?  │
                                    └────────┘
                                        │
                                       yes
                                        │
                                ┌──────────────┐
                                │ End of program│
                                └──────────────┘
```

$$\Delta t = 0.95 \times dy/(\rho c)$$

Calculate maximum time increment from stability condition

Calculate and store new values p,V,u,E,Q,X,τ,t with Lax scheme, eq. of state, and heat release subroutines

Evaluate boundary values with piston subroutine

Print?   yes   print results

no

Stop?

no

yes

End of program

Appendix VI The interaction of a shock and detonation wave with an
               interface

When a plane shock wave is incident on an interface which separates
two different media it is physically obvious that a shock wave is trans-
mitted[89]. The reflected wave will in general be a shock or rarefaction
wave depending on the relative shock impedances of the media. The shock
impedance is defined as the product of the original density of the me-
dium and the speed of the shock wave moving through it. In fig. VI-1
the interaction process is sketched in the X,t-plane.
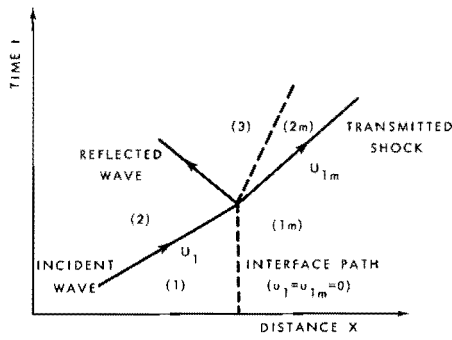
Fig. VI-1   Distance-time representation of the interaction process at
            an interface

From the equations of conservation of mass and momentum for a strong
shock wave $(p_2 \gg p_1)$ it follows for the

incident shock wave $p_2 = \rho_1 u_2 U_1$ VI-1

transmitted shock wave $p_{2m} = \rho_{1m} u_{2m} U_{1m}$ VI-2

When the reflected wave is a shock wave we find similarly

$\quad p_3 - p_2 = \rho_2 v_2 (u_2 - u_3)$ VI-3

where v_2 is the speed of the reflected shock wave relative to the me-
dium upstream of it, which is positive.

The boundary conditions across the interface require

$$p_3 = p_{2m} \quad ; \quad u_3 = u_{2m} \qquad \text{VI-4}$$

Elimination of u_2 and u_3 gives from VI-1 to VI-4

$$\frac{p_{2m}}{p_2} = \frac{\rho_{1m}U_{1m}}{\rho_1 U_1} \frac{\rho_1 U_1 + \rho_2 v_2}{\rho_{1m}U_{1m} + \rho_2 v_2} \qquad \text{VI-5}$$

In a different form

$$\frac{p_3 - p_2}{p_2} = \frac{\rho_2 v_2}{\rho_1 U_1} \frac{\rho_{1m}U_{1m} - \rho_1 U_1}{\rho_{1m}U_{1m} + \rho_2 v_2} \qquad \text{VI-6}$$

From the latter equation it is seen that a reflected shock wave $(p_3 > p_2)$ is only possible if the shock impedances $\rho_{1m}U_{1m} > \rho_1 U_1$. Analogously it can be shown that a rarefaction wave $(p_3 < p_2)$ is only possible if the shock impedance $\rho_{1m}U_{1m} < \rho_1 U_1$.

In case the media may be described by a constant gamma equation of state and assuming strong shock waves, we may put this result in a different form. For a reflected shock wave it is required that $p_3 = p_{2m} > p_2$ and also $u_2 > u_3$. In other words

$$p_{2m} = \frac{\gamma_m + 1}{2} \rho_{1m} u_{2m}^2 = \frac{\gamma_m + 1}{2} \rho_{1m} u_3^2 > p_2 = \frac{\gamma_1 + 1}{2} \rho_1 u_3^2 \qquad \text{VI-7}$$

This results in [90]

$$\rho_{1m} > \frac{\gamma_1 + 1}{\gamma_m + 1} \rho_1 \qquad \text{VI-8}$$

for a shock wave to be reflected.

If one would consider the incident wave to be a detonation wave with negligible reaction zone (CJ model) the above derivations of VI-5 and VI-6 remain essentially the same. Therefore if we identify p_2 as p_{CJ}

and U_1 as D and make the usual acoustical approximation[82] $\rho_2 v_2 = \rho_1 D$ we find from VI-5 in the case of a reflected shock wave

$$\frac{P_{CJ}}{P_{2m}} = \frac{\rho_{1m}U_{1m}+\rho_1 D}{2\rho_{1m}U_{1m}} \qquad\qquad VI-9$$

In a different form for a reflected shock wave we have

$$P_{2m} = \frac{\gamma_m+1}{2} \rho_{1m}u_3^2 > P_{CJ} = (\gamma_1+1)\rho_1 u_2^2 \qquad\qquad VI-10$$

Hence in case of an incident detonation wave with negligible reaction zone we find the condition for a reflected shock wave

$$\rho_{1m} > 2 \frac{\gamma_1+1}{\gamma_m+1} \rho_1 \qquad\qquad VI-11$$

In case of an appreciable reaction zone length it may be expected that, when the transient processes due to the presence of the spike have died down, Eqs. VI-9 and VI-11 will apply for the final state. This assumption was made by Deal for the determination of the CJ pressures of high explosives.

REFERENCES

1. Courant, R. and Friedrichs, K.O., Supersonic Flow and Shock Waves, Interscience Publ.Inc., New York, 1948.
2. Stanyukovich, K.P., Unsteady Motion of Continuous Media, ed. by Holt, M., Pergamon Press, Oxford, 1960.
3. Zeldovich, Ya.B. and Raizer, Yu.P., Physics of Shock Waves and High-Temperature Hydrodynamic Phenomena, ed.by Hayes, W.D. and Probstein, R.F., Academic Press, New York, London, 1966.
4. Jouguet, M.J., Sur la propagation des réactions chimiques dans les gaz, J.Math.Pure et Appl., 60 (1905) 347.
5. Oppenheim, A.K., Manson, N., and Wagner, H.Gg., Recent Progress in Detonation Research, AIAA J., 1 (1963) 2243.
6. Shchelkin, K.I., and Troshin, Ya.K., Gasdynamics of Combustion, Izd.Ak.Nauk SSSR, Moscow, 1963. NASA TT F-231, 1964.
7. Soloukhin, R.I., Detonation Waves in Gases, Sov.Phys. USP 6 (1964) 523.
8. Soloukhin, R.I., Shock Waves and Detonations in Gases, Mono Book Corp., Baltimore, 1966.
9. Shchelkin, K.I., Instability of Combustion and Detonation of Gases, Sov.Phys. USP 8 (1966) 780.
10. van Tiggelen, A., and de Soete, G., Rev.Inst. Franc. Pétrole, Ann. Comb. Liquides, 21 (1966) 239; 21 (1966) 455; 21 (1966) 604.
11. Strehlow, R.A., Detonation and the Hydrodynamics of Reactive Shock Waves, Am.Chem.Soc.Div.Fuel Chem., 11 (1967) 1.
12. Strehlow, R.A., Gas Phase Detonations: Recent Developments, Combustion and Flame 12 (1968) 81.
13. Edwards, D.H., A Survey of Recent Work on the Structure of Detonation Waves, 12th Symp. (Int.) on Combustion, p. 819, The Combustion Institute, Pittsburgh, Pa, 1970.
14. Chapman, D.L., Phil.Mag. 47 (1899) 90.
15. Zeldovich, Ya.B. and Kompaneets, A.S., Theories of Detonation, Academic Press, New York, London, 1960.
16. Zeldovich, Ya.B., Theory of Propagation in Gaseous Systems, JETP 10 (1940) 542.
17. Von Neumann, J., Progress Report on Theory of Detonation Waves, Office of Sci.Res. and Dev.Rep. No. 549 (1942).
18. Doering, W., Über den Detonationsvorgang in Gasen, Ann.Physik 43 (1943) 421.
19. Duff, R.E., Calculation of Reaction Profiles behind Steady-State Shock Waves. I. Application to Detonation Waves, J.Chem. Phys. 28 (1958) 1193.
20. Kystiakowsky, G.B. and Kydd, P.H., Gaseous Detonations, IXA. Study of the Reaction Zone by gas Density Measurements, J.Chem.Phys. 25 (1956) 824.
21. Cook, M.A., Keyes, R.T. and Filler, A.S., Mechanism of Detonation, Trans.Far.Sic. 52 (1956) 369.
22. Kistiakowsky, G.B. and coworkers, Gaseous Detonations,
    I.   J.Am.Chem.Soc. 72 (1950) 1080; II. J.Am.Chem.Soc. 72 (1950) 1086; III. J.Chem.Phys. 20 (1952) 876; IV. J.Chem. Phys. 20 (1952) 884; V. J.Chem.Phys. 20 (1952) 994; VI. J. Chem.Phys. 23 (1955) 271; VII. J.Chem.Phys. 23 (1955) 1889; VIII. J.Chem.Phys. 25 (1956) 516.

23. Manson, N., and Guénoche, H., Etude de l'influence du diamètre des tubes sur la célérité des ondes explosives, Rev.Inst.Franc. Pétrole, Ann.Comb.Liquides, 9 (1954) 214.

24. Cheswick, J.P. and Kistiakowsky, G.B., Gaseous Detonations, X. Study of Reaction Zones, J.Chem.Phys. 28 (1958) 956.

25. Edwards, D.H., Williams, G.T. and Breeze, J.C., Pressure and Velocity Measurements on Detonation Waves in Hydrogen-Oxygen Mixtures, J.Fluid Mech. 6 (1959) 947.

26. Guerraud, C., Leyer, J. and Brochet, C., Mesure de la variation de la pression de detonation dans les mélanges gazeux, C.R.Acad. Sc.Paris 264 (1967) 5.

27. Just, Th. and Wagner, H.Gg., Untersuchung der Reaktionszone von Detonationen in Knallgas, Z.Elektrochem. 64 (1960) 501.

28. Soloukhin, R.I., Multiheaded Structure of Gaseous Detonation, Combustion and Flame 10 (1966) 51.

29. Jones, T.G. and Vlases, G.C., Pressure Probes for Research in Plasma Dynamics and Detonation, Rev.Sci.Instr. 38 (1967) 1038.

30. Baganoff, D., Pressure Gauge with 0.1 microsecond Risetime for Shock Reflection Studies, Rev.Sci.Instr. 35 (1964) 288.

31. Gaydon, A.G. and Hurle, I.R., Temperature Measurements behind Shock Initiated Detonations in CO/O_2 Mixtures, Les Ondes de Détonations (CNRS), Paris, 1962.

32. Campbell, C. and Woodhead, D., The Ignition of Gases by an Explosion Wave. Part I. Carbon Monoxide-Hydrogen Mixture, J.Chem. Soc. 129 (1926) 3010.

33. White, D.R., Turbulent Structure of Gaseous Detonation, Phys. Fluids 4 (1961) 465.

34. Denisov, Yu.N., Shchelkin, K.I. and Troshin, Ya.K., Some Questions of Analogy between Combustion in a Thrust Chamber and in a Detonation Wave, 8th Symp. (Int.) on Combustion, p. 1152, Williams and Wilkins, 1962.

35. Erpenbeck, J.J., Stability of Steady State Equilibrium Detonation, Phys.Fluids 5 (1962) 604.

36. Oppenheim, A.K., Development and Structure of Plane Detonation Waves, Combustion and Propulsion: 4th AGARD Coll., Pergamon Press, New York, p. 186, 1961.

37. Gilbert, R.B. and Strehlow, R.A., Theory of Detonation Initiation behind Reflected Shock Waves, AIAA J. 4 (1966) 1777.

38. Broekstra, G., Detonatie, De Ingenieur 82 (1970) 033.

39. Taylor, C.I., Dynamics of the Combustion Products behind Planar and Spherical Detonation Fronts in Explosives, Proc.Roy.Soc. A 200 (1950) 235.

40. Gordon, W.E., Pressure Measurements in gaseous Detonation by means of Piezoelectric Gauges, 3rd Symp. (Int.) on Combustion, p. 579, Williams and Wilkins, 1949.

41. Hicks, B.L., Montgomery, D.J. and Wasserman, R.H., On the One-Dimensional Theory of Steady Compressible Fluid Flow in Ducts with Friction and Heat Addition, J.Appl.Phys. 18 (1947).

42. Sedov, L.I., Similarity and Dimensional Methods in Mechanics, Academic Press, New York, 1959.

43. Huni, J.P., Ardila, H. and Ahlborn, P., Calibration of Piezoelectric Pressure Probe, Rev.Sci.Instr. 41 (1970) 1074.

44. Soloukhin, R.I., Structure of a Multifront Detonation Wave in a Gas, Combustion, Explosion and Shock Waves, 1 (1965) 23.

45. Glass, I.I., Martin, W.A., and Patterson, C.N., A Theoretical and Experimental Study of the Shock Tube, UTIA Rep. No. 2 (1953).

46. Oppenheim, A.K., Gasdynamic Analysis of the Development of Gaseous Detonation and its Hydraulic Analogy, 4th Symp. (Int.) on Combustion, p. 471, Williams and Wilkins, 1953.

47. Boa-Teh Chu, On the Generation of Pressure Waves at a Plane Flame Front, 4th Symp. (Int.) on Combustion, p. 603, Williams and Wilkins, 1953.

48. Schott, G.L. and Getzinger, R.W., Kinetic Studies of Hydroxyl Radicals in Shock Waves, J.Chem.Phys. 43 (1965) 3237.

49. White, D.R., Moore, G.E., Structure of Gaseous Detonations. IV. Induction Zone Studies in H_2-O_2 and CO-O_2 Mixtures, 10th Symp. (Int.) on Combustion, p. 785, The Combustion Institute, Pittsburgh, Pa, 1965.

50. White, D.R., Density Induction Times in very lean Mixtures of D_2, H_2, C_2H_2, and C_2H_4, with O_2, 11th Symp. (Int.) on Combustion, p. 147, The Combustion Institute, Pittsburgh, Pa, 1967.

51. Kistiakowsky, G.B. and Richards, L.W., Emission of Vacuum Ultraviolet Radiation from the Acetylene-Oxygen and the Methane-Oxygen Reactions in Shock Waves, J.Chem.Phys. 36 (1962) 1707.

52. Schott, G.L. and Kinsey, J.L., Kinetic Studies of Hydroxyl Radicals in Shock Waves, II, J.Chem.Phys. 29 (1958) 1177.

53. Strehlow, R.A. and Cohen, A., Initiation of Detonation, Phys.Fluids 5 (1962) 97.

54. Glass, G.P., Kistiakowsky, G.B., Michael, J.V. and Niki, H., Mechanism of the Acetylene-Oxygen Reaction in Shock Waves, J.Chem. Phys. 42 (1965) 608.

55. Urtiew, P.A. and Oppenheim, A.K., Detonative Ignition induced by Shock Merging, 11th Symp. (Int.) on Combustion, p. 665, The Combustion Institute, Pittsburgh, Pa, 1967.

56. Strehlow, R.A., Maurer, R.E. and Rajan, S., Transverse Waves in Detonations: I. Spacing in the Hydrogen-Oxygen System, AIAA J. 7 (1969) 323.

57. Jost, W., Just, Th. and Wagner, H.Gg., Investigation of the Reaction Zone of Gaseous Detonations, 8th Symp. (Int.) on Combustion, p. 582, Williams and Wilkins, 1962.

58. Lee, J.H., The Propagation of Shocks and Blast Waves in a Detonating Gas, Thesis, McGill University, Montreal, 1965.

59. Richtmyer, R.D. and Morton, K.W., Difference Methods for Initial-Value Problems, Interscience Publ., New York, 1967.

60. Fox, L., Numerical Solution of Ordinary and Partial Differential Equations, Pergamon Press, Oxford, 1962.

61. Von Neumann, J. and Richtmyer, R.D., A Method for the Numerical Calculation of Hydrodynamic Shocks, J.Appl.Phys. 21 (1950) 232.

62. Zovko, C.T. and Macek, A., A Computational Treatment of the Transition from Deflagration to Detonation in Solids, 3th Symp. on Detonation, 1960.

63. Lax, P.D., Weak Solutions of Nonlinear Hyperbolic Equations and their Numerical Computation, Comm.Pure and Appl.Math. $\underline{7}$ (1954) 159.

64. Lax, P.D. and Wendroff, B., Systems of Conservation Laws, Comm. Pure and Appl.Math. $\underline{8}$ (1960) 217.

65. Söderberg, S., Numerical Solution of the Generation of a Hydrodynamic Shock caused by a Moving Piston, FOA Report B 4008-23, Res.Inst.Nat.Def. Sweden, 1968.

66. Edwards, D.H., Jones, T.G. and Price B., Observations on Oblique Shock Waves in Gaseous Detonations, J.Fluid Mech. $\underline{17}$ (1963) 21.

67. Fay, J.A. and Opel, G., Two-Dimensional Effects in Gaseous Detonation Waves, J.Chem.Phys. $\underline{29}$ (1958) 955.

68. Fay, J.A., The Structure of Gaseous Detonation Waves, 8th Symp. (Int.) on Combustion, p. 30, Williams and Wilkins, 1962.

69. Strehlow, R.A. and Cohen, A., Shock-Initiated Detonations, Phys. Fluids $\underline{3}$ (1960) 319.

70. Lu, P.H., Dabora, E.K. and Nicholls, J.A., The Structure of H_2-CO-O_2 Detonations, Combustion Science and Technology, $\underline{1}$ (1969) 65.

71. Denisov, Iu.N., Collision with a Wall of Waves of a One-Dimensional Gaseous Detonation with Large and Negligibly Small Periods of Induction of Combustion, Transl.f.Russian, PMTF $\underline{2}$ (1966) 96. (courtesy of Dr. D.H. Edwards)

72. Droppleman, J.D., An experimental and analytical Investigation of the Reflection Process of a Detonation Wave, Thesis, Un. of Colorado, USA, 1967. (courtesy of Dr. D.H. Edwards)

73. Knight, H.T. and Duff, R.E., Precision Measurements of Detonation and Strong Shock Velocity in Gases, Rev.Sci.Instr. $\underline{26}$ (1955) 257.

74. Edwards, D.H., A Piezo-electric Pressure Bar Gauge, J.Sci.Instr. $\underline{35}$ (1958) 346.

75. Edwards, D.H., Davies, L. and Lawrence, T.R., The Application of a Piezoelectric Bar Gauge to Shock Tube Studies, J.Sci.Instr. $\underline{41}$ (1964) 609.

76. Ragland, K.W. and Cullen, R.E., Piezoelectric Pressure Transducer with Acoustic Absorbing Rod, Rev.Sci.Instr. $\underline{38}$ (1967) 740.

77. Lee, J.H., private communication (Aug. 1969).

78. Knystautas, R., An Experimental Study of Spherical Gaseous Detonation Waves, MERL Report 69-2, Dep.Mech.Eng., McGill Un., Montreal, 1969.

79. Jones, I.R., Beryllium Pressure Bar Having Submicrosecond Risetime Rev.Sci.Instr. $\underline{37}$ (1966) 1059.

80. Duff, R.E. and Houston, E., Measurement of the Chapman-Jouguet Pressure and Reaction Zone Length in a Detonating High Explosive, J.Chem.Phys. $\underline{23}$ (1955) 1268.

81. Deal, W.E., Measurement of Chapman-Jouguet Pressure for Explosives, J.Chem.Phys. $\underline{27}$ (1957) 796.

82. Walsh, J.M. and Christian, R.H., Equation of State of Metals from Shock Wave Measurements, Phys.Rev. $\underline{97}$ (1955) 1544.

83. Cowan, R.D. and Fickett, W. Calculation of the Detonation Proper-
        ties of Solid Explosives with the Kistiakowsky-Wilson Equa-
        tion of State, J.Chem.Phys. 24 (1956) 932.
84. Craig, B.G., Measurements of the Detonation-Front Structure in
        Condensed-Phase Explosives, 10th Symp. (Int.) on Combustion,
        p. 863, The Combustion Institute, Pittsburgh, Pa, 1965.
85. Hauver, G.E. and Eichelberger, R.J. , Solid State Transducers for
        Recording of Intense Pressure Pulses, Les Ondes de Détonation,
        CNRS, p. 363, Paris, 1962.
86. Veretennikov, V.A., Dremin, A.N., Rozanov, O.K. and Shvedov, K.K.,
        Applicability of Hydrodynamic Theory to the Detonation of
        Condensed Explosives, Fiz.Goreniya Vzryva 1 (1965) 3.
        (Combustion, Explosion and Shock Waves, 1 (1967) 1).
87. Petrone, F.J., Validity of the Classical Detonation Wave Structure
        for Condensed Explosives, Phys.Fluids, 11 (1968) 1473.
88. Jameson, R.L. and Hawkins, A., Shock Velocity Measurements in Inert
        Monitors Placed on Several Explosives, 5th Symp. on Detonation,
        p. 17. Preprints August 1970, Pasadena, California.
89. Pack, D.C., The Reflection and Transmission of Shock Waves, Phil.
        Mag. 2 (1957) 182.
90. Paterson, S., Contact Transmission of Detonation, 4th Symp. (Int.)
        on Combustion, p. 468, Williams and Wilkins, 1953.
91. Broekstra, G., Note on Detonation and Blast Wave Theory; Part I.
        Detonation Theory, Defence Res.Establishment Suffield, Ral-
        ston, Canada, Rep. No. 24/68, 1968.
92. Eisen, C.L., Gross, R.A. and Rivlin, T.J., Theoretical Calculations
        in Gaseous Detonations, Combustion and Flame, 4 (1960) 137.

SUMMARY

Historically the structure of a steady one-dimensional detonation wave
was first described by Chapman and Jouguet (CJ). The CJ model of a de-
tonation wave assumes instantaneous and complete combustion immediately
behind the leading shock front of a detonation wave. The CJ model
enables one to derive theoretically the detonation velocity and thermo
and gasdynamical variables for complete combustion.
Zeldovich, Von Neumann and Doering described the structure of a steady
detonation wave to consist of a leading shock front, which initiates
chemical reaction, followed by a reaction zone which is terminated by
the CJ surface where combustion is completed.
During the last decade convincing theoretical and experimental evidence
has been provided that the structure of a detonation wave in gases is
far from one-dimensional. Instead of laminar flow behind a plane shock
front a three-dimensional transverse "turbulent" wave pattern governs
the detonation wave structure. A mathematical analysis of the complete
multiheaded detonation wave seems not within reach yet.
Detonation waves in gases or liquid and solid high explosives occurring
either accidently or purposely in both commercial and military appli-
cations generally interact with their immediate surroundings creating
strong shock waves. The shattering action or the ability of an explo-
sive to demolish a hard object when fired in direct contact is called
brisance. The object in contact with the explosive in turn influences
the detonation process.
The basic mechanisms underlying the interaction of detonation waves
with their surroundings are at present poorly understood. In order to
gain a better insight into the nature and the origin of such interac-
tions a possible approach of the problem is suggested in this work. To
do so effectively we propose an approximate description of the detona-
tion wave structure. Essentially this is tantamount to assuming that
from a gasdynamics point of view a detonation wave may be modelled by
a one-dimensional double wave complex consisting of a shock wave, which
initiates chemical reaction by adiabatic compression of the original
explosive, and of a combustion wave in which the conversion of reac-

tants to products attended by release of the heat of explosion actually occurs.

The concept of a detonation wave as consisting of a double wave complex is not new in itself. In this work, however, we derive and study the physical implications of such a concept to some extent, while the concept of a combustion wave as an elementary wave is made amenable to a theoretical analysis of interaction processes.

The description of interactions of non-reactive elementary waves, i.e. shock, compression and rarefaction waves, by means of an analysis in a pressure-particle velocity diagram is a well-known technique. In this work we will show that the introduction of the combustion wave as a reactive elementary wave permits one to perform a theoretical analysis of interaction processes involving both reactive and non-reactive waves in the same diagram.

We will show that two fundamental interaction rules may be derived that have important applications in detonation research. These concern the head-on collision of a combustion wave with a shock wave, and with a rarefaction wave.

Two specific applications are dealt with in this work, namely, the reflection of a gaseous detonation wave against a solid wall and the transmission of a detonation wave in a high explosive into an inert medium and in particular the so-called plate velocity method.

Besides the aforementioned points, we consider some properties of the non-reactive elementary waves, i.e. shock, compression and rarefaction waves, in PART A - Chapter AI. A survey of detonation wave models is presented in PART A - Chapter AII. In the same Chapter we discuss some properties of one-dimensional detonation waves. We performed accurate calculations of the thermo and gasdynamical variables of detonation waves in stoichiometric hydrogen-oxygen and equimolar acetylene-oxygen mixtures at several initial pressures, which are compared with our experimental values. More particularly, we developed a precision pin-raster-oscilloscope technique for the measurements of detonation wave velocities of these mixtures, while we measured detonation pressures with specially developed pressure bar transducers with a piezoelectric

sensing element (2 mm dia x 1 mm) matched to a tin rod. We have given
some attention to the flow of the combustion products behind a detona-
tion wave in gases in the Taylor rarefaction wave. In the same Chapter
we develop the theory of the combustion wave for a constant gamma -
constant molecular weight ideal gas. Our accurate calculations of the
states ahead of and behind combustion waves in the aforementioned mix-
tures are presented in Appendix I.

In PART B - Chapter BI we summarize the pressure-particle velocity loci
of the non-reactive elementary waves. Their applicability is illustrated
qualitatively by considering the shock tube problem. In the same Chapter
we derive the pressure-particle velocity loci of reactive combustion
waves. This Chapter provides the ingredients for the study of two inter-
action rules that we derive in PART B - Chapter BII. We will demonstrate
that the head-on collision of a backward facing shock wave (rarefaction
wave) with a forward facing combustion wave will result in a transmitted
backward facing shock wave (rarefaction wave), and a reflected forward
facing rarefaction wave (shock wave).

PART C begins with a discussion of three different detonation wave mo-
dels, I, II and III employed in this work each of which is less res-
trictive than the preceding one. Model I and II are characterized by a
constant induction time, while in Model I the heat of explosion is re-
leased instantaneously at the end of the induction period and in Model
II a heat release equation is applied which is characterized by a heat
release "relaxation time". Model III is given by a density and temper-
ature dependent induction time and the heat release equation of Model
II. The reflection of a gaseous detonation wave against a solid wall is
studied by means of these three Models. We performed computer simula-
tions of the interaction process with the aid of a finite difference
method for the approximate solution of the gasdynamical equations. With
reasonable assumptions as to the values of the induction time, the
reaction zone length and the heat of explosion we achieved a favourable
comparison with experimental values obtained by Droppleman of a charac-
teristic decay time of the pressure profile at the wall. It appears

from a parameter study that the induction time is the parameter that
dominates the profile of the reflected pressure at the wall. We de-
veloped a special reflection pressure bar transducer (sensing element
10 mm dia x 0.2 mm) which exhibits a rise time of about 200 nanoseconds,
which is substantially faster than any other gauge of this type hither-
to reported. Although the response of the gauge to a pressure step
function is not completely satisfactory, experimental results of the
reflected pressure at the wall are in qualitative agreement with our
computed results.

In PART D the interaction rules are suggested to explain some anomalies
that have appeared in determining the structure and, more particularly,
the reaction zone lengths of solid high explosives by the plate-veloci-
ty technique. A typical free-surface velocity versus plate thickness
profile is produced when a detonation wave impinges on an inert mate-
rial plate which we examined by means of a computer simulation.

CURRICULUM VITAE

Gerrit Broekstra was born in Alkmaar on 1st August 1941. In this city
he completed the Gymnasium-Beta. He started his studies at the Techno-
logical University of Delft in 1960 and obtained his degree in Applied
Physics in 1966. To this end he wrote a thesis on optimizing techniques
followed by a publication as a co-author with Prof.Dr.Ir. C.J.D.M.
Verhagen on "A multi-dimensional self-optimizing control system invol-
ving dynamics and disturbances, employing relay extremum control"
("Theory of self-adaptive control systems", a publication of the In-
strument Society of America, Ed. by P.H. Hammond, Plenum Press, New
York, 1966).
During his military service in the Royal Dutch Army he was detached as
a physicist at the Technological Laboratory of the National Defence
Research Organization TNO. At this laboratory he has been employed since
1966 as head of the department "Shock waves and High Explosives". In
1967 he was detached for a period of one year to the Defence Research
Establishment Suffield, Alberta, of the Defence Research Board of
Canada to study the physics and chemistry of shock tubes and high ex-
plosive detonations. During this period he participated in several
multi-ton blast and detonation projects, a joint venture of Canada,
United Kingdom and United States of America. He wrote several reports
on shock tube performance and blast and detonation theory.

STELLINGEN

I

Het verdient aanbeveling de grote discrepantie tussen inductietijden,
verkregen langs theoretische weg en door schokbuisexperimenten, van
waterstof-zuurstofmengsels in het gebied van hoge druk en lage tempe-
ratuur te onderzoeken met behulp van een adiabatische-compressie-
apparaat.

Jost W., 9th Symp. (Int.) on Combustion, Ac. Press, New York,
London (1963) 1013.
Wakefield, C.B., Ripley, D.L. and Gardiner, W.C., J.Chem.Phys.
50 (1969) 325.

II

De door Cosner c.s. experimenteel gevonden relatie, die de getransmit-
teerde druk in een acceptorlading als functie van de initiatie-afstand
in de acceptor geeft, leidt bij vergelijking met Warner's c.s. theore-
tische analyse van het initiatieproces in heterogene springstoffen tot
een interessante conclusie met betrekking tot de grootte van de expo-
nent van de drukterm in de reaktievergelijking van het "brandende-
korrelmodel" van Eyring.

Cosner, L.N., Sewell, R.G.S. and Sinclair, J.E., Explosivstoffe
10 (1969) 230.
Warner, F.J. and Pack, D.C., 10th Symp. (Int.) on Combustion,
Ac. Press, New York, London (1965) 845.

III

Een "adiabatic compression apparatus" kan goed gebruikt worden voor de
bestudering van het dynamische gedrag van breekmembranen, bestemd voor
het beheersen van de druk bij gasexplosies in een gesloten ruimte.

Martinengo, A., Oxidation and Combustion Review, Elsevier Publ.
Comp., Amsterdam, 2 (1967) 209.

IV

Naar analogie van de reaktievergelijking voor het "brandende-korrel-
model" van Eyring en de toepassing daarvan voor het detonatiegolfmodel
van heterogene springstoffen, kan gezien de structuur van de detonatie-
golf in gassen een dergelijke reaktievergelijking opgesteld worden,
die een verbetering zou kunnen betekenen van het model van Zeldovich,
Von Neumann en Döring.

V

Bij de afleiding van de energiebalans-vergelijking voor de explosie in
een gesloten vat past Trense ongebruikelijke definities toe van de
begrippen inwendige energie en explosiewarmte.

Trense, R.W., TNO-Nieuws 26 (1971) 73.

VI

Bij de opleiding van technologen verdient het aanbeveling aandacht te
besteden aan de wetenschappelijke grondslagen van explosieveiligheid.

VII

Uit de resultaten van de bepaling van de relatie tussen schoksnelheid
en deeltjessnelheid met behulp van verschillende meetmethoden bij
polymethylmethacrylaat kan geconcludeerd worden dat de zgn. aquarium-
methode, waarbij de schokgolf van deze stof overgaat in water, met
enige voorzichtigheid dient te worden gehanteerd.

Jaffe, I., Beauregard R., and Amster, A., ARS J. 32 (1962) 22.
Liddiard, T.P., 4th Symp. (Int.) on Detonation, White Oak, Mary-
    land, ACR-126 (1965) 214.
Barker, L.M. and Hollenbach, R.E., J.Appl.Phys. 41 (1970) 4208.

VIII

De resultaten van de door York ontwikkelde drukopnemers van het "pressure-bar" type, gebaseerd op een alternatief criterium voor de aanpassing van de componenten van de "pressure bar", suggereren dat een aanvaardbare responsie van dit soort opnemers meer bepaald wordt door grote aandacht voor de constructie van de gehele opnemer dan door toepassing van overwegingen op grond van de theorie van spanningsgolf-voortplanting in de "pressure bar".

York, T.H., Rev.Sci.Instr., 41 (1970) 519.
Dit proefschrift.

IX

De justitie gaat er van uit dat invaliden, aan wie een ontheffing van het parkeerverbod is verleend, uitsluitend in de plaats van inwoning gehandicapt zijn.

G. Broekstra